Ultimate Strength of Steel-Elastomer Sandwich Panels Under Combined Loadings Including In-Plane Shear

by

JOSTEIN FLADBY

THESIS

for the degree of

MASTER OF SCIENCE

(Master i Anvendt matematikk og mekanikk)

Faculty of Mathematics and Natural Sciences
University of Oslo

May 2010

Det matematisk- naturvitenskapelige fakultet
Universitetet i Oslo

Preface

This thesis is written to complete the MSc degree at the University of Oslo.

I would especially like to thank my supervisor dr. Brian Hayman, Senior Principal Engineer at DNV, and Adjunct Professor at UiO for his guidance during the whole process. It is highly appreciated. I would also like to thank Det Norske Veritas (DNV), the NTANO715 section particularily, for support and access to their facilities.

I would also like to thank Professor Jostein Hellesland at UiO and my fellow students Håkon Andersen and Geir Ole Guthu particularily, for good discussions around my study.

Oslo, May 30, 2010
Jostein Fladby

Abstract

Sandwich Plate System (SPS) is a sandwich construction consisting of steel face sheets and polyurethane core. The main objective for the steel faces is to resist bending and in-plane loads, while the compliant core transfers shear between the faces. One important benefit with sandwich panels is the elimination of the need for intermediate stiffeners. SPS panels are today used in stadium and arena terraces, bridges, ships and as structural flooring.

Det Norske Veritas (DNV) is currently developing rules and guidelines for design and installation of SPS in ship newbuildings. To do this it is important to study how the SPS panels behave under a variety of loads such as lateral pressure load, in-plane shear load and in-plane uni-axial compression load. Combinations of these loads are important to study to establish strength criterias for SPS panels. Studying these load combinations is the objective for the current study as a collaboration between the University of Oslo (UiO) and Det Norske Veritas (DNV).

In the current study the ultimate capacity of SPS panels under lateral pressure load and in-plane shear load has been studied both separately and in combination. In-plane uni-axial compression load is also included in three-way interactions. Both simply supported and clamped boundary conditions are studied to see the effect of these. Theories that can model the separate load cases are described and compared to each other and to the finite element results. Some theory for load combinations are reviewed, and a slightly conservative interaction curve for different load combinations on SPS panels is suggested.

Contents

Notation

a – panel length
b – panel width
d – distance from mid-face to mid-face
D – flexural rigidity
E – modulus of elasticity
G – shear modulus
k_a – factor used for lateral pressure theories to compare results
$k_a^{'}$ – correction factor used in DNV Classification Rules
K – buckling coefficient
l – length of a yield line (Y-L theory)
l – length of stiffener (often equal to a)
M_p – plastic bending moment
N – in-plane uni-axial compression load
N_{ult} – ultimate in-plane uni-axial compression load
p – lateral pressure load
p_{ult} – ultimate lateral pressure load
p_{YL} – yield line pressure
Q – in-plane shear load
Q_{ult} – ultimate in-plane shear load
s – spacing between stiffeners (often equal to b)
S – shear stiffness
t – thickness of a standard isotropic plate
t_c – thickness of the core in a sandwich
t_f – thickness of a face in a sandwich
t_k – thickness added for corrosion
W_{ext} – external virtual work
W_{int} – internal virtual work
α – angle between shortest panel edge and diagonal yield line (Y-L theory)
β – width over length ratio
δ – mid-panel out-of-plane dispaclement
θ – rotation of the cross section (Y-L theory)
ν – Poisson's ratio
σ_Y – yield stress
τ_c – transverse shear stress
τ_Y – yield stress in shear
ϕ – panel aspect ratio

Chapter 1

Introduction

1.1 Background

Sandwich Plate System (SPS) is a type of sandwich plate where the faces are made of steel that resists bending and various in-plane loads, and the core is made of polyurethane that transfers shear stresses between the two faces. One large benefit with sandwich plates is the large increase in flexural rigidity and bending strength per unit weight. This eliminates the need for the lowest level of stiffeners, and can simplify many constructions. SPS is currently being used in many applications such as bridges, arena terraces and in ships. Because of the advantages that follow with sandwich structures, it is of interest to use this type of plates in newbuildings of ship as well. Two principal figures of SPS is shown in Figure 1.1.

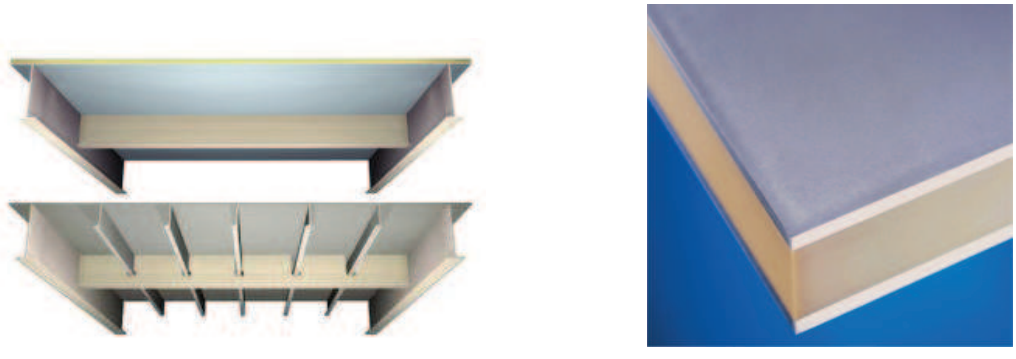

(a) **(b)**

Figure 1.1: SPS structure compared to conventional stiffened structure (a) and SPS cross section (b)

A panel in a ship hull structure can be subjected to a variety of loads. For instance lateral pressure loads, in-plane uni-axial and bi-axial compression and tension loads and in-plane shear loads. Ultimate capacity for these different loadings and combinations of them are important under the process of dimensioning these panels. Det Norske Veritas

(DNV) is currently making rules for the design of these panels and is therefore in collaboration with the current study, analysing a wide range of panels subjected to these different loadings to get a well understanding on how the panels behaves.

1.2 Previous Work

A wide range of theories has been reviewed in connection to this work, from theories for the separate loading cases to the theories for combination of loads in conventional structures and stiffened plates in ships.

Yield line theory is an easy and powerful tool to estimate an upper bound for slabs and plates. This theory was firstly used for concrete slabs, before it was adapted to steel plates. The theory is based on the principle of virtual work. Zhou [1] also adapted this theory to SPS panels which will be one of the theories described in this report. Small adjustments are made to the roof-shaped mechanism assumed in this theory to see if this gives a better estimate, or if the difference is negligible.

Jones [2] develop a lower bound theory for steel plates by suggesting a stress field and using the differential equation for plates. This theory is also used in this work to make a similar lower bound solution for SPS panels. It turns out for the simply supported SPS panels, that this value is not a lower bound solution, but almost equal to the upper bound theory.

DNV's rules [3] are also studied to compare the SPS panels with stiffened plates in ships. Both pure lateral load and in-plane shear buckling are described separately, and also how these are combined in different plating structures in a ship are included.

Paik and Thayamballi [4] gives a good description of the different load combinations and how to dimension them in conventional steel-plated structures. This theory is reviewed in this report, together with a similar approach for SPS panels.

Few experiments are performed on ultimate capacity of SPS panels, but Little [5] has performed some tests on a panel subjected to in-plane uni-axial compression load and uniform lateral pressure load. These tests were compared to finite element analyses. A preliminary project written before the current study goes through the results obtained in Little's report and explains the differences between the finite element analyses and the experiments [6].

Intelligent Engineering has also performed many analyses for different load combinations and submitted papers on their findings.

1.3 Objectives for the Present Study

The main objective in this project is to study ultimate capacity of SPS under the combination of in-plane shear loading, uni-axial compression load and lateral pressure load. Analysing failure modes for the separate loading cases and theory that can describe this behaviour are of great importance. The findings will be used to find slightly conservative interaction curves for all sorts of load combinations of the three load cases on various panel geometries, which can serve a basis for design rules in the future. To reach this goal the following stages are included in the project description.

1. The available literature on ultimate strength of SPS panels under the listed loading cases will be reviewed, together with relevant literature on modelling of sandwich panels in general.

2. On the basis of this and the experience gained in the pre-project, a modelling strategy will be defined for use in a parametric study of the ultimate strength of SPS plates. In addition to FE analysis, analytical or semi-analytical methods may be used if these are fond to be consistent with FE results. This stage may involve deeper investigation of some of the aspects studied in the pre-project.

3. Based on the above, SPS plates will be modelled with both simply supported and clamped boundary conditions under the separate loading cases:

   - uniform lateral pressure
   - uniform in-plane uni-axial compression
   - uniform in-plane shear

   so as to obtain the variation of ultimate strength and deformation modes with plate dimensions for a comprehensive range of SPS plate parameters. In order to limit the number of cases analysed, existing results obtained by IE and others may be included where these are available and considered reliable.

4. A range of combined loading cases will be analysed so as to produce a set of strength interaction curves for two-way combinations and interaction surfaces for three-way interactions. As for the individual loading cases, special attention will be paid to the deformation modes failure mechanisms.

5. If possible, conservative approximations to these interaction curves and surfaces will be established in a simplified form that is convenient for use in design codes and classification rules.

6. Ways in which the results might be incorporated in DNV Rules will be proposed.

7. The results and recommendations will be presented in a comprehensive report.

There were a few challenges during this project. The first of these challenges was to find a good reference value for lateral pressure. Both upper bound and lower bound theories and also even first surface yield are considered to find a good value that can be used in the class rules. All of the theories described can be used in the class rules, but they would need different safety factors with respect to how conservative they need to be. First yield is not described further in this report since this would require much more time to make a "similar" criterion for the in-plane shear load.

During the work with lateral pressure load another discussion came up. How is the transverse shear stress in the core influencing the ultimate capacity? If the core shear stress is higher than the bonding strength, debonding might be the governing failure mechanism. It was decided that bonding strength needs further investigations before a clear strength criterion on this can be made. For the interaction curves in the current study, it is however assumed that debonding will not occur.

The last major challenge in this work was to model boundary conditions in ABAQUS that allow all the different loading combinations and model the actual boundary conditions with straight edges.

Since all these challenges took more time than anticipated, the study on pure in-plane uni-axial compression load was very limited, and the interaction surfaces was limited to two panels with clamped boundary conditions. The pre-project [6] gave however insights in ultimate behaviour for uni-axial compression load, so a reference value was possible to obtain. From this, an interaction surface formula was suggested. This formula needs nevertheless testing on a larger range of panels to provide a check of more general performance.

1.4 Presentation of Chapters in This Report

First part of this report, Chapter 2, consists of two parts; governing theory for lateral pressure loads, and theory for in-plane shear load. Different approaches for the two loading conditions are discussed and compared.

Finite element modelling in ABAQUS is the topic of Chapter 3. Here, all aspects and difficulties discovered during the modelling are described. Also figures of the loading and boundary conditions are included.

The main part of this report is Chapters 4, 5 and 6 where all the results are presented. Both the separate loading cases and the different interaction combinations can be found here. There is also included some discussions and observations in this section that addresses irregularities in the results and how these factors can be solved.

Last chapter in this study is devoted to conclusions found in the other chapters and also

suggestions to what could and what should be studied further to get a more complete picture of ultimate capacity of the SPS panels.

Chapter 2

Governing Theory

2.1 Lateral Pressure Load on SPS Panels

2.1.1 Upper Bound (Yield Line Theory)

One way of estimating ultimate strength of a panel subjected to pure lateral pressure is to use the yield line theory. The theory was originally developed by Professor K.W. Johansen, and published in his doctoral thesis in 1843 at the Danish Technical University. His analysis was based on one-dimensional beams, but the theory has later been extended to two-dimensional slabs and panels. A formula based on this theory was made for SPS panels by Zhou [1] in 2008. The major advantage of this theory is the simplicity of the explicit formula obtained, and for many years it has proved to be a powerful tool for estimating ultimate capacity of concrete slabs and steel plates. There is however a disadvantage with the theory as well; it gives no indication about the deflection of the panel.

The basic assumptions behind the theory are that the deflections are small compared to the overall geometry, the in-plane forces are neglected, and the collapse must be due to moments.

The first step in a yield line analysis is to establish a collapse mechanism for the panel studied. It is important to bear in mind that the choice of collapse mechanism needs to be compatible with the kinematic boundary conditions. A poor choice of collapse mechanism gives a non-conservative solution, even though the kinematic boundary conditions are satisfied, since yield line theory give an upper-bound solution for collapse load, Buyukozturk [7].

A very common collapse mechanism used for concrete slabs and steel plates is the roof-shaped plastic mechanism shown in Figure 2.1. In the limit state, where the plastic hinges form and the panel is divided as shown on Figure 2.1, external virtual work from the lateral pressure p_{YL} is equal to the inner virtual work from the resisting internal plastic bending moment M_p.

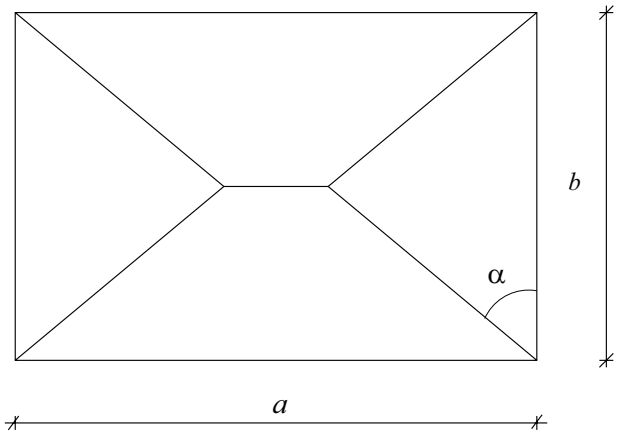

Figure 2.1: Collapse mechanism commonly used for concrete slabs and steel plates. With clamped boundary conditions all four boundaries are also yield lines

By known principles the work is given by load times displacement. For this case, it will be the sum of applied pressure on each part, times the area of each part, times the distance the centroid of the part is displaced. When the length of the panel is given as a, the width is given as b and the angle between the diagonal yield lines and the edges are 45°, the panel can be divided into eight equal triangles and two equal rectangles. Each triangle has the area of $\frac{b^2}{8}$ and each rectangle has the area of $(a-b)\frac{b}{2}$. If the displacement in the middle of the panel is given as δ, it can be shown that the displacement on each of the triangles' centroids will be $\frac{\delta}{3}$ and the displacement on each of the rectangles' centroids will be $\frac{\delta}{2}$. Combining these gives the total external virtual work

$$W_{ext} = 8p_{YL}\frac{b^2}{8}\frac{\delta}{3} + 2p_{YL}(a-b)\frac{b}{2}\frac{\delta}{2} = \frac{p_{YL}\delta}{6}\left(3ab - b^2\right) \tag{2.1}$$

The internal virtual work is the work done by the internal bending moment. In the limit state, this moment will be the plastic moment of the cross section, M_p. For steel and other single layered isotropic plates, this moment will be given as $M_p = \sigma_Y\frac{t^2}{4}$. M_p is the only thing in the derivation of the formula that changes when the theory is adopted to sandwich panels. For a sandwich panel, it is assumed that only the faces can take up the yield stress, so the plastic moment for a sandwich panel will be $M_p = \sigma_Y t_f(t_f + t_c)$ where t_f is the thickness of the face, and t_c is the thickness of the core. The reasoning behind this is illustrated in Zhou's report [1]. The internal work is given by $W_{int} = M_p\theta l$, where θ is the rotation of the cross section, and l is the length of the yield line. Sobotka [8] shows how the rotation can be found by geometry consideration and integration for arbitrarily placed yield lines and can be expressed as a function of δ defined in the paragraph above. The internal work is connected to the choice of boundary conditions. For clamped panels yield lines along the entire perimeter need to be included in contrast to simply supported panels where only the internal yield lines are included. This results in higher bending resistance for the clamped panels which again shows that the clamped panel can carry a

higher lateral pressure load than the simply supported panel can. The full expression for internal work become for clamped panels

$$\begin{aligned} W_{int} &= M_p \theta l = 8\sigma_Y t_f \left(t_f + t_c\right) \delta + \sigma_Y t_f \left(t_f + t_c\right) \delta \left(4\frac{a}{b} + 4\right) + \sigma_Y t_f \left(t_f + t_c\right) \delta \left(4\frac{a}{b} - 4\right) \\ &= 8\sigma_Y t_f \left(t_f + t_c\right) \delta \left(\frac{a}{b} + 1\right) \end{aligned} \tag{2.2}$$

Ultimate limit state for a general clamped plate is then given as

$$W_{ext} = W_{int} \Longrightarrow p_{YL} = \frac{16 M_p k_a}{b^2} \tag{2.3}$$

with $k_a = \frac{a/b+1}{(a/b-1)+2/3}$ and

$$\begin{aligned} M_p &= \sigma_Y \frac{t^2}{4} && \text{for standard isotropic plates} \\ M_p &= \sigma_Y t_f \left(t_f + t_c\right) && \text{for sandwich panels} \end{aligned} \tag{2.4}$$

Since simply supported panels only have the internal yield lines shown in Figure 2.1, the expression for internal work simplifies to

$$W_{int} = 8\sigma_Y t_f \left(t_f + t_c\right) \delta + \sigma_Y t_f \left(t_f + t_c\right) \delta \left(4\frac{a}{b} - 4\right) = 4\sigma_Y t_f \left(t_f + t_c\right) \delta \left(\frac{a}{b} + 1\right) \tag{2.5}$$

Ultimate limit state becomes

$$W_{ext} = W_{int} \Longrightarrow p_{YL} = \frac{8 M_p k_a}{b^2} \tag{2.6}$$

with the same k_a defined for the clamped panel. As can be seen above, the yield line pressure on clamped panels is exactly twice the yield line pressure of similar simply supported panels.

Another similar derivation is made by Wood in 1961 for the same roof-shaped failure mechanism. The only difference from this derivation is that Wood allows the angle between the shortest edge and the diagonal yield lines, α, to vary. In the end the angle that gives the lowest lateral pressure is calculated. Since the yield line method is an upper bound solution, this method will be a slightly better approximation than the one where 45° angles are assumed. For square plates, however, the 45° angle is the most critical angle.

External virtual energy for a panel where the angle between the shortest edge and the diagonal yield line can vary, is given as

$$W_{ext} = \frac{1}{2} b^2 \delta p_{YL} \left(\frac{a}{b} - \frac{1}{3}\tan\alpha\right) \tag{2.7}$$

where α is the angle, and the rest of the parameters are the same as earlier in this section.

For the simply supported panel described in Jones [2], the internal virtual work is given as

$$W_{int} = 4M_p\delta\left(\frac{a}{b} + \frac{\cos\alpha}{\sin\alpha}\right) \tag{2.8}$$

For the clamped panel, yield lines along the perimeter must be included. This gives the internal virtual work

$$W_{int} = 8M_p\delta\left(\frac{a}{b} + \frac{\cos\alpha}{\sin\alpha}\right) \tag{2.9}$$

which again is twice as much as for the simply supported panel. Equating the external and internal virtual work gives the following expression for the lateral pressure on a clamped panel

$$p_{YL} = \frac{24M_p}{b^2\left(\frac{3}{\beta} - \frac{\sin\alpha}{\cos\alpha}\right)}\left[\frac{1}{\beta} + \frac{\cos\alpha}{\sin\alpha}\right] \tag{2.10}$$

where $\beta = b/a$.

To find the angle that gives the lowest lateral pressure, the stationary value, $\frac{\partial p_{YL}}{\partial(\tan\alpha)} = 0$, need to be found. This gives

$$\frac{-\frac{\beta}{\sin^2\alpha}\left(3 - \beta\tan\alpha\right) - \left(1 + \frac{\beta}{\tan\alpha}\right)\left(-\frac{\beta}{\cos^2\alpha}\right)}{3 - \beta\tan\alpha} = 0 \Longrightarrow \tan^2\alpha = \frac{3 - \beta\tan\alpha}{1 + \frac{\beta}{\tan\alpha}} \tag{2.11}$$

$$\Longrightarrow \tan\alpha = -\beta \pm \sqrt{\beta^2 + 3} \tag{2.12}$$

Since $0 < \alpha < \pi/2$,

$$\tan\alpha = -\beta + \sqrt{\beta^2 + 3} \tag{2.13}$$

Equation 2.13 inserted in equation 2.10 gives

$$p_{YL} = \frac{16M_pk_a}{b^2} \tag{2.14}$$

for clamped panels, and

$$p_{YL} = \frac{8M_pk_a}{b^2} \tag{2.15}$$

for simply supported panels, with $k_a = \frac{3}{\left(\sqrt{3+(b/a)^2} - b/a\right)^2}$ for both boundary conditions.

2.1.2 Lower Bound (Jones)

Since upper bound solutions always are non-conservative, it is useful to also study lower bound solutions to get an indication of how close the actual solution is. If the span between upper and lower bound is small, it can be concluded that the theoretical and actual values are close. A lower bound solution for clamped panels is derived by Jones [9].

The principle behind the lower bound theory is to find a stress field for the panel that satisfies the equilibrium equation found by studying force and moment equilibrium of an infinitesimal piece of a plate. This theory lies under the assumption of small deformations which is important to keep in mind when evaluating the results of analyses later.

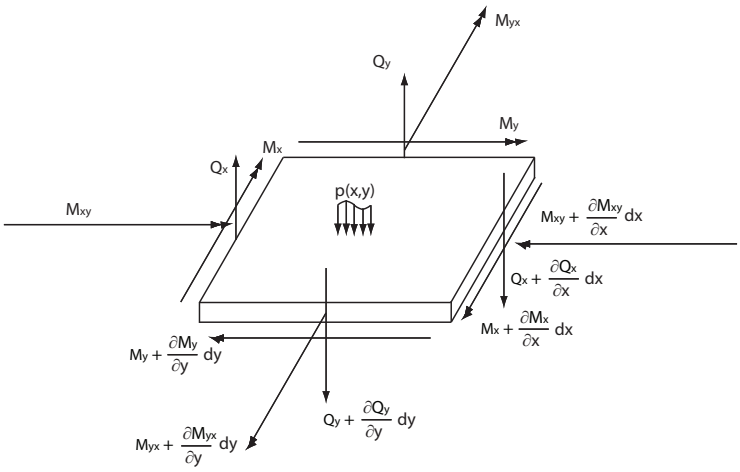

Figure 2.2: Infinitesimal piece of a plate. The x-axis lies horizontal on the figure, the y-axis is the other in-plane axis, and the z-axis is the out of plane axis

In Figure 2.2, the forces and moments that act on an infinitesimal element, with dimensions dx and dy in x- and y-directions respectively, are plotted. The only load applied is the lateral pressure, which for this derivation can be considered as a constant for the whole panel. It can also be noted that $M_{xy} = M_{yx}$ since $\tau_{xy} = \tau_{yx}$ is given by moment equilibrium with respect to the z-axis.

There are three equilibrium equations the panel above can satisfy. Vertical force equilibrium, moment equilibrium in x-direction and moment equilibrium in y-direction. These three equations become

$$\frac{\partial Q_x}{\partial x} + \frac{\partial Q_y}{\partial y} + p = 0 \tag{2.16}$$

$$\frac{\partial M_x}{\partial x} + \frac{\partial M_{xy}}{\partial y} - Q_x = 0 \tag{2.17}$$

$$\frac{\partial M_y}{\partial y} + \frac{\partial M_{xy}}{\partial x} - Q_y = 0 \tag{2.18}$$

Equation 2.17 and 2.18 can be rewritten with respect to Q_x and Q_y and substituted into Equation 2.16. This gives the differential equation for a panel subjected to lateral pressure only.

$$\frac{\partial^2 M_x}{\partial x^2} + 2\frac{\partial^2 M_{xy}}{\partial x \partial y} + \frac{\partial^2 M_y}{\partial y^2} + p = 0 \tag{2.19}$$

The expressions for moments over the panel are found through series expansion. If one origin is assumed to be in the centre of the panel, it can directly be concluded that odd terms in the expansion (i.e. x, x^3, ...) cannot be present. This comes from symmetry requirements. The moment at $x = a/2$ is equal to the moment at $x = -a/2$. For the simply supported panel the natural boundary conditions are [2]

$$M_x = 0 \qquad \text{for } x = \pm a/2 \tag{2.20}$$
$$M_y = 0 \qquad \text{for } y = \pm b/2 \tag{2.21}$$
$$M_x = M_p \qquad \text{for } x = 0 \tag{2.22}$$
$$M_y = M_p \qquad \text{for } y = 0 \tag{2.23}$$
$$M_{xy} = \pm M_p \qquad \text{in the corners} \tag{2.24}$$

The following series expansions for the moments are proposed

$$M_x = c_1 + c_2 x^2 \tag{2.25}$$
$$M_y = d_1 + d_2 y^2 \tag{2.26}$$
$$M_{xy} = e_1 xy \tag{2.27}$$

Higher order terms are not included since it would be difficult to solve the partial differential equation (Equation 2.19) with these higher terms. Applying the boundary conditions (Equations 2.20 - 2.24) gives the following expressions

$$M_x = M_p \left(1 - 4x^2/a^2\right) \tag{2.28}$$
$$M_y = M_p \left(1 - 4y^2/b^2\right) \tag{2.29}$$
$$M_{xy} = -4M_p xy/ab \tag{2.30}$$

These expressions are then substituted into Equation 2.19 and solved with respect to the pressure p.

$$p = \frac{8M_p}{b^2}\left[1 + b/a + (b/a)^2\right] = \frac{8M_p k_a}{b^2} \tag{2.31}$$

where $k_a = \left[1 + b/a + (b/a)^2\right]$.

The clamped panel has another set of natural boundary conditions

$$M_x = -M_p \qquad \text{for } x = \pm a/2 \tag{2.32}$$
$$M_y = -M_p \qquad \text{for } y = \pm b/2 \tag{2.33}$$
$$M_x = M_p \qquad \text{for } x = 0 \tag{2.34}$$
$$M_y = M_p \qquad \text{for } y = 0 \tag{2.35}$$

Jones [9] neglects M_{xy} for this boundary condition. This results in a value higher than the true lower bound solution. The main difference between the boundary conditions on clamped panels and simply supported panels is that clamped panels develop plastic

moment on the panel edges too. If the same series expansion as for the simply supported panels are used, Equations 2.25-2.26 and the clamped boundary conditions are applied, the following expressions are obtained.

$$M_x = M_p\left(1 - 8x^2/a^2\right) \tag{2.36}$$

$$M_y = M_p\left(1 - 8y^2/b^2\right) \tag{2.37}$$

Inserted in Equation 2.19 and solved with respect to the pressure p gives

$$p = \frac{16M_p}{b^2}\left[1 + (b/a)^2\right] = \frac{16M_p k_a}{b^2} \tag{2.38}$$

where $k_a = \left[1 + (b/a)^2\right]$.

2.1.3 DNV Classification Rules

The DNV Classification Rules [3] consider the panel subjected to a lateral pressure as an elastic bending problem. This is quite conservative since the bending stresses are reduced due to the membrane effect after the panel reaches the elastic limit. According to Mürer [10] this is compensated in the rules by allowing bending stress above the yield stress. The panel will still have a large reserve until we have a fully plastic membrane, but this capacity is only interesting for special cases.

The thickness requirement for plates subjected to a lateral pressure is given in the DNV Rules as

$$t = \frac{Ck'_a s\sqrt{p}}{\sqrt{\sigma}} + t_k \text{ mm} \tag{2.39}$$

where

C = is a boundary dependent factor, which normally has a value of 15.8 with equally spaced stiffeners. The value may change depending on the local structure.

k'_a = a correction factor for the aspect ratio of a plate field
= $(1.1 - 0.25s/l)^2$
= max 1.0 for $s/l \leq 0.4$
= min 0.72 for $s/l \geq 1.0$

s = stiffener spacing in m

l = stiffener span in m

p = design lateral pressure in kN/m^2

σ = nominal allowable bending stress in N/mm^2

t_k = additional thickness to account for corrosion

An approximation to find this formula, will be to use the elasto-plastic theory on an infinitely long plate between two stiffeners.

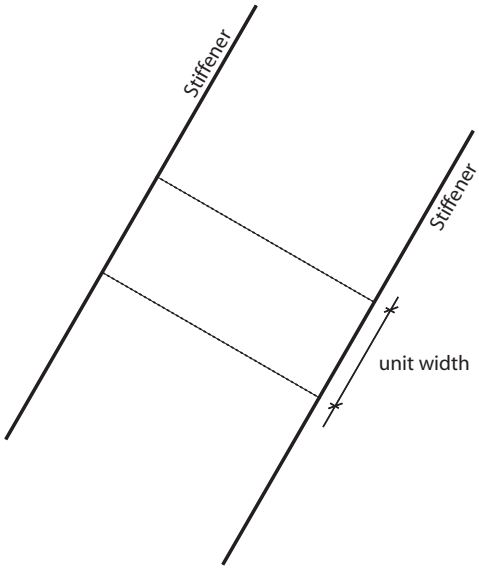

Figure 2.3: Infinitely long plate between two stiffeners

Figure 2.3 shows a unit width transverse plate strip between two stiffeners. This strip is considered to be a beam, clamped on both edges. A local coordinate system is defined with the x-axis along the unit width strip, and the y-axis parallel to the stiffeners. From kinematic compatibility and the assumption of infinitely long plate in y-direction, $\varepsilon_y = 0$. From normal plate assumptions, out-of-plane stresses are also neglected, $\sigma_z = 0$. This simplifies Hook's law

$$\varepsilon_x E = \sigma_x - \nu\sigma_y \tag{2.40}$$

$$0 = \sigma_y - \nu\sigma_x \Longrightarrow \sigma_y = \nu\sigma_x \tag{2.41}$$

The von-Mises yield criterion for principal stresses under the assumption of plane stress says

$$(\sigma_x)_Y^2 + (\sigma_y)_Y^2 - (\sigma_x)_Y (\sigma_y)_Y = \sigma_Y^2 \tag{2.42}$$

Inserting Equation 2.41 into 2.42 give

$$(\sigma_x)_Y = \frac{\sigma_Y}{\sqrt{1 - \nu + \nu^2}} \tag{2.43}$$

The plastic bending moment, M_p, along this plate strip beam is, for a homogenous isotropic cross section, given as

$$M_p = (\sigma_x)_Y \frac{t^2}{4} \tag{2.44}$$

The plastic moment occurs first on the two boundaries.

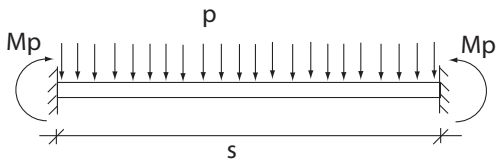

Figure 2.4: Clamped beam subjected to pressure load

The relation between the pressure and the plastic moment illustrated in Figure 2.4 can be found with classic beam theory to be

$$p = \frac{12M_p}{s^2} \tag{2.45}$$

where s is the distance between the stiffeners, or the length of the plate strip beam. If the equation is solved with respect to the thickness, t, and the same units as in the formula in the class rules are used, the following expression with the elasto-plastic theory is obtained

$$t = 17.2s\sqrt{\frac{p}{\sigma_Y}} \tag{2.46}$$

The formula in the rules is using an allowable stress instead of yield stress. In order to compare the rules to the elasto-plastic theory, allowable stress must be converted to yield stress. This gives the following expression

$$t = 19.15s\sqrt{\frac{p}{\sigma_Y}} \tag{2.47}$$

The difference between the two formulas are 11%. Mürer [10] also says that this elasto-plastic theory seems to be sufficient for normal ship plates in the plate range $s/l < 80$.

To compare the class rule with the other theories described in the previous Sections, 2.1.1 and 2.1.2, the units must be changed and the expression rewritten. This give

$$p = \frac{16M_p}{k_a'^2 s^2} = \frac{16M_p}{s^2}k_a \tag{2.48}$$

where $k_a = 1/k_a'^2$. s will be the same parameter as b for the other theories.

2.1.4 Comparison

All formulas derived in Sections 2.1.1 to 2.1.3 are written on the form

$$p = C\frac{M_p}{b^2}k_a \tag{2.49}$$

where $C = 8$ for simply supported panels, $C = 16$ for clamped panels and k_a varies with the different methods and panel aspect ratios. This form makes it easy to compare the

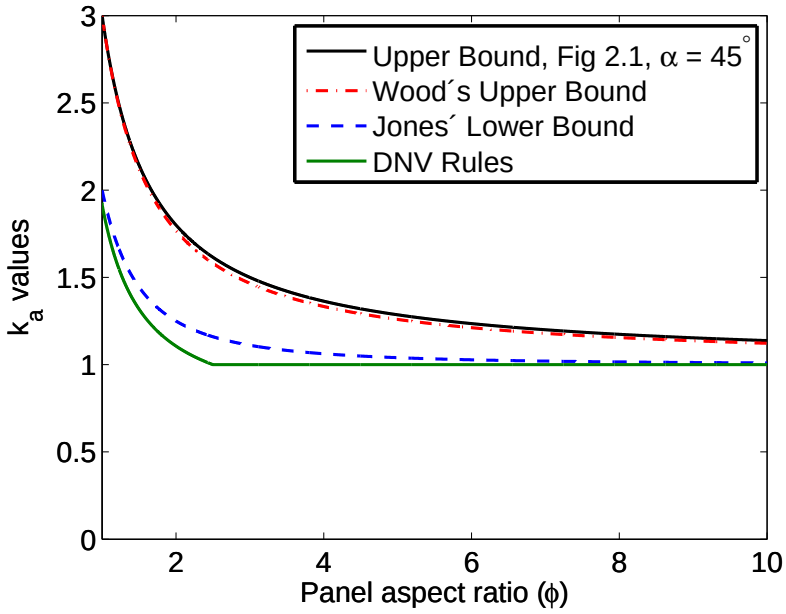

Figure 2.5: k_a values for clamped panels with various panel aspect ratios, ϕ

different methods, simply by comparing the k_a values for different aspect ratios.

Figure 2.5 shows k_a-values for clamped panels. First thing to notice is the marginal difference between the two yield line theories. This means that letting the angle shown in Figure 2.1 vary, does not influence the results greatly.

The difference between the upper bound solutions and lower bound solutions is largest for square panels. The upper bound is 50% higher than the lower bound, but as the panel aspect ratio increases to infinity the two different bounds approach the same value. In this work, only the aspect ratios between 1 and 2 are studied, so the variation between the different k_a-values are for these cases large.

DNV class rules are conservative for all aspect ratios, but when the aspect ratio moves towards infinity, all the values are the same. For square panels the DNV rules and the Jones lower bound solution are almost identical, but for an aspect ratio between 2 and 3, the difference between these two solutions is around 16%.

For SPS panels the plastic moment is given as $M_p = \sigma_Y t_f (t_f + t_c)$. It has been suggested as another approach to consider the two face sheets in the sandwich as equivalent to a steel plate with $M_p = 2\sigma_Y \frac{t_f^2}{4}$. This means that the two face sheets develop a roof-shaped mechanism separately. Following this approach leads to a far too conservative capacity. The support gained from the core cannot be neglected.

2.1.5 Core Shear Strength

When applying lateral loads on a sandwich panel, core shear stress also needs some attention. There are two modes of failure that can occur. The first one is core shear failure in the middle of the cross section, and the second one is debonding between the core and the faces.

A quick way of estimating the shear stress in the core is to find the total transverse force on the panel, divide the force on the length of the perimeter and the distance between the midplanes of the steel faces.

$$\tau_c = \frac{pab}{(2a + 2b)(t_f + t_c)} \tag{2.50}$$

This expression gives a constant average transverse shear stress over the whole perimeter. It is however known that the transverse shear stress is higher in the middle of the long edges, so Equation 2.50 can only indicate whether the core shear stress is a critical phenomenon or not.

The material data for the core, which is described in Chapter 3, indicates that the tensile ultimate strength is around 39 MPa. This means that ultimate shear strength in the core will be roughly around 20 MPa depending on which yield criterion is used, Tresca or Mises. Bond strength between the faces and the core is highly dependent on the surface preparation of the face material, so bond strength might be lower than the core shear strength.

Intelligent Engineering (IE), Daewoo Shipbuilding and Marine Engineering (DSME) and Lloyd's Register (LR) have suggested a design rule for bond strength in a conference paper [11]. This rule is given as

$$t_n + d_c \geq \frac{\beta\gamma q b}{\tau_{limit}} \tag{2.51}$$

where t_n is the faceplate net thickness, d_c is the thickness of the core, τ_{limit} is the bond shear stress capacity given as 6.0 MPa for watertight and deep tank bulkhead, b is the width of the panel, β and γ are factors that vary with the panel aspect ratio and q is the design pressure included a safety factor of 1.5.

The analyses indicate that core shear stresses of 6 MPa and higher occur in some of the thicker panels, so bonding strength requires further study including extensive testing and data analysis that is ongoing.

2.2 In-Plane Shear Load on SPS Panels

2.2.1 Shear Yield

There are two different failure mechanisms studied in this work related to the ultimate capacity for in-plane shear load. The first is when the panel yields over the entire cross

section due to high shear stress and yield lines occur with 45° to the panel edges. A theory that describes this failure mechanism will be presented in this section.

Next theory studied in this work will be shear buckling followed by yield over the cross section again followed by failure. Shear buckling will be studied closer in the next section.

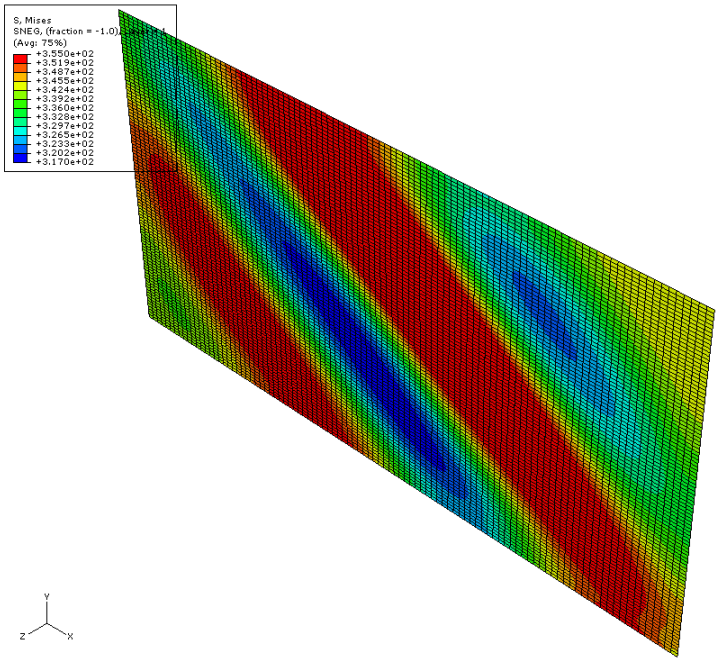

Figure 2.6: Failure on a SPS panel due to shear yield over the cross section. Von Mises stress is given in MPa

As can be seen in Figure 2.6, a 45° yield line is stretching from one of the long edges to the other. After the panel reaches this point, it cannot carry any higher shear load. A formula to predict this load has been based on the von-Mises yield criterion for pure shear. Von-Mises criterion for pure shear is given as

$$\tau_Y = \frac{\sigma_Y}{\sqrt{3}} \tag{2.52}$$

where τ_Y is the shear stress when yield occurs and σ_Y is the tensile yield stress for the panel. As the criterion shows, the shear yield stress is lower than the tensile yield stress.

For SPS and sandwiches in general, there are at least two different materials present, and these materials have different yield stresses. This effect must be included in the final expression. The ultimate load the panel can carry per unit length is the sum of the ultimate load per unit length for the face sheets, and the ultimate load per unit length for the

core.

$$Q_{ult} = 2\tau_{Yf}t_f + \tau_{Yc}t_c = \frac{\sigma_{Yf}}{\sqrt{3}}2t_f + \frac{\sigma_{Yc}}{\sqrt{3}}t_c = \frac{1}{\sqrt{3}}\left(2\sigma_{Yf}t_f + \sigma_{Yc}t_c\right) \tag{2.53}$$

where Q_{ult} is the ultimate load per unit length, t_f is the thickness of the faces, σ_{Yf} is the yield stress in the faces, t_c is the thickness of the core and σ_{Yc} is the yield stress in the core. Since the yield stress in the faces is much greater than the yield stress in the core, the contribution gained from the core can be neglected in a simplified expression for ultimate capacity

$$Q_{ult} = 2\tau_{Yf}t_f = 2\frac{\sigma_{Yf}t_f}{\sqrt{3}} \tag{2.54}$$

2.2.2 Shear Buckling

Figure 2.7 shows the second failure mechanism studied

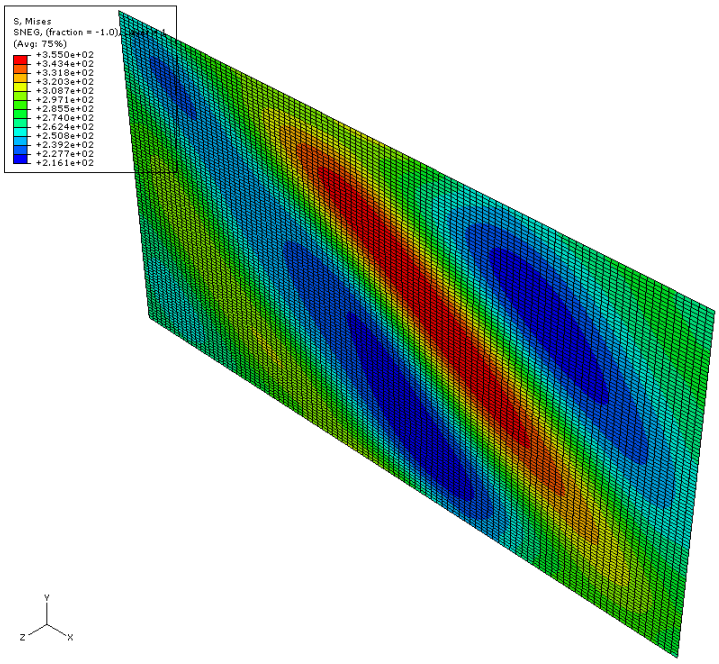

Figure 2.7: Failure on a SPS panel due to shear buckling. Von Mises stress is given in MPa

As can be seen in Figure 2.7, yield is developed on one of the buckles and failure follows right after. How soon the yield develops after buckling occur, depend on the initial imperfection of the panel. In a later chapter, results from such analyses will be presented. It turns out that the elastic critical load is a good estimate of the ultimate capacity of the panel. Kuenzi, Ericksen and Zahn [12] presents a formula for the buckling load based on the principle of stationary potential energy.

The potential energy is divided in two parts; the strain energy and the potential energy from applied loads. When linear elastic isotropic material is assumed, the following expression for the strain energy is obtained

$$U_{strain} = \int_V \int_\varepsilon \{\boldsymbol{\sigma}\}^T \{d\boldsymbol{\varepsilon}\} dV = \int_V \frac{1}{2} \{\boldsymbol{\sigma}\}^T \{\boldsymbol{\varepsilon}\} \, dV = \int_V \frac{1}{2} \{\boldsymbol{\varepsilon}\}^T \{\mathbf{E}\} \{\boldsymbol{\varepsilon}\} \, dV \tag{2.55}$$

where $\{\boldsymbol{\varepsilon}\} = \left\{ \begin{array}{ccccc} \varepsilon_{xx} & \varepsilon_{yy} & \varepsilon_{xy} & \varepsilon_{yz} & \varepsilon_{zx} \end{array} \right\}^T$, ε_{**} are the strain components in the sandwich, and for panels where plain stress is assumed, $\sigma_z = 0$,

$$\{\mathbf{E}\} = \frac{E}{1-\nu^2} \begin{bmatrix} 1 & \nu & 0 & 0 & 0 \\ \nu & 1 & 0 & 0 & 0 \\ 0 & 0 & \frac{1-\nu}{2} & 0 & 0 \\ 0 & 0 & 0 & \frac{1-\nu}{2} & 0 \\ 0 & 0 & 0 & 0 & \frac{1-\nu}{2} \end{bmatrix} \tag{2.56}$$

where E is the Young's modulus and ν is the Poisson's ratio. This gives the strain energy expression

$$\begin{aligned} U_{strain} = \frac{1}{2(1-\nu^2)} \int_V & \left[E\varepsilon_{xx}^2 + E\varepsilon_{yy}^2 + 2\nu E \varepsilon_{xx}\varepsilon_{yy} + (1-\nu^2) G \varepsilon_{xy}^2 \right. \\ & \left. + (1-\nu^2) G \varepsilon_{yz}^2 + (1-\nu^2) G \varepsilon_{zx}^2 \right] dV \end{aligned} \tag{2.57}$$

where G is the shear modulus. The potential energy from the applied shear load can be expressed as

$$U_p = \int_A N_{xy} \left(\frac{\partial w}{\partial x} \right) \left(\frac{\partial w}{\partial y} \right) dA \tag{2.58}$$

where N_{xy} is applied shear load per unit length and w is out-of-plane displacement.

Kuenzi, Ericksen and Zahn, [12], starts their analysis by assuming the out-of-plane displacement. For a simply supported panel, this expression will be

$$w = \sum_{m=1}^{\infty} \sum_{n=1}^{\infty} C_{mn} \sin\left(\frac{m\pi x}{a} \right) \sin\left(\frac{n\pi y}{b} \right) \tag{2.59}$$

where x and y are the in-plane coordinates, and a and b are the length and width of the panel respectively. This assumption holds through the whole thickness of the sandwich. Kuenzi, Ericksen and Zahn [12] choose the $x-y$-plane to lie between one of the faces and the core. It is also assumed that the transverse shear stresses in the core are constant throughout the thickness. The in-plane displacements are also double infinite sums, with coefficients that need to be chosen such that the total potential energy becomes as low as possible. The following displacement components are suggested in Kuenzi et al. [12].

The core:

$$u_{c_{mn}} = (k_{mn}z + q_{mn}) \frac{\partial w_{mn}}{\partial x} \tag{2.60}$$

$$v_{c_{mn}} = (h_{mn}z + r_{mn}) \frac{\partial w_{mn}}{\partial y} \tag{2.61}$$

The faces:

$$u_{1_{mn}} = (q_{mn} - z) \frac{\partial w_{mn}}{\partial x} \tag{2.62}$$

$$v_{1_{mn}} = (r_{mn} - z) \frac{\partial w_{mn}}{\partial y} \tag{2.63}$$

$$u_{2_{mn}} = (k_{mn}t_c + q_{mn} - z + t_c) \frac{\partial w_{mn}}{\partial x} \tag{2.64}$$

$$v_{2_{mn}} = (h_{mn}t_c + r_{mn} - z + t_c) \frac{\partial w_{mn}}{\partial y} \tag{2.65}$$

where u and v are displacements in x- and y- direction respectively, and the subscript c, 1, 2 refers to the core and the two faces.

It is important, when assuming displacement functions, to ensure that kinematic compatibility is satisfied between the faces and the core, hence for $z = 0$ and $z = t_c$. To be able to use the strain energy expression shown in Equation 2.57, the strain components

from the displacement assumptions needs to be derived.

$$\varepsilon^{(1)}_{xx_{mn}} = \frac{\partial u_{1_{mn}}}{\partial x} = (q_{mn} - z)\frac{\partial^2 w_{mn}}{\partial x^2} \tag{2.66}$$

$$\varepsilon^{(1)}_{yy_{mn}} = \frac{\partial v_{1_{mn}}}{\partial x} = (r_{mn} - z)\frac{\partial^2 w_{mn}}{\partial y^2} \tag{2.67}$$

$$\varepsilon^{(1)}_{xy_{mn}} = \frac{\partial u_{1_{mn}}}{\partial y} + \frac{\partial v_{1_{mn}}}{\partial x} = (q_{mn} + r_{mn} - 2z)\frac{\partial^2 w_{mn}}{\partial x \partial y} \tag{2.68}$$

$$\varepsilon^{(2)}_{xx_{mn}} = \frac{\partial u_{2_{mn}}}{\partial x} = (k_{mn}t_c + q_{mn} - z + t_c)\frac{\partial^2 w_{mn}}{\partial x^2} \tag{2.69}$$

$$\varepsilon^{(2)}_{yy_{mn}} = \frac{\partial v_{2_{mn}}}{\partial x} = (h_{mn}t_c + r_{mn} - z + t_c)\frac{\partial^2 w_{mn}}{\partial y^2} \tag{2.70}$$

$$\varepsilon^{(2)}_{xy_{mn}} = \frac{\partial u_{2_{mn}}}{\partial y} + \frac{\partial v_{2_{mn}}}{\partial x} = (k_{mn}t_c + h_{mn}t_c + q_{mn} + r_{mn} - 2z + 2t_c)\frac{\partial^2 w_{mn}}{\partial x \partial y} \tag{2.71}$$

$$\varepsilon^{(c)}_{zx_{mn}} = \frac{\partial w_{mn}}{\partial x} + \frac{\partial u_{c_{mn}}}{\partial z} = (1 + k_{mn})\frac{\partial w_{mn}}{\partial x} \tag{2.72}$$

$$\varepsilon^{(c)}_{yz_{mn}} = \frac{\partial w_{mn}}{\partial y} + \frac{\partial v_{c_{mn}}}{\partial z} = (1 + h_{mn})\frac{\partial w_{mn}}{\partial y} \tag{2.73}$$

Inserted in the equation for strain energy, the following components of energy are given

$$U_{1_{mn}} = C^2_{mn}\frac{abE_f}{8\left(1-\nu_f^2\right)}\left[\begin{array}{l}\left(\frac{m\pi}{a}\right)^4\left[\left(q_{mn}+\frac{1}{2}t_f\right)^2 t_f + \frac{1}{12}t_f^3\right] + \left(\frac{n\pi}{b}\right)^4\left[\left(r_{mn}+\frac{1}{2}t_f\right)^2 t_f + \frac{1}{12}t_f^3\right] \\ + 2\nu_f\left(\frac{m\pi}{a}\right)^2\left(\frac{n\pi}{b}\right)^2\left[\left(q_{mn}+\frac{1}{2}t_f\right)\left(r_{mn}+\frac{1}{2}t_f\right)t_f + \frac{1}{6}t_f^3\right] \\ + \frac{1}{2}\left(1-\nu_f\right)\left(\frac{m\pi}{a}\right)^2\left(\frac{n\pi}{b}\right)^2\left[\left(q_{mn}+r_{mn}+t_f\right)^2 t_f + \frac{2}{3}t_f^3\right]\end{array}\right] \tag{2.74}$$

$$U_{2_{mn}} = \frac{C^2_{mn}abE_f}{8\left(1-\nu_f^2\right)}\left[\begin{array}{l}\left(\frac{m\pi}{a}\right)^4\left[\left(k_{mn}t_c+q_{mn}-\frac{1}{2}t_f\right)^2 t_f + \frac{1}{12}t_f^3\right] \\ + \left(\frac{n\pi}{b}\right)^4\left[\left(h_{mn}t_c+r_{mn}-\frac{1}{2}t_f\right)^2 t_f + \frac{1}{12}t_f^3\right] \\ + 2\nu_f\left(\frac{m\pi}{a}\right)^2\left(\frac{n\pi}{b}\right)^2\left[\left(k_{mn}t_c+q_{mn}-\frac{1}{2}t_f\right)\left(h_{mn}t_c+r_{mn}-\frac{1}{2}t_f\right)t_f + \frac{1}{6}t_f^3\right] \\ + \frac{1}{2}\left(1-\nu_f\right)\left(\frac{m\pi}{a}\right)\left(\frac{n\pi}{b}\right)^2\left[\left(k_{mn}t_c+h_{mn}t_c+q_{mn}+r_{mn}-t_f\right)^2 t_f + \frac{2}{3}t_f^3\right]\end{array}\right] \tag{2.75}$$

$$U_{c_{mn}} = C_{mn}^2 \frac{ab}{8}\left[G_c t_c\left(\left(\frac{m\pi}{a}\right)^2(1+k_{mn})^2+\left(\frac{n\pi}{b}\right)^2(1+h_{mn})^2\right)\right] \tag{2.76}$$

$$U_{strain} = \sum_{m=1}^{\infty}\sum_{n=1}^{\infty}\left(U_{1_{mn}}+U_{2_{mn}}+U_{c_{mn}}\right) = \frac{ab}{8}\sum_{m=1}^{\infty}\sum_{n=1}^{\infty}\left(C_{mn}^2 T_{mn}\right) \tag{2.77}$$

Since an out-of-plane deflection on the panel is assumed, the potential energy from the applied shear load can also be found

$$U_p = N_x y \sum_{m=1}^{\infty}\sum_{n=1}^{\infty}\sum_{p=1}^{\infty}\sum_{q=1}^{\infty}\int_0^a\int_0^b C_{mn}\left(\frac{m\pi}{a}\right)\cos\left(\frac{m\pi x}{a}\right)\sin\left(\frac{n\pi y}{b}\right)C_{pq}\left(\frac{q\pi}{b}\right)\sin\left(\frac{p\pi x}{a}\right)\cos\left(\frac{q\pi y}{b}\right)dydx$$

$$= \begin{cases} -N_{xy}\displaystyle\sum_{m=1}^{\infty}\sum_{n=1}^{\infty}\sum_{p=1}^{\infty}\sum_{q=1}^{\infty}\int_0^a C_{mn}C_{pq}\left(\frac{m\pi}{a}\right)\left(\frac{q\pi}{b}\right)\cos\left(\frac{m\pi x}{a}\right)\sin\left(\frac{p\pi x}{a}\right)\frac{2nb}{\pi\left(q^2-n^2\right)} & \text{if } n+q \text{ is odd} \\ 0 & \text{if } n+q \text{ is even} \end{cases}$$

$$= \begin{cases} -N_{xy}\displaystyle\sum_{m=1}^{\infty}\sum_{n=1}^{\infty}\sum_{p=1}^{\infty}\sum_{q=1}^{\infty}C_{mn}C_{pq}\left(\frac{m\pi}{a}\right)\left(\frac{q\pi}{b}\right)\frac{4abnp}{\pi^2\left(m^2-p^2\right)\left(q^2-n^2\right)} & \text{if } n+q \text{ and } m+p \text{ is odd} \\ 0 & \text{if } n+q \text{ or } m+p \text{ is even} \end{cases} \tag{2.78}$$

As can be seen above, both $n+q$ and $m+p$ needs to be odd in order to have a nonzero contribution from the potential energy from the load.

The total energy on the panel can then be written as

$$U_{tot} = U_{strain} - U_p = \frac{ab}{8}\sum_{m=1}^{\infty}\sum_{n=1}^{\infty}\left(C_{mn}^2 T_{mn}\right) + 4N_{xy}\sum_{m=1}^{\infty}\sum_{n=1}^{\infty}\sum_{p=1}^{\infty}\sum_{q=1}^{\infty}C_{mn}C_{pq}\frac{mnpq}{\left(m^2-p^2\right)\left(n^2-q^2\right)} \tag{2.79}$$

Next step in the analysis will be to find the stationary value. In other words, the five following sets of conditions must be satisfied

$$\frac{\partial U_{tot}}{\partial C_{mn}} = 0 \qquad \frac{\partial T_{mn}}{\partial q_{mn}} = 0 \qquad \frac{\partial T_{mn}}{\partial r_{mn}} = 0 \qquad \frac{\partial T_{mn}}{\partial k_{mn}} = 0 \qquad \frac{\partial T_{mn}}{\partial h_{mn}} = 0 \tag{2.80}$$

The four last conditions in Equation 2.80 give the following relations

$$\begin{aligned} q_{mn} &= -\frac{1}{2}k_{mn}t_c \\ r_{mn} &= -\frac{1}{2}h_{mn}t_c \\ k_{mn} &= \frac{1}{t_c}\frac{t_f\left[\left(\frac{m\pi}{a}\right)^2+\left(\frac{n\pi}{b}\right)^2\right]-\frac{2G_c\left(1-\nu_f^2\right)}{E_f t_f}}{\frac{S}{D}+\left[\left(\frac{m\pi}{a}\right)^2+\left(\frac{n\pi}{b}\right)^2\right]} \\ h_{mn} &= k_{mn} \end{aligned} \tag{2.81}$$

where $S=\frac{G_c d^2}{t_c}$, $D=\frac{E_f t_f d^2}{2\left(1-\nu_f^2\right)}$(thin-face and compliant core approximation), and $d=t_f+t_c$. When the four parameters above is inserted into the expression for total potential energy, the first of the five conditions above yields

$$\begin{aligned} &\frac{b}{8a^3}D\pi^4 C_{mn}\left(\frac{\left[m^2+\phi^2n^2\right]^2}{1+\pi^2\frac{D}{Sb^2}\left[\frac{m^2}{\phi^2}+n^2\right]}+\frac{E_f t_f^3}{6D\left(1-\nu_f^2\right)}\left[m^2+\phi^2n^2\right]^2\right) \\ &\qquad +4N_{xy}\sum_{p=1}^{\infty}\sum_{q=1}^{\infty}C_{pq}\frac{mnpq}{\left(m^2-p^2\right)\left(n^2-q^2\right)}=0 \qquad \text{where } m,n\in\mathbb{N} \end{aligned} \tag{2.82}$$

where $\phi=\frac{a}{b}$ is the length over width ratio. N_{xy} can be written as $N_{xy}=D\frac{\pi^2}{b^2}K$ where K is the buckling coefficient.

$$\begin{aligned} &\frac{\pi^2 C_{mn}}{32\phi^3 K}\left(\frac{\left[m^2+\phi^2n^2\right]^2}{1+\pi^2\frac{D}{Sb^2}\left[\frac{m^2}{\phi^2}+n^2\right]}+\frac{E_f t_f^3}{6D\left(1-\nu_f^2\right)}\left[m^2+\phi^2n^2\right]^2\right) \\ &\qquad +\sum_{p=1}^{\infty}\sum_{q=1}^{\infty}C_{pq}\frac{mnpq}{\left(m^2-p^2\right)\left(n^2-q^2\right)}=0 \qquad \text{where } m,n\in\mathbb{N} \end{aligned} \tag{2.83}$$

To find the non-trivial solution of this matrix, the determinant must be equal to zero. Stein and Neff [13] showed that for shear buckling in standard plates the determinant could be split in two smaller determinants. One determinant represents the symmetrical buckling and one represents the anti-symmetrical buckling. The reason why this is possible comes from the criteria that $n+q$ and $m+p$ are both odd. When all these parameters are summed, $m+n+p+q$, this number must be even. This means that if $m+n$ is even, $p+q$ needs to be even as well, and if $m+n$ is odd, $p+q$ needs to be odd. The combinations of m and n that gives even numbers are representing the symmetrical buckling, and the combinations that gives odd numbers are representing the anti-symmetrical buckling. These determinants are implemented in a MATLAB code which is attached in Appendix A. Clamped panels need another assumed displacement field and a similar derivation as shown for the simply supported boundary conditions.

Kuenzi, Ericksen and Zahn [12] also made formulas for solving these shear buckling problems with both clamped and simply supported boundaries. These are handy, since they are easy to use, and the critical load can be found fast. For a clamped panel the approximate formula for the buckling coefficient yields

$$K = \frac{K_{0Clamped}}{1 + \pi^2 \frac{D}{Sb^2}\left(K_{0Clamped} - \frac{4}{3}\left[1 + \frac{b^2}{a^2}\right]\right)} \quad \text{for } 0 \leq \pi^2 \frac{D}{Sb^2} \leq \frac{3}{4}\left(1 + \frac{b^2}{a^2}\right)^{-1} \tag{2.84}$$

where $K_{0Clamped} = 9 + \frac{17}{3}\frac{b^2}{a^2}$ is the buckling coefficient for an ordinary isotropic homogenous plate. For the simply supported panel the following formula is given

$$K = \frac{K_{0SS}}{1 + \pi^2 \frac{D}{Sb^2}\left(K_{0SS} - 1 - \frac{b^2}{a^2}\right)} \quad \text{for } 0 \leq \pi^2 \frac{D}{Sb^2} \leq \left(1 + \frac{b^2}{a^2}\right)^{-1} \tag{2.85}$$

where $K_{0SS} = \frac{16}{3} + 4\frac{b^2}{a^2}$ is the buckling coefficient for an ordinary isotropic homogenous plate. These formulas can also be found in Zenkert [14]. The criteria set after the buckling coefficient, comes from core shear instability. It is found that when the core is very weak, the buckling coefficient will only depend on the shear parameters $K = \frac{1}{\pi^2 \frac{D}{Sb^2}}$. This is not, however of practical importance, since the core would need to be really thick and soft in order to experience this instability behaviour. An ABAQUS analysis of an SPS3-15-3 3200x6400 mm^2 panel has been made to show the accuracy of the formulas described above.

In Figure 2.8 is the eigenmode given from the ABAQUS analysis. This panel gives an anti-symmetric eigenmode with two buckles. In Figure 2.9, the buckling coefficients for SPS3-15-3 panels with different aspect ratios are presented. The values on the vertical axis should be noted.

The 3200x6400 mm^2 panel corresponds to a panel aspect ratio of 2, which in the graph will be 0.5 with the axis currently used in Figure 2.9. The determinant solution with this panel aspect ratio, corresponds to an anti-symmetric eigenmode with two buckles. This agrees with Figure 2.8. Compared to the finite element analysis we can see that the determinant solution is slightly non-conservative by around 2.8%, and that the approximate design formula is slightly conservative by around 3.4%.

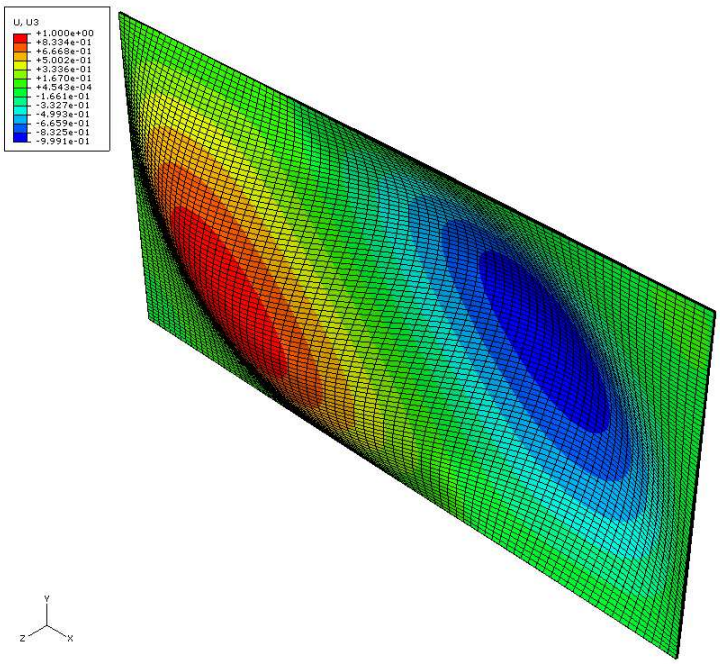

Figure 2.8: Eigenmode of an SPS3-15-3 3200x6400 mm^2 panel. Displacements are given in mm

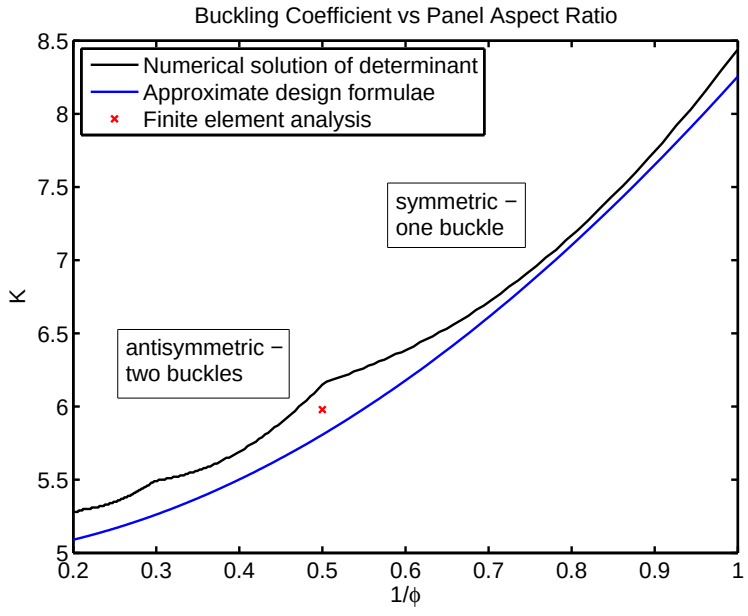

Figure 2.9: Shear buckling coefficient versus panel aspect ratio

Chapter 3

Finite Element Modelling

3.0 History and Background of the Finite Element Method

According to Cook [15] the origin of the finite element analysis as it is known today comes from a paper by Courant in 1943 where he determined the torsional rigidity of a hollow shaft by dividing the cross section into triangles and interpolated a stress function linearly over each triangle from the stresses at the nodes. The first practical applications came with the aeronautical industry in the beginning of the 1950s and finite element method proved to be an efficient tool for several applications. In 1963, the finite element method was recognised as a form of the Rayleigh-Ritz method and after that time, the use and research of the finite element method has escalated significantly.

In this chapter the modelling procedure for the SPS panels will be presented along with challenges experienced during the process and how these were dealt with. All finite element analyses performed in this study are done with the ABAQUS software from Simulia.

3.1 Panel Geometry

To get a broad understanding of sandwich panels' performance, it is in this study chosen a range of quite extreme geometries with regard to the following three ratios

- face to core thickness
- panel aspect ratio
- panel thickness to width (or length)

All panels studied can be found in Table 3.1

Table 3.1: Geometries studied in this work

Panel Aspect Ratio (a/b)	Panel Width (mm)	Face Thickness (mm)	Core Thickness (mm)
1.0	2000	3	35
	2000	10	15
	2000	10	35
1.5	1200	5	32
	2800	6	25
2.0	3200	3	15
	3200	3	35
	3200	7	35
	3200	10	15

SPS panel layups are commonly written on the form SPS3-35-3 after how the cross section is built. The first and last number describes the two face thicknesses and the middle number describes the core thickness. All numbers are given in mm. In table 3.1 it can be seen that there are panels with a thick core and very thin faces, and there are panels with thick faces and a thin core. There are also panels with thin core and thin faces and thick core and thick faces. For the completeness of the study some panels in the middle range with more standard cross sections are included as well. Panel aspect ratio is also, as can be seen in table 3.1, varied between 1.0 and 2.0.

3.2 Material Data

SPS is made out of two main ingredients; steel faces and a polyurethane core. The mechanical properties of these materials are given in Table 3.2 and Figures 3.1 and 3.2

Table 3.2: Material properties for the face and core in the SPS panel

Material	Modulus of Elasticity (MPa)	Poisson's Ratio	Yield Stress (MPa)
Steel	206 000	0.3	355
Polyurethane	750	0.36	0.75

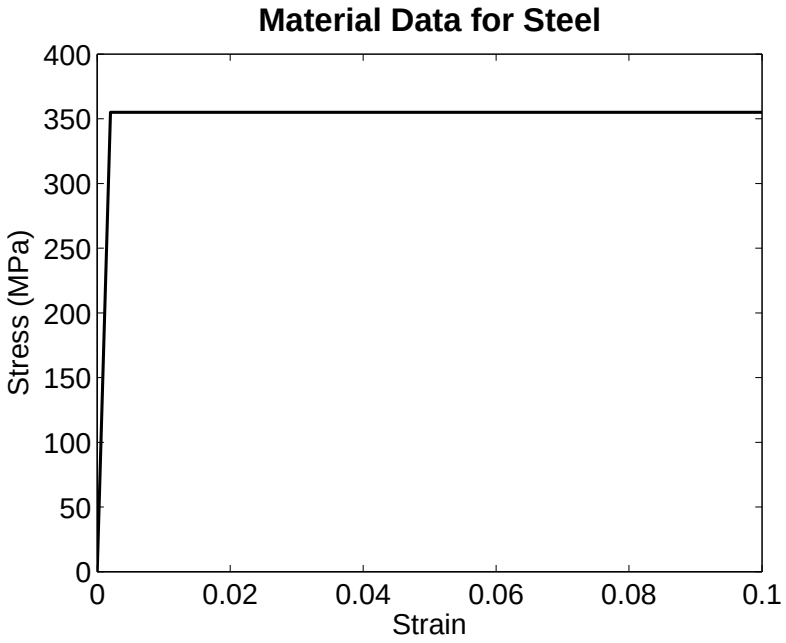

Figure 3.1: True stress-strain curve for the face material

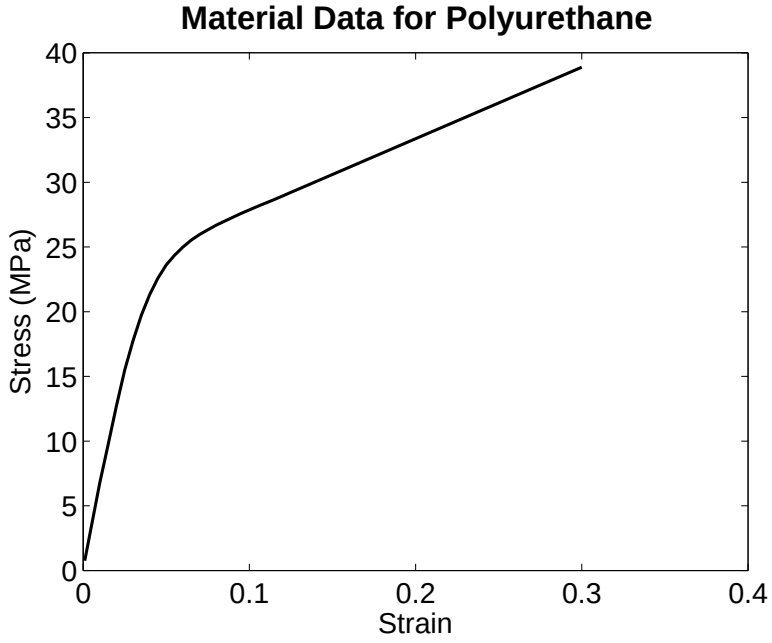

Figure 3.2: True stress-strain curve for the core material

As can be seen in Figures 3.1 and 3.2, non-linear material curves are used for both the steel and the polyurethane. Table 3.2 shows the difference in yield stress for the core material and the face material. The steel is so much stronger than the elastomer, so for in-plane loading, the contribution from the core becomes insignificant even though the core

is much thicker than the faces.

In a later chapter another steel type will be used. That is a normal strength structural steel with 235 MPa yield stress instead of the 355 MPa described above. It is assumed bi-linear steel for the normal strength steel as well.

3.3 Elements and Meshing

3.3.1 Elements

There are two different types of elements used in this study. The first element is the 8-noded brick element in ABAQUS called C3D8R where the C stands for continuum stress and displacement, 3D tells that this is a three dimensional element, 8 is the amount of nodes on the brick, and R means that reduced integration is included.

Second type of elements used in this study is the 4-noded doubly curved thick shell element in ABAQUS called S4R where the S stands for stress and displacement shell, 4 is the number of nodes and R stands for reduced integration. A small part of the study has been to decide what element type is most suited for modelling SPS panels for the various loadings and boundary conditions.

One of the main advantages with the solid elements over the shell elements is the ability to model very local bending effects such as local bending on the boundaries. This is especially important for welded structures where local stresses can lead to fatigue problems.

In Figure 3.3 it can be seen that the strain is high at the edge, and is quickly reduced towards the centre of the panel. A model with shell elements will not spot this sudden increase in strain towards the edge of the plate.

A problem with the C3D8R elements used in this study is that it only has one integration point in each element. This makes it vulnerable for hourglassing. There is a form of hourglass control for this type of elements, but as can be seen on Figure 3.4, this did not help for this case.

This particular case shown in Figure 3.4 was from a shear buckling analysis. As can be seen, the core has formed to a shape that is completely physically irrelevant. According to the ABAQUS Documentation [16] this occurs since the elements only have one integration point. This makes it possible for the elements to distort excessively with the strain in the integration points still equal to zero, and a mode that requires no energy emerges.

There are two solutions to this problem. First solution is to use full integration instead

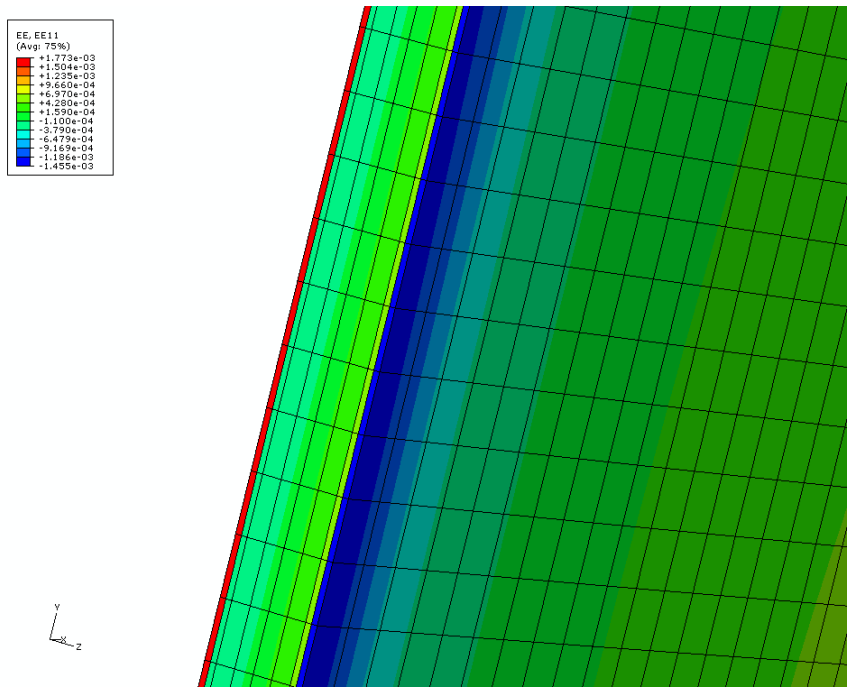

Figure 3.3: Solid elements can model local bending effects on the edges that the shell elements cannot. The contour plot in this figure is of elastic strain in the x-direction

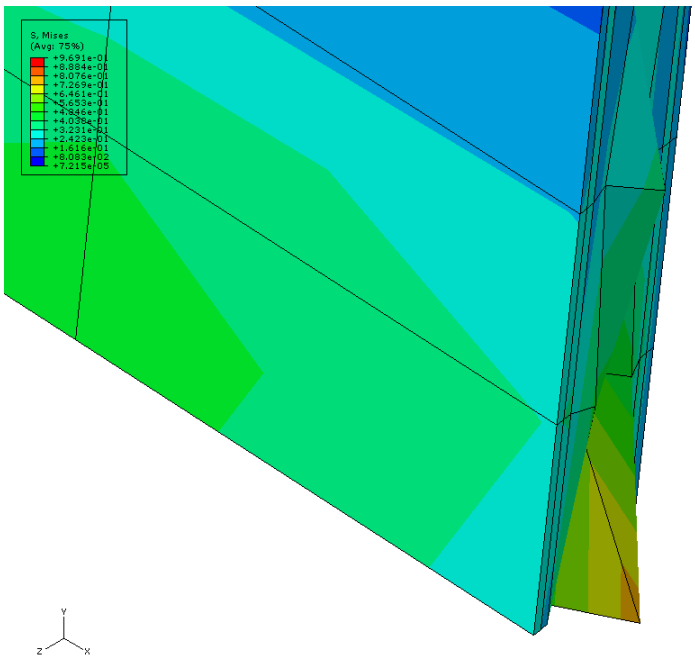

Figure 3.4: Hourglassing of the core in a solid model of SPS. Von Mises stress is given in MPa

of the reduced integration. When the full integration is used the correct eigenmode can be obtained, but the eigenvalue is far too high. In other words, the elements are too stiff. This can only be solved by either increasing the number of elements over the thickness, or using 20-noded brick elements instead of the 8-noded brick elements. With this change in elements, the same eigenvalues for the solid model and the thick shell model are found, which is promising for the thick shell model used in the analyses.

Second solution to the hourglassing problem is to use the second order element C3D20R. These elements have more than one integration point in each element such that the zero modes cease to exist.

Both these solutions results in a far higher amount of nodes in the analysis which requires much more computer resources. Based on the experienced gained from the points above, thick shell S4R elements has been used to run analyses on ultimate capacity in this study with an occasional check of the results with the solid C3D8R elements.

3.3.2 Meshing

For all cases studied, a mesh consisting of 10 000 thick shell elements have been used, 100 elements in each direction for all aspect ratios. Mesh refinement analysis is performed on the roughest mesh and shows convergence. The solid model has 75 elements along the long edges and 50 elements along the short edge on each layer. Through the thickness, there are two layers in each of the faces and four in the core. This gives a total of 30 000 solid elements.

3.4 Loading

3.4.1 Load Sequence for combined in-plane shear load and lateral pressure

Two loads are applied to the system. In-plane shear load and lateral pressure load. There are several ways these loads can be applied. Since non-linearity and plasticity is considered, it is necessary to consider the effect of path-dependent ultimate strength. For that reason two different loading sequences has been analysed. The first one was proportional increase of loads, meaning that the shear load and pressure load were increased at the same time in a fixed ratio until failure. The second type of loading is to first apply a certain amount of lateral pressure, before an increasing shear load is applied with the lateral pressure held constant.

Based on the results and the experienced gained from the testing of the two different load sequences, only the proportional increase of loads is used for the three-way interaction.

3.4.2 Load Steps

The main method used to find the load-displacement curve was the static riks method in ABAQUS, or more generally called the arc length method based on incremental equilibrium. The riks method is used for both of the load sequence; when the two loads are applied proportionally and when the shear load is increased alone up to failure. All analyses are made with non-linear geometry assumptions.

The second method is also based on incremental equilibrium, but does not use arc length to find the next increment. One problem with this method is that the panel behaviour need to be known to find the load-displacement curve. For instance if two buckling modes have close eigenvalues, an eventual snap back cannot be modelled unless load control is used, and if load control is used, it will not model a snap through or local peaks. For that a displacement control is needed. This method is used when applying the lateral pressure load alone first, as described in Section 3.4.1 above since the panel behaviour in this case is known.

It is important to note that for the first sequence, initial imperfection should be applied when the transverse lateral load is very low compared to the shear force. As soon as the lateral pressure load is considerable, the influence of the imperfection becomes negligible and can be excluded.

3.5 Boundary Conditions

3.5.1 Simply Supported

The most difficult part to implement in the model is the boundary conditions to avoid singularities and represent the real situation in the best possible way. In this work both clamped panels and simply supported panels with straight edges are considered. The first boundary condition described is the simply supported one.

Firstly the whole perimeter is fixed such that it cannot translate out-of-plane. One of the corners is restrained in both the in-plane directions, and another corner is restrained in one of the in-plane direction. This is to prevent rigid rotation of the whole panel. The last necessary boundary condition is the one that keeps the edges straight when loads are applied. By coupling the nodes along the boundary such that the third rotational degree of freedom is equal for all nodes along an edge, it seems that this requirement is fulfilled as well. The corner nodes need special attentions in this process since they belong to two edges. In this work, this is solved by excluding the corner nodes from the coupling on two of the parallel edges. Since only first order elements are used, this approach seems to work well.

3.5.2 Clamped

Clamped panels are similar to the simply supported panels, except that the two first rotational degrees of freedom are fixed along the entire perimeter as well.

Figure 3.5 shows a sketch of the boundary conditions and the applied stresses on the SPS panels studied in this work.

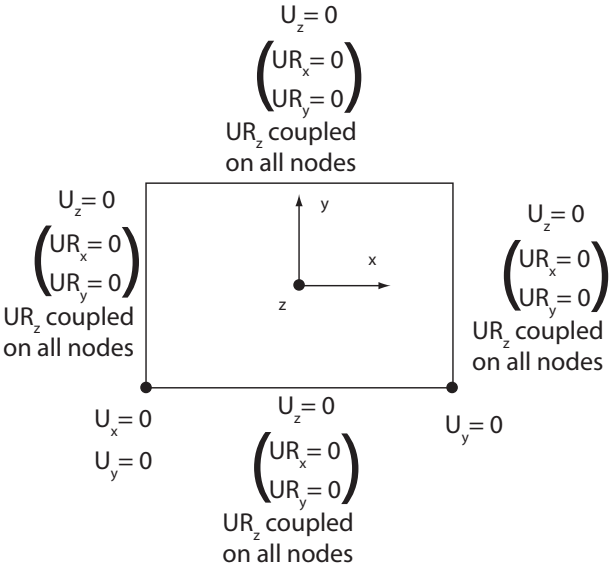

(a) Boundary conditions on the SPS panels. The conditions in the parenthesis are the extra constraints for the clamped version

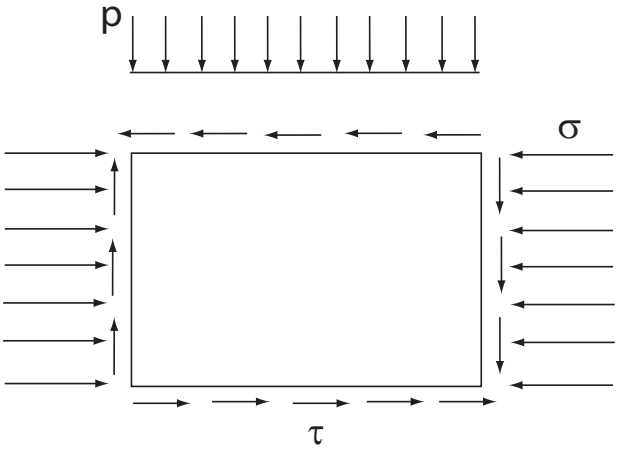

(b) Applied stresses on the panel. In-plane shear (τ), uni-axial compression (σ) and lateral pressure (p)

Figure 3.5: Boundary conditions and stresses on the SPS panels in the current study

Chapter 4

Pure Lateral Pressure Load

4.0 General

Finite element analyses have been performed to study the behaviour of SPS panels loaded with lateral pressure. Both the upper bound estimate from the yield line theory and the lower bound estimate from Jones [2] are included in the load-displacement curves from the element analyses.

4.1 SPS3-15-3 3200x6400 mm^2

In the first case a SPS3-15-3 panel is studied with dimension 3200x6400 mm^2. The load-displacement curve for this panel with clamped and simply supported boundaries can be found in Figures 4.1 and 4.2.

As can be seen in Figure 4.1 the deflection under the loads specified by both the upper bound theory and the lower bound theory are both within the range of acceptable deflections. The deflection under the pressure load estimated by Jones' lower bound is around 60 mm which is below 2% of the panel width. Yield line pressure load gives a deflection of 2.6% of the panel width. Von Mises stress at the point where the yield line theory predicts failure is plotted in Figure 4.3.

Figure 4.3 shows that yield is developed along the edges, but this alone is not enough to experience failure after the yield line theory.

Considering the shape of the load-displacement curve, there is nothing that indicates a change in panel properties between the upper bound solution and the lower bound solution. This can indicate that the deformation of the panel does not satisfy the assumption of small deformations in the theory, thus making the theory invalid.

Figure 4.4 shows the same panel with clamped boundaries. The only difference is that

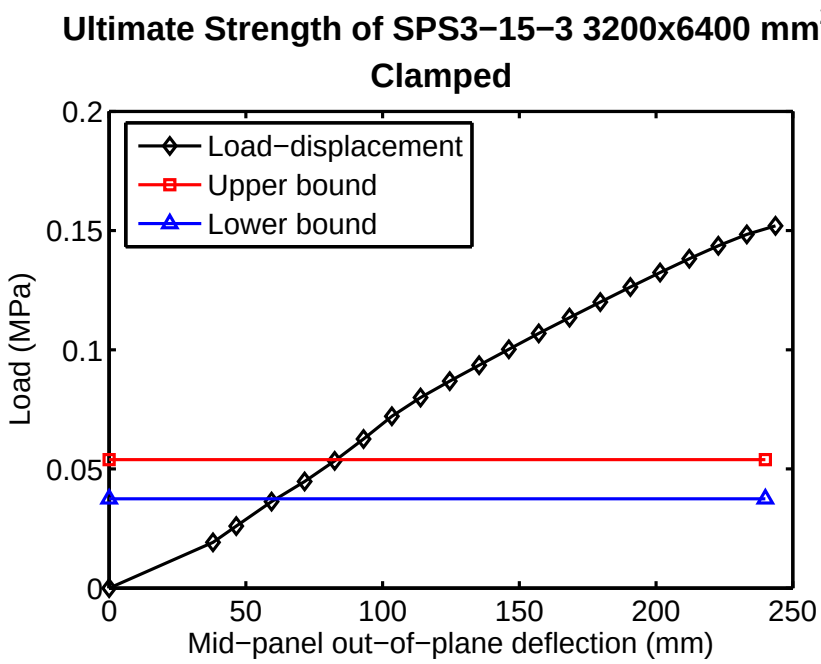

Figure 4.1: Load-displacement curve for a SPS3-15-3 3200x6400 mm^2 panel with clamped boundary conditions

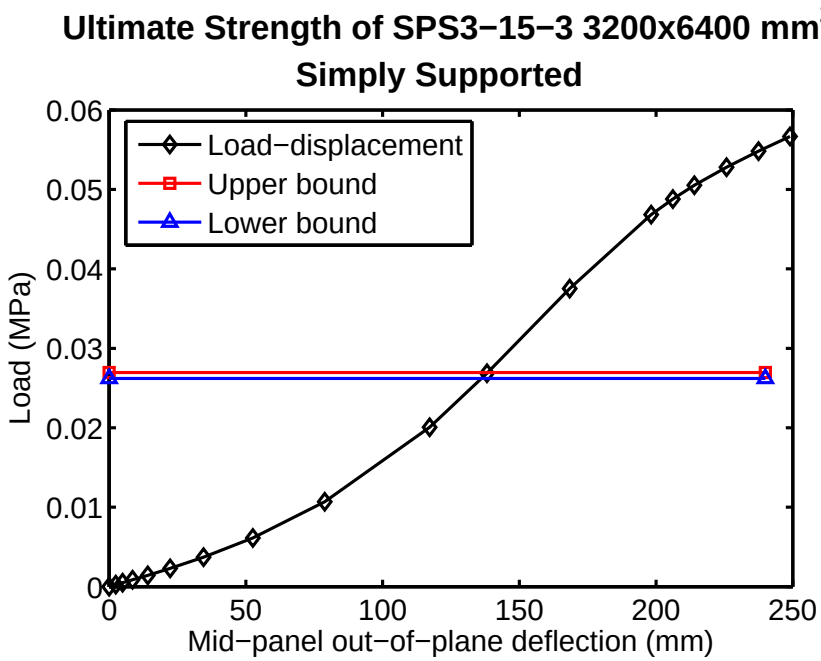

Figure 4.2: Load-displacement curve for a SPS3-15-3 3200x6400 mm^2 panel with simply supported boundary conditions

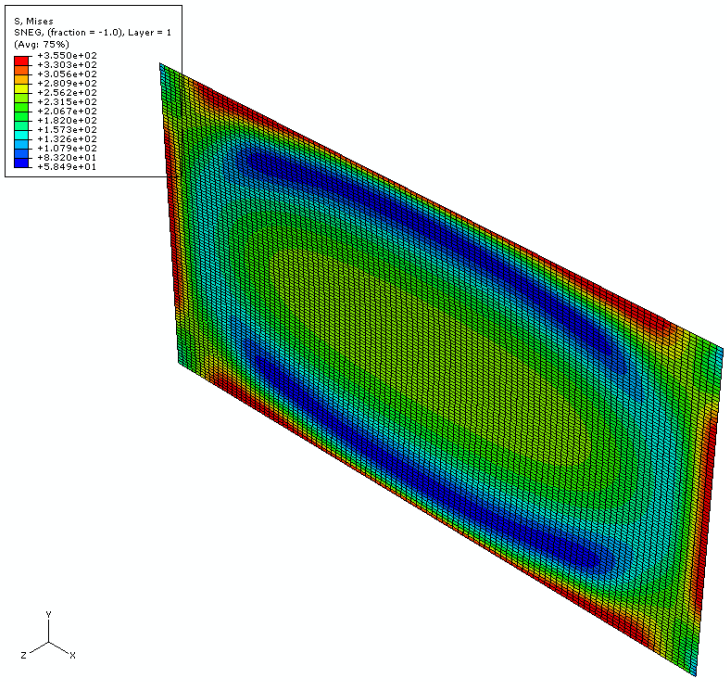

Figure 4.3: Von Mises stress contour plot for a SPS3-15-3 3200x6400 mm^2 panel with clamped boundaries. Von Mises stress is given in MPa

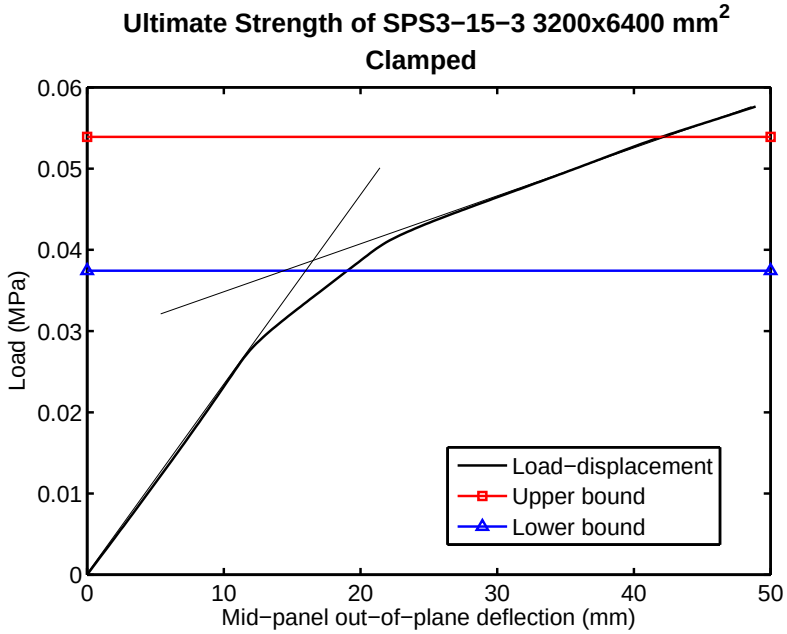

Figure 4.4: Load-displacement curve for a SPS3-15-3 3200x6400 mm^2 panel with clamped boundary conditions (10 times higher modulus of elasticity)

the modulus of elasticity in the steel is multiplied by a factor of 10. This is done to make the panel stiffer and thereby reduce the deformation such that the assumption of small deformation is valid. As can be seen in Figure 4.4 the lower bound solution corresponds now very well to the "knee" in the curve.

Since the panel is flexible, the deformations increases quickly and the lateral load is transferred to membrane stress in the faces instead of forming plastic moments on the panel. Failure of the panel happens when the membranes become fully plastic. This load is however extremely high, with very large deformations and cannot be used for dimensioning purposes. Flexible panels like this should only be used in places where the lateral pressure load is small or non-existent.

Figure 4.2 shows a similar behaviour for the simply supported panel as for the clamped one. As was mentioned in the theory, Section 2.1.5, transverse shear stress also needs some attention. The shear stress distribution over the cross section on the middle of the long edges on the clamped panel described above can be seen in Figure 4.5.

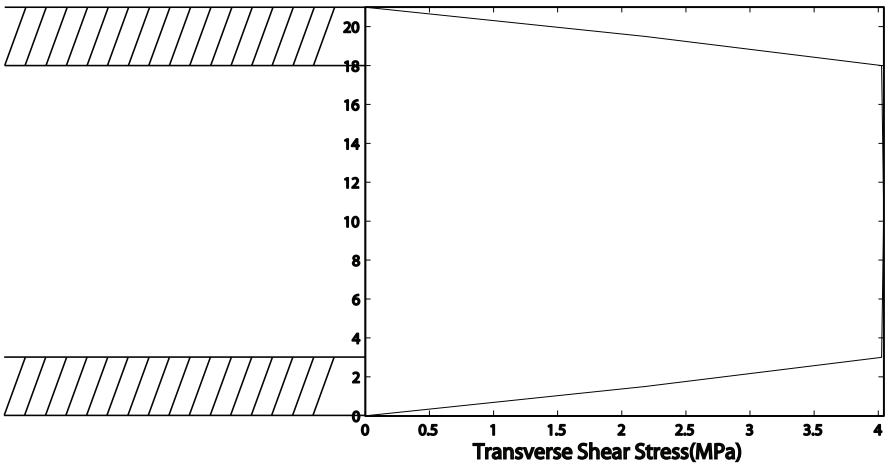

Figure 4.5: Shear stress over the cross section on a SPS3-15-3 3200x6400 mm^2 clamped panel at the upper bound pressure

Shear stress for both these two boundary conditions seems to be of no concern for this geometry and lay-up. That counts for both the two failure mechanism; core shear failure and debonding, since stresses for both boundary conditions are well below the critical value given as 6.0 MPa.

4.2 SPS10-35-10 2000x2000 mm^2

The previous panel was the most slender panel in this study. Next panel described is the thickest panel in the study, with both a thick core and thick faces. This panel is a SPS10-

35-10 with dimensions 2000x2000 mm^2.

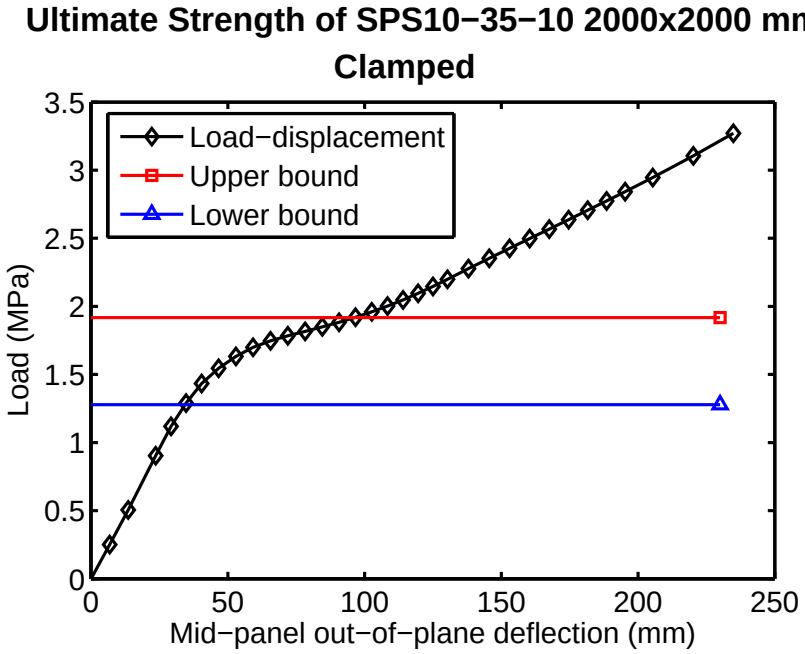

Figure 4.6: Load-displacement curve for a SPS10-35-10 2000x2000 mm^2 panel with clamped boundary conditions

Figures 4.6 and 4.7 both show well-defined "knee" values. This is where the panel forms into a mechanism and the point where the yield line theory should predict collapse. The yield pattern assumed in Figure 2.1 result in the red value in the graph. This value is slightly higher than the "knee" value, but since yield line theory is an upper-bound theory, this is expected.

The contour plot in Figure 4.8 show that the mechanism assumed in the yield line theory fits the stress distribution on the panel. After the mechanism is created, the load increases rapidly with increasing deflection since the membrane effect is taking over. This result shows that yield line pressure can be used for thick panels.

For the clamped panel in Figure 4.6 the "knee" value is lying between the upper bound and lower bound solution which is expected. The upper bound and lower bound solution are equal for the simply supported panel. By the definition of the theory this should only happen if this is the 'exact' value. The upper and lower bound solution predicts a value around 14% above the "knee" value. Out-of-plane deformations are for these panels 2.3% of the panel width for both sets of boundary conditions.

Maximum transverse shear stress over the cross section is found to be 18 MPa for the

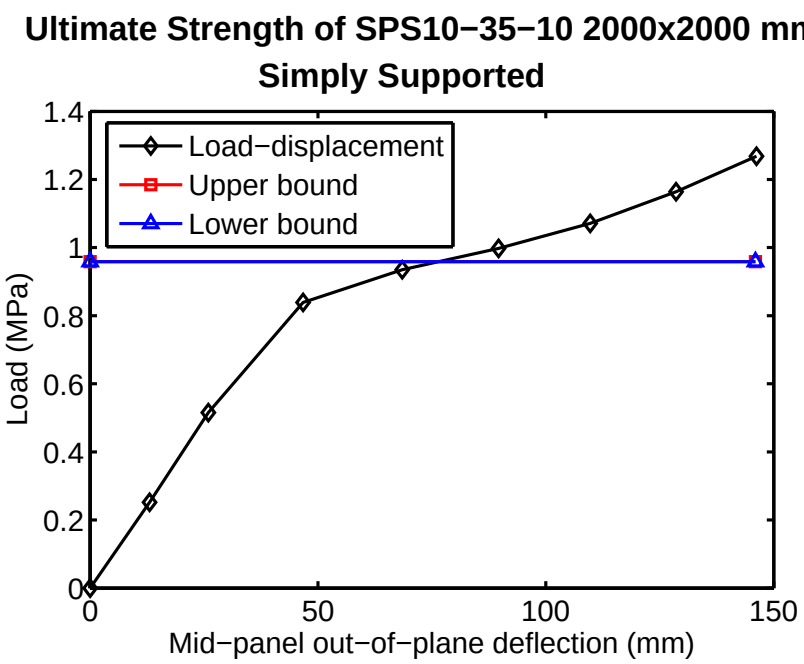

Figure 4.7: Load-displacement curve for a SPS10-35-10 2000x2000 mm^2 panel with simply supported boundary conditions

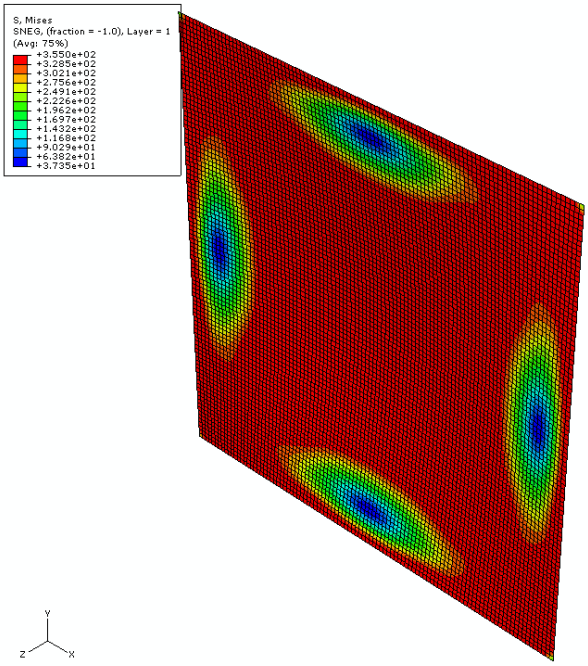

Figure 4.8: Von Mises stress of the panel when first mechanism is created. Von Mises stress is given in MPa

clamped panel and 15 MPa for the simply supported panel for the lower bound pressure. In this report it is assumed that debonding and core shear failure will not occur, but the factor needs attention in further studies. Maybe cut-offs in the final interaction curves must be included at a later stage.

4.3 SPS3-35-3 2000x2000 mm^2 and 3200x6400 mm^2

The next two cases will be with a cross section with thin faces and a thick core on the small panel (2000x2000 mm^2), and on the large panel (3200x6400 mm^2). The square panel is presented first.

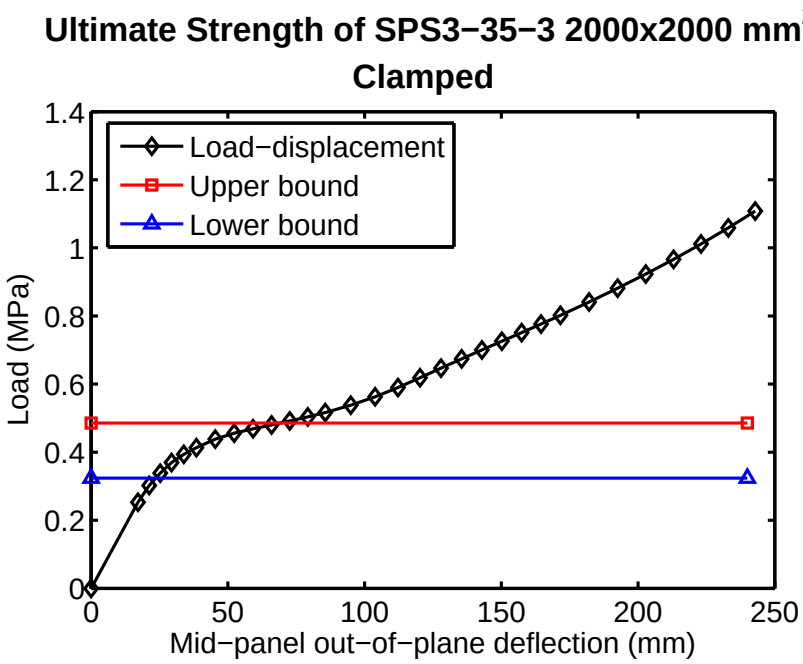

Figure 4.9: Load-displacement curve for an SPS3-35-3 2000x2000 mm^2 panel with clamped boundary conditions

Figures 4.9 and 4.10 shows similar behaviour to the thick SPS10-35-10 panels presented earlier. For the clamped panel, upper bound theory predicts failure slightly above the "knee" value, and lower bound slightly below the "knee" value. Upper bound solution and lower bound solution give the same prediction for the simply supported panel which is 12% above the "knee" value.

Core shear stresses are 6 MPa and 5 MPa for the clamped and simply supported panel. This should be well within the limits for core shear failure, but bonding seems to be more critical and needs further studies.

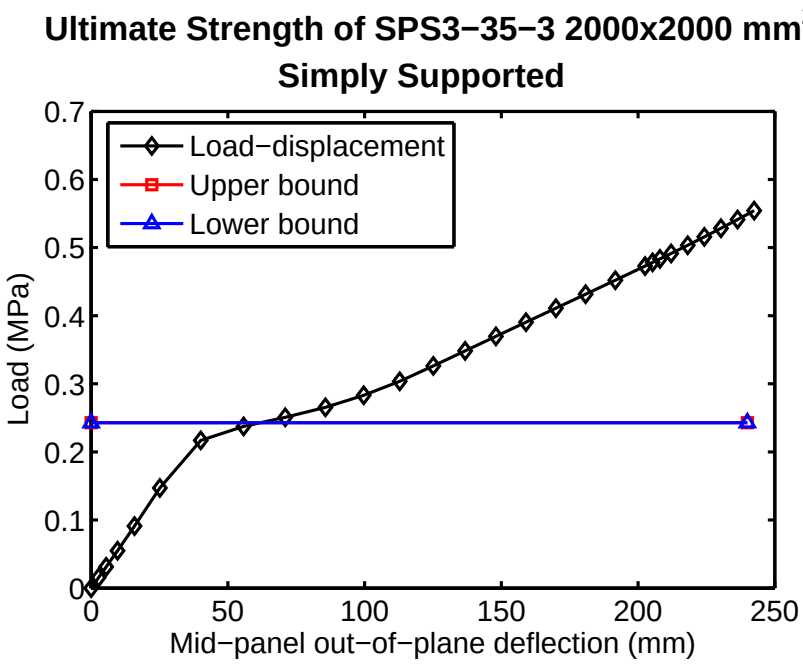

Figure 4.10: Load-displacement curve for an SPS3-35-3 2000x2000 mm^2 panel with simply supported boundary conditions

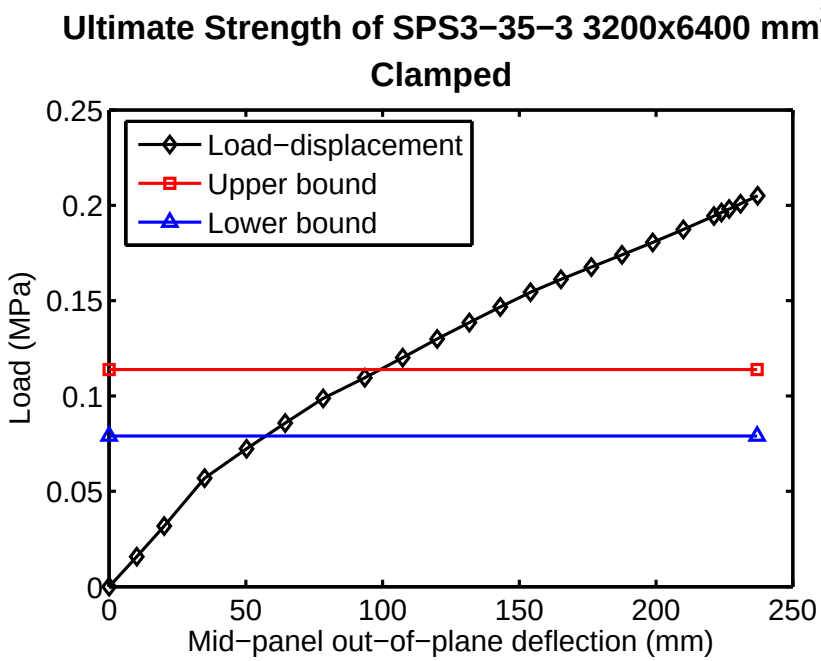

Figure 4.11: Load-displacement curve for an SPS3-35-3 3200x6400 mm^2 panel with clamped boundary conditions

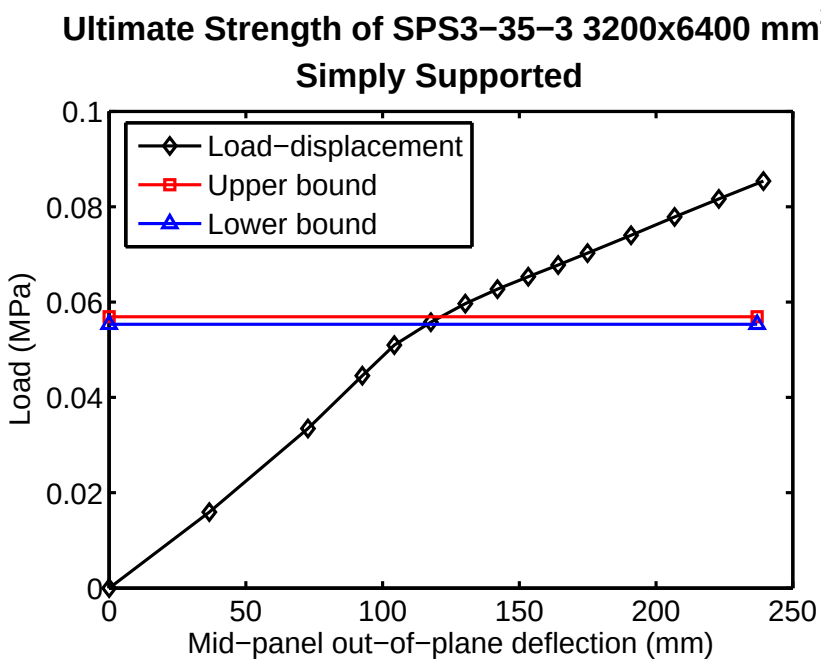

Figure 4.12: Load-displacement curve for an SPS3-35-3 3200x6400 mm^2 panel with simply supported boundary conditions

SPS3-35-3 with an aspect ratio of 2 gives the load-displacement curve shown in Figures 4.11 and 4.12. This panel has similar properties to the SPS3-15-3 panel with the same panel dimension. If the modulus of elasticity for the steel is increased with a factor of ten, a curve with a well-defined "knee" appears. This "knee" value lies between the calculated upper bound and lower bound solution. From this, it can be concluded that the assumption of small deformations for the theories is violated, but they still may be used as a reference value.

The deflection under the upper bound theory might be a bit too large for some applications. At least the deformation needs to be taken into account when the construction is dimensioned.

Transverse shear stress in the core is not an issue for neither of the boundary conditions. Magnitudes of the shear stresses are slightly above 4 MPa and 2 MPa for the clamped and the simply supported panel respectively.

4.4 SPS10-15-10 2000x2000 mm^2 and 3200x6400 mm^2

The next sets of panels analysed are panels with 10 mm faces and 15 mm core. This is a lay-up with thick faces and a thin core. Both the 2000x2000 mm^2 geometry and the 3200x6400 mm^2 geometry are considered.

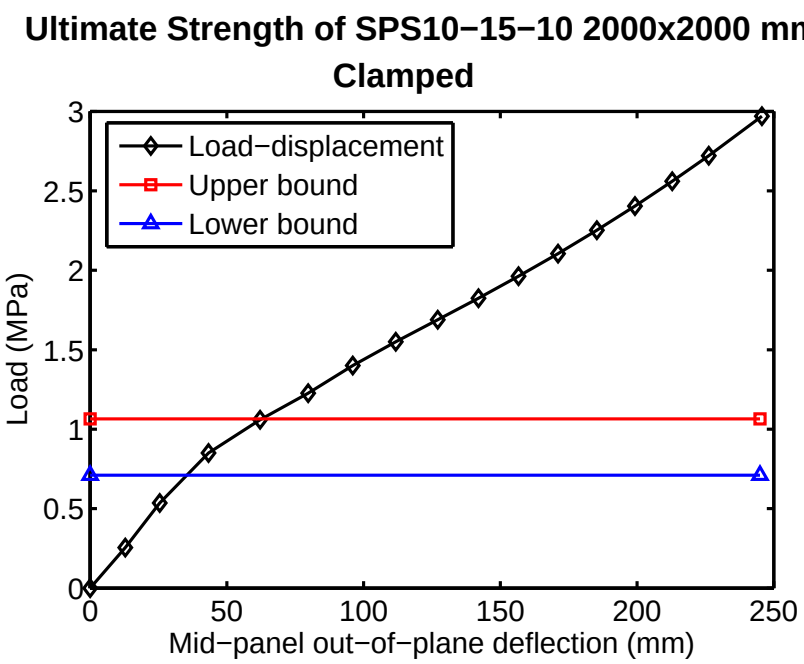

Figure 4.13: Load-displacement curve for a SPS10-15-10 2000x2000 mm^2 panel with clamped boundary conditions

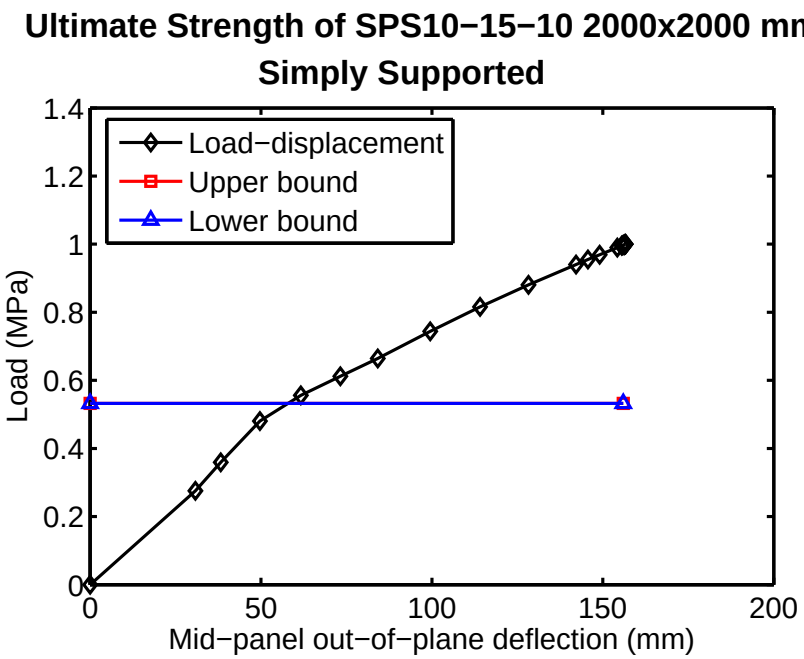

Figure 4.14: Load-displacement curve for a SPS10-15-10 2000x2000 mm^2 panel with simply supported boundary conditions

Both Figures 4.13 and 4.14 indicates a vague "knee" value. The stress plots for the panels at the load level where yield line theory predicts the forming of a mechanism show that the mechanism is not fully formed at this stage. It is however very close, so this is on the limit of what can be said to be small deformations with respect to the theory. This applies to both boundary conditions. How critical the mid-panel out-of-plane deflection is, must be decided for each and every application.

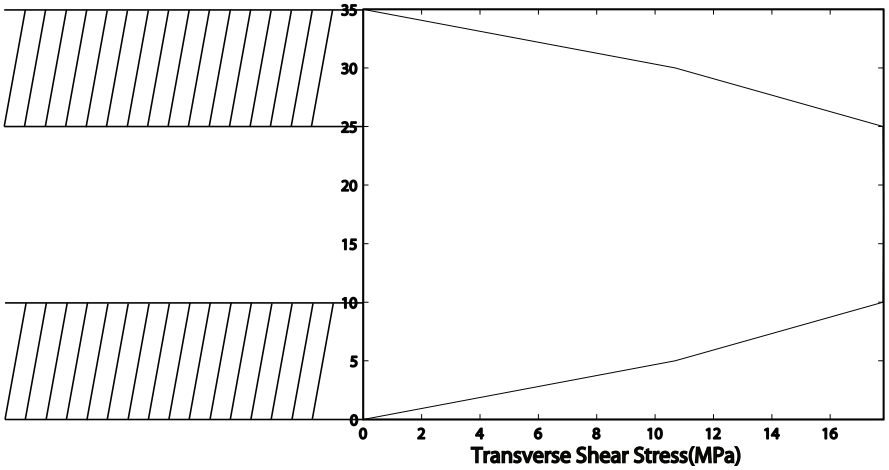

Figure 4.15: Shear stress over the cross section on a SPS10-15-10 2000x2000 mm^2 clamped panel at the lower bound pressure

Shear stress is quite high for these panels with almost 18 MPa for the clamped panel and slightly above 14 MPa for the simply supported panel. This seems to be particularily critical for the bonding. Figure 4.15 also show that the transverse shear stress in the faces varies parabolic.

The panels in Figures 4.16 and 4.17 have a problem with flexibility. As for the other panels in this report with dimensions 3200x6400 mm^2, the deflection becomes large so fast, that the forming of a mechanism does not happen. The deflections under the load found by the yield line theory are 2.8% and 4.2% of the panel width for the clamped and simply supported panel respectively.

Transverse shear stresses are for these panels 9 MPa and 5.5 MPa.

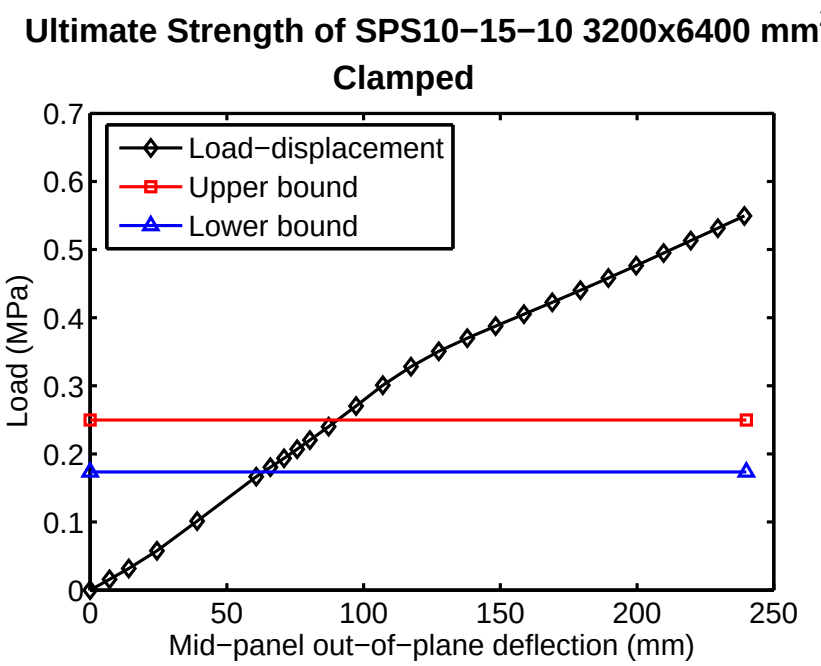

Figure 4.16: Load-displacement curve for a SPS10-15-10 3200x6400 mm^2 panel with clamped boundary conditions

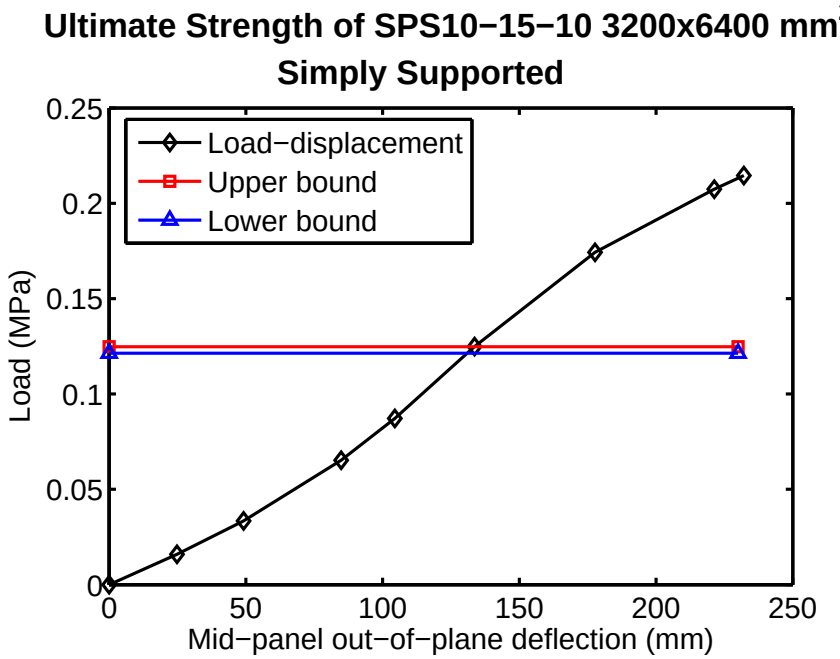

Figure 4.17: Load-displacement curve for a SPS10-15-10 3200x6400 mm^2 panel with simply supported boundary conditions

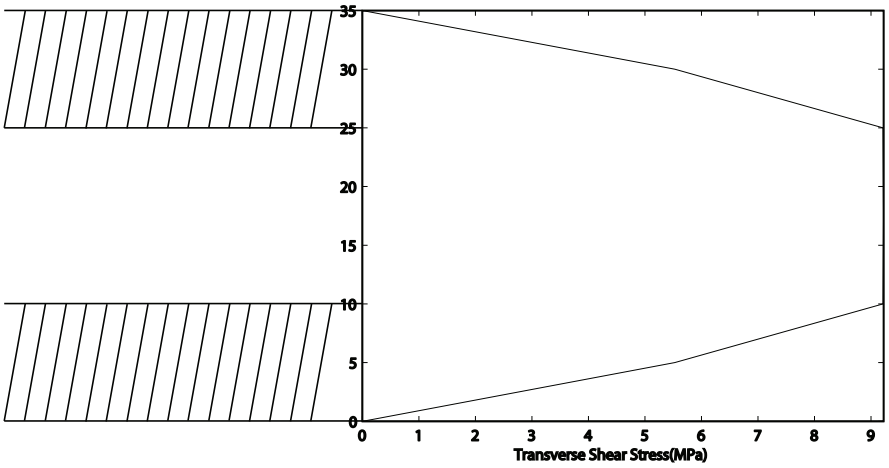

Figure 4.18: Shear stress over the cross section on a SPS10-15-10 3200x6400 mm^2 clamped panel at the lower bound pressure

4.5 SPS5-32-5 1200x1800 mm^2

Since most of the panels in this study are of the extreme type, it is also included a panel with more standard lay-up and geometry. The results from an analysis with SPS5-32-5 1200x1800 mm^2 is plotted in Figure 4.18.

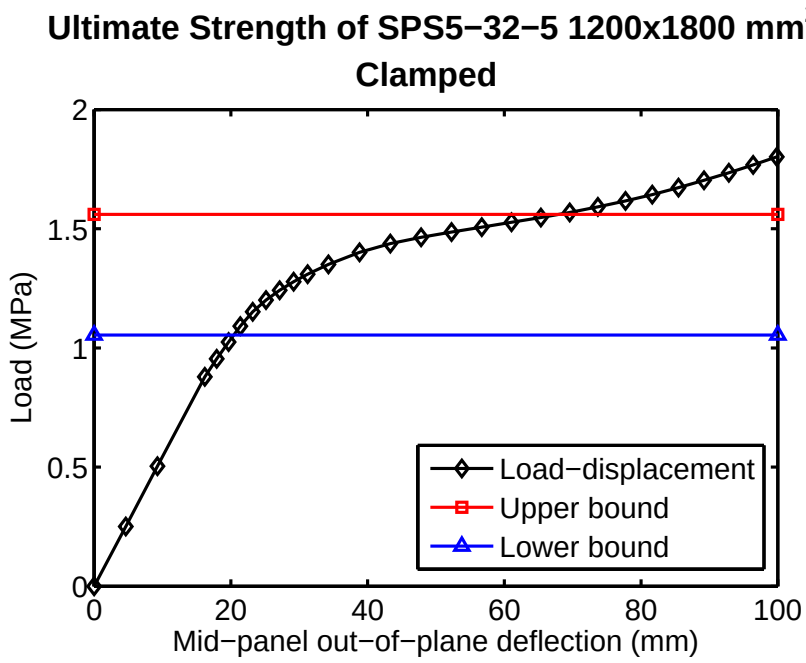

Figure 4.19: Load-displacement curve for a SPS5-32-5 1200x1800 mm^2 panel with clamped boundary conditions

According to the Mises stress plot, the mechanism assumed in the theory is formed at a lateral pressure load of 1.44 MPa. This is a little above the "knee" value, but between the upper and lower bound. The out-of-plane deflection under the yield line pressure for this panel is 5.8% of the panel width. Under the lower bound pressure, deflection for this panel is 1.7%.

Transverse shear stress over the cross section is for this panel a little above 14 MPa when the lateral pressure load is the lower bound pressure. When the lateral pressure load is the upper bound pressure, the transverse shear stress can be estimated to be around 20 MPa based on roughly linear properties in this region for the elastomer material. This stress is quite high and the core strength must be evaluated.

4.6 Summary

All panels studied in this report can be divided into two groups. The first group is panels that can be loaded up to a certain point where the forming of a mechanism starts. After this point, the load-displacement curve flattens out until the mechanism is fully formed. When the mechanism is formed, all loads are carried by the membranes.

The other group is the flexible panels. In this case the deformation becomes larger faster, and the membrane takes over the load before a mechanism can be formed. This is reflected in the load-displacement curve by a nearly linear curve instead of a curve with a well-defined "knee". For the range of panels in this study it seems to be only the panels with dimensions 3200x6400 mm^2 that falls into the group of flexible panels.

It was stated earlier that the assumption of small displacements was violated for the flexible panels, but it is also shown that when the upper and lower bounds are used on the flexible panels, they give a value that corresponds well to the "knee" value which the panel would have if the membranes were stiffer. This means that the bounds can be used in the interaction curves as a common reference value.

Chapter 5

Pure In-Plane Shear Load

5.0 General

To be able to say something general about how the SPS panels respond to in-plane shear load, it is vital to perform some finite element analyses. The analyses are then compared to the theories described in Section 2.2 to see if these theories can be used, or if other factors also need consideration.

5.1 SPS3-15-3 3200x6400 mm^2

The first panel studied is a SPS3-15-3 panel with dimensions 3200x6400 mm^2 which is a thin panel. The results from the analyses are plotted in Figure 5.1.

In Figure 5.1, the yield load is far above the load-displacement curves, so in this case it is not possible to load the panel up to this level. For the case with 1.0 mm maximum initial imperfection, the load-displacement curve can reach over the critical buckling load. However, when the initial imperfection is increased to 5.0 mm amplitude, the increased imperfection leads to a load-displacement curve that is closer to the critical buckling load. 5 mm imperfection on a 3200 mm width panel is not a large imperfection, so for dimensioning purposes, the extra capacity the finite element analysis show after the critical buckling load is exceeded, is not recommended to include in the total strength estimate.

For the clamped boundaries in Figure 5.2, there is a similar behavior. The panel cannot be loaded beyond the critical buckling load. Since the clamped boundaries are stiffer than the simply supported boundaries, this also immediately result in a higher critical buckling load for the clamped panel. It also seems that the simply supported panel is more sensitive to initial imperfection than the clamped panel is.

For both the two cases above, the approximate design formula seems to agree well with the finite element analyses.

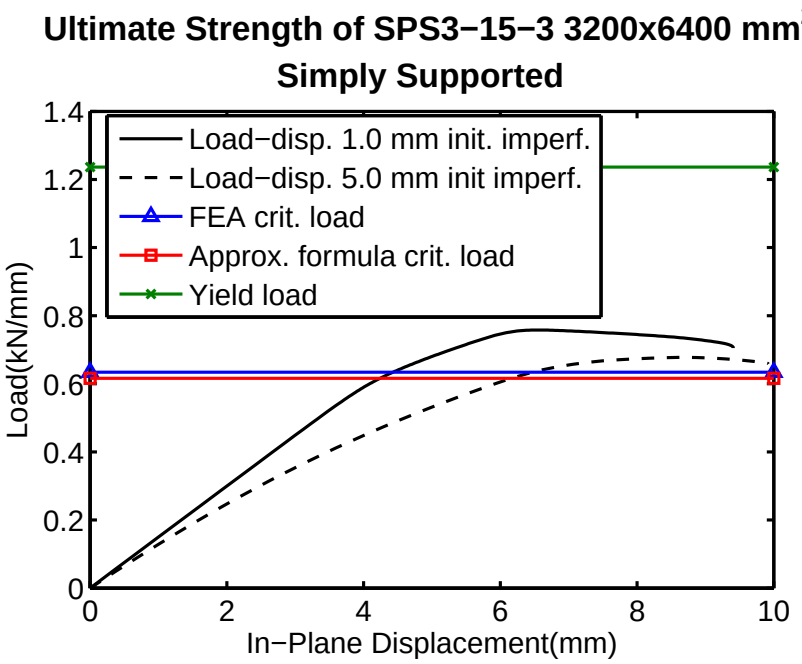

Figure 5.1: SPS3-15-3 3200x6400 mm^2 panel with simply supported boundaries subjected to in-plane shear load

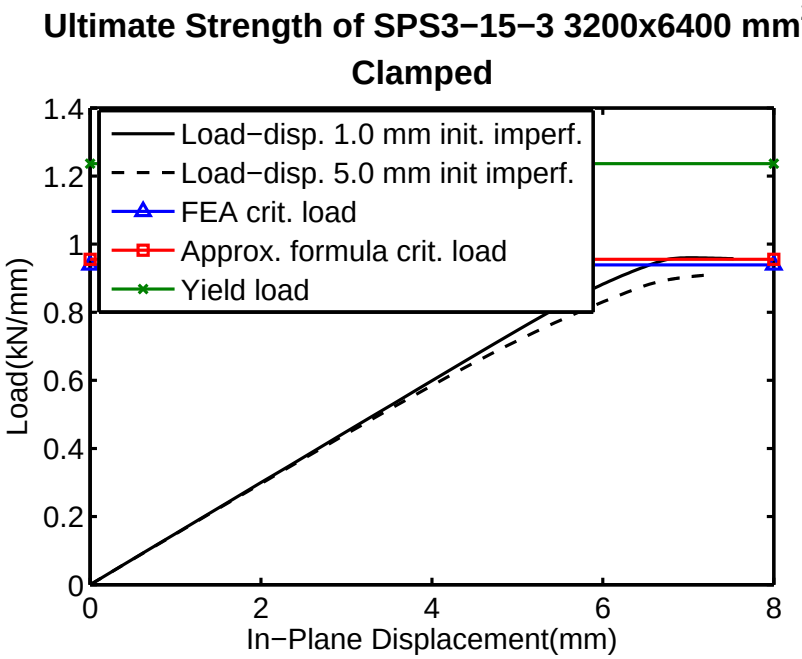

Figure 5.2: SPS3-15-3 3200x6400 mm^2 panel with clamped boundaries subjected to in-plane shear load

5.2 SPS3-35-3 2000x2000 mm^2

The next panel studied is SPS3-35-3 panel with dimensions 2000x2000 mm^2. The Figures 5.3 and 5.4 show the results from these analyses.

For these panels the yield load is critical. The critical buckling load is in fact much higher than the yield load. When failure due to yield occurs, boundary conditions does not influence the result at all. Both panels shown in Figures 5.3 and 5.4 fail at a shear load of 1.25kN/mm. There is good correspondence between the approximated buckling load and the eigenvalue found by the finite element method.

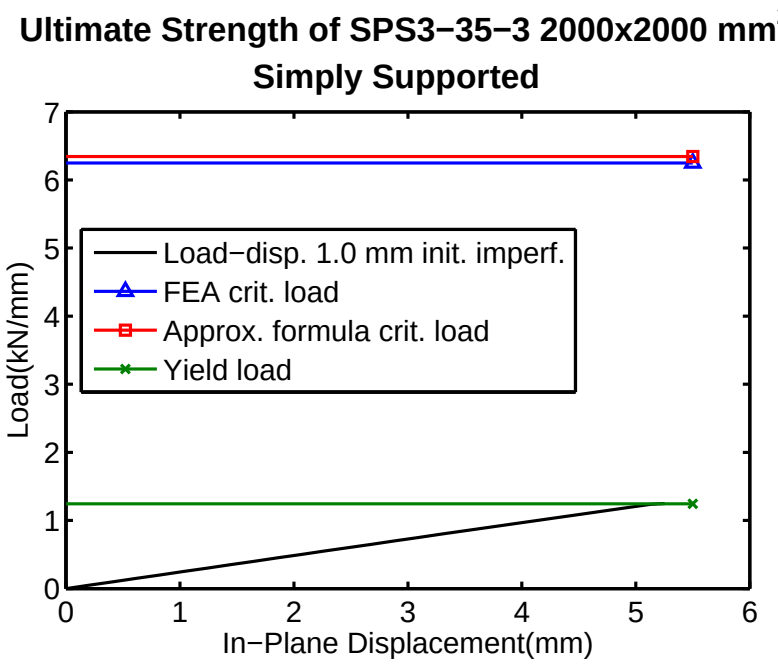

Figure 5.3: SPS3-35-3 2000x2000 mm^2 panel with simply supported boundaries subjected to in-plane shear load

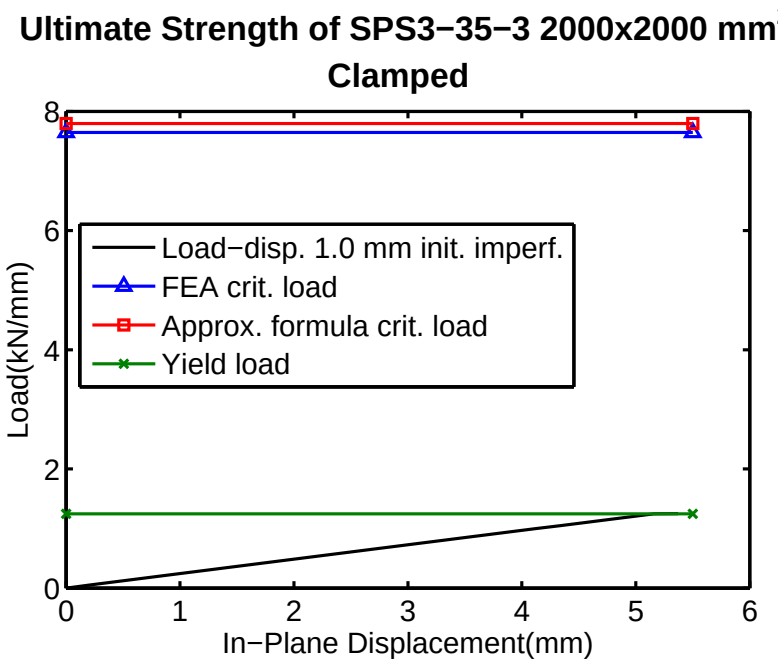

Figure 5.4: SPS3-35-3 2000x2000 mm^2 panel with clamped boundaries subjected to in-plane shear load

5.3 SPS3-35-3 3200x6400 mm^2

The next panel has the same cross section as the previous one, but the dimensions have changed to 3200x6400 mm^2. The load-displacement curve is presented in Figures 5.5 and 5.6.

Since these panels have the same cross section as the previous panel, the yield load will be the same for these panels too. The critical buckling load is greatly reduced from the previous panel because of the increase in panel dimension, but the critical buckling load is still far higher than the yield load. Also for these panels the approximated design formula corresponds well with the finite element method.

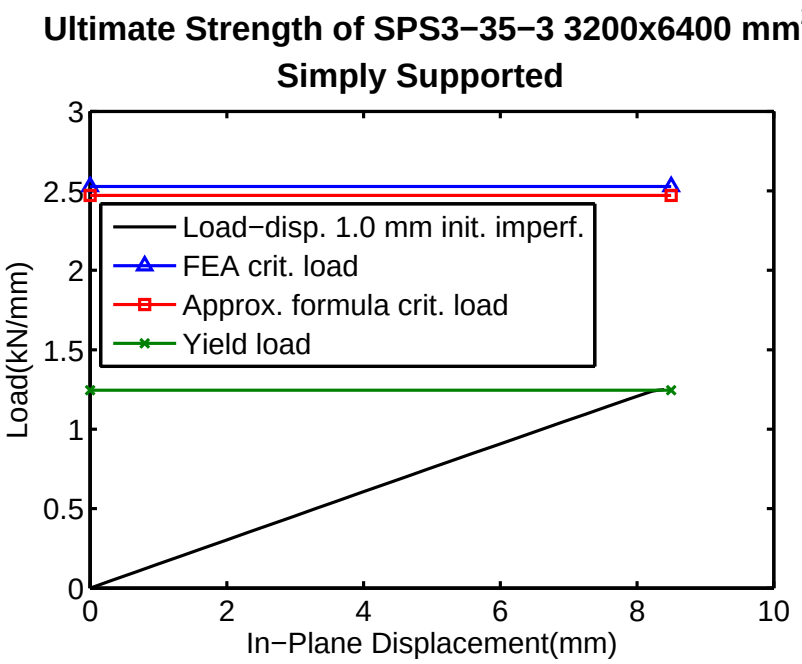

Figure 5.5: SPS3-35-3 3200x6400 mm^2 panel with simply supported boundaries subjected to in-plane shear load

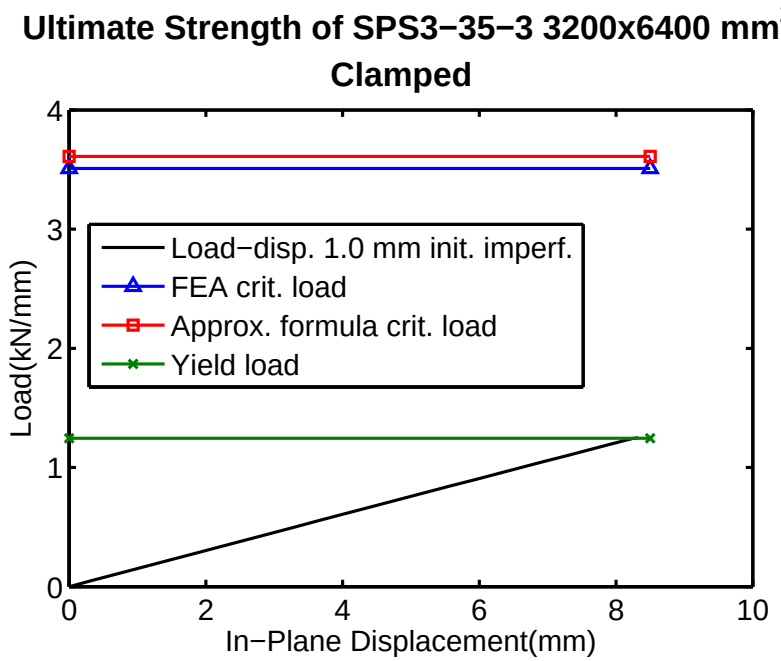

Figure 5.6: SPS3-35-3 3200x6400 mm^2 panel with clamped boundaries subjected to in-plane shear load

5.4 SPS10-15-10 2000x2000 mm^2 and 3200x6400 mm^2

These panels had relatively thin faces and a thick core. The next two panels have two thick faces and a relatively thin core. Figures 5.7, 5.8, 5.9 and 5.10 shows the load displacement curves for SPS10-15-10 panels with dimensions 2000x2000 mm^2 and 3200x6400 mm^2.

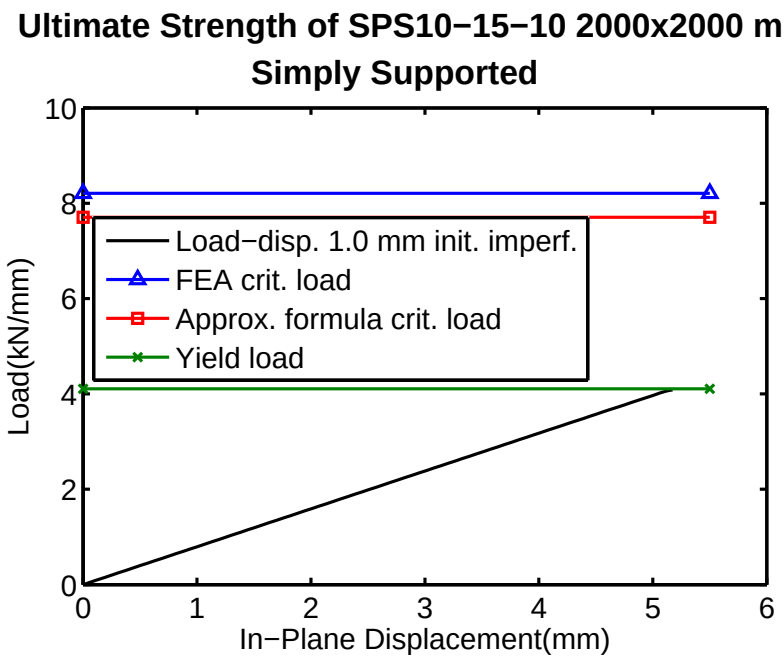

Figure 5.7: SPS10-15-10 2000x2000 mm^2 panel with simply supported boundaries subjected to in-plane shear load

Figures 5.7 and 5.8 shows the square panel with simply supported and clamped boundaries. The clamped and the simply supported panels have the same ultimate load in this case, and that load is the theoretical yield load.

The rectangular panel on Figure 5.9 and 5.10 with the SPS10-15-10 cross section is somehow more interesting. The critical buckling load and the theoretical yield load is much closer here than in the previous analyses. This results in a different failure mode for the simply supported panel and the clamped one. Since the simply supported panel is more flexible, the critical buckling load lies below the yield load, and failure occurs right after buckling. For the clamped panel which is stiffer, the critical buckling load lies a little above the yield load, so this panel fails due to the yield load again.

Another thing that need to be taken into account on this cross section is that the thickness of the face can no longer be considered as thin compared to the core. This is one of the fundamental assumptions when the buckling expressions are derived. For the clamped

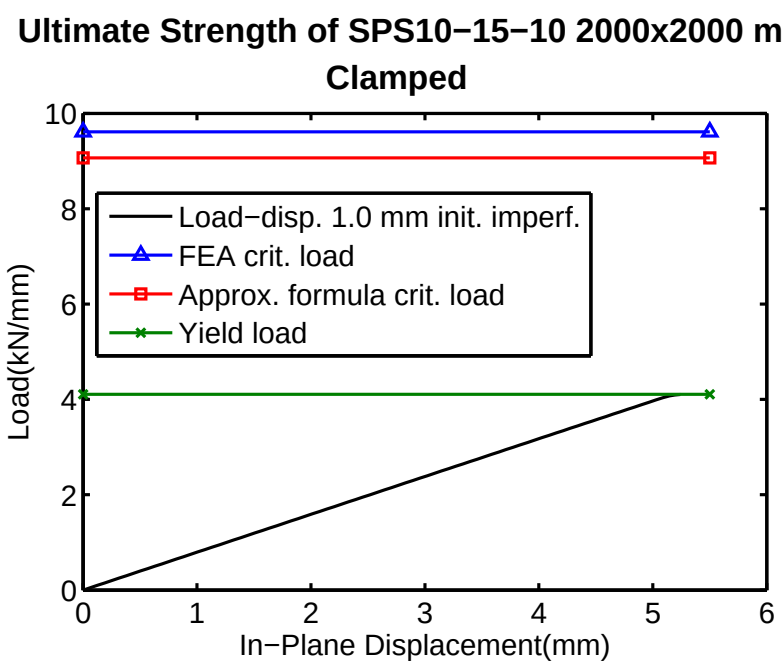

Figure 5.8: SPS10-15-10 2000x2000 mm^2 panel with clamped boundaries subjected to in-plane shear load

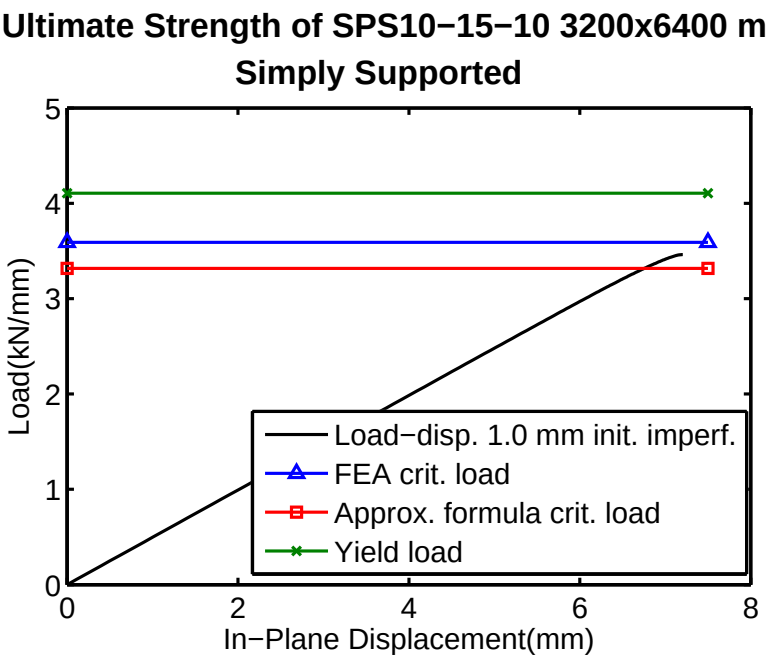

Figure 5.9: SPS10-15-10 3200x6400 mm^2 panel with simply supported boundaries subjected to in-plane shear load

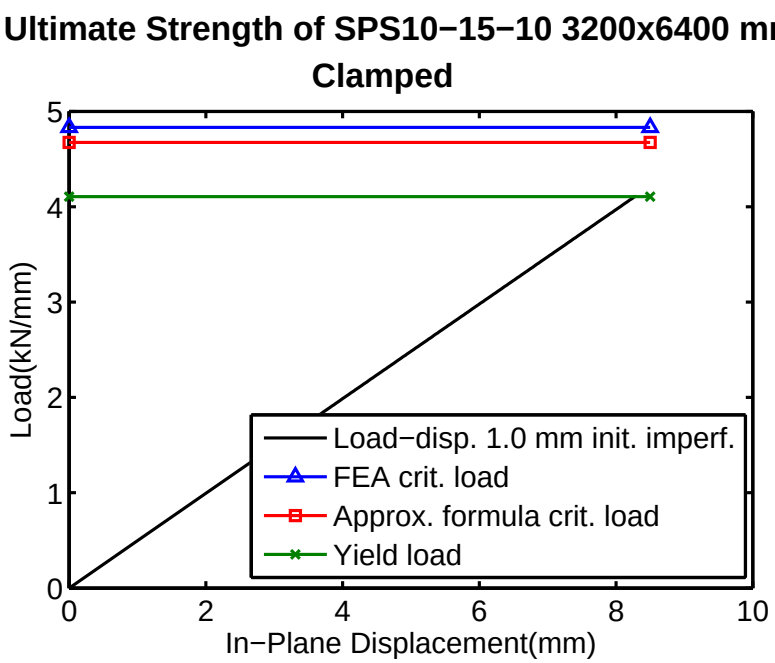

Figure 5.10: SPS10-15-10 3200x6400 mm^2 panel with clamped boundaries subjected to in-plane shear load

panel, this matters little since the yield load theory does not assume thin faces, but for the simply supported panel, this needs to be considered. However, since both the finite element analysis and the numerically solved determinant give about the same critical buckling load, the effect of thick faces does not seem to influence greatly these results.

5.5 SPS10-35-10 2000x2000 mm^2

The next panel analysed is an SPS10-35-10 panel with dimensions 2000x2000 mm^2.

Also for these two panels the thin face assumption is not valid. The critical buckling load is 3-4 times the yield load, so for these thick panels buckling is not an issue.

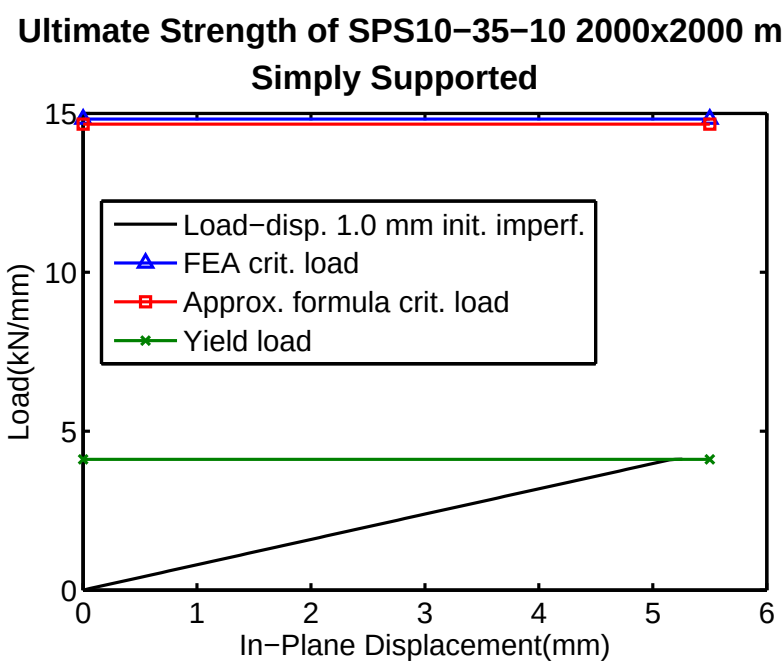

Figure 5.11: SPS10-35-10 2000x2000 mm^2 panel with simply supported boundaries subjected to in-plane shear load

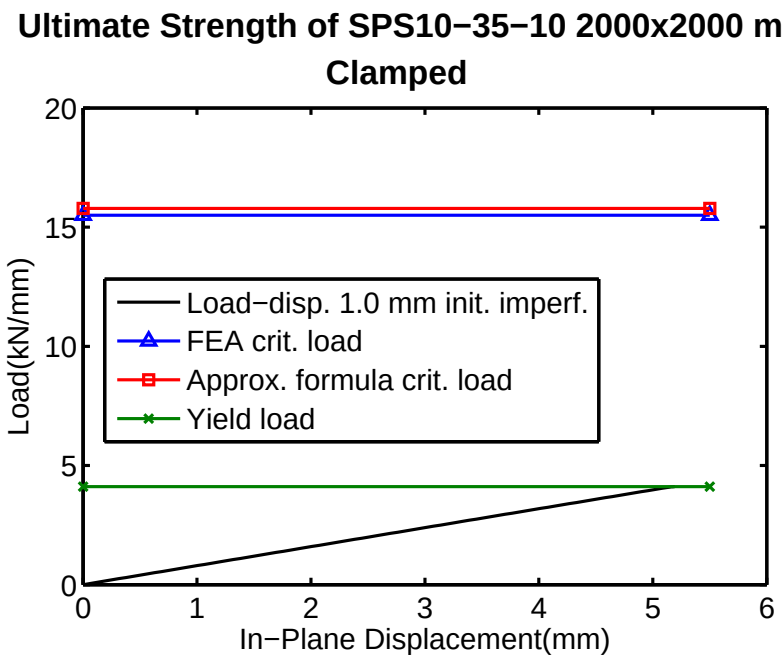

Figure 5.12: SPS10-35-10 2000x2000 mm^2 panel with clamped boundaries subjected to in-plane shear load

5.6 SPS5-32-5 1200x1800 mm^2 and SPS7-35-7 3200x6400 mm^2

The last analyses performed on pure in-plane shear are of two panels, a SPS5-32-5 panel with a dimension of 1200x1800 mm^2 and a SPS7-35-7 panel with a dimension of 3200x6400 mm^2. Both panels are clamped and the results can be seen in Figures 5.13 and 5.14.

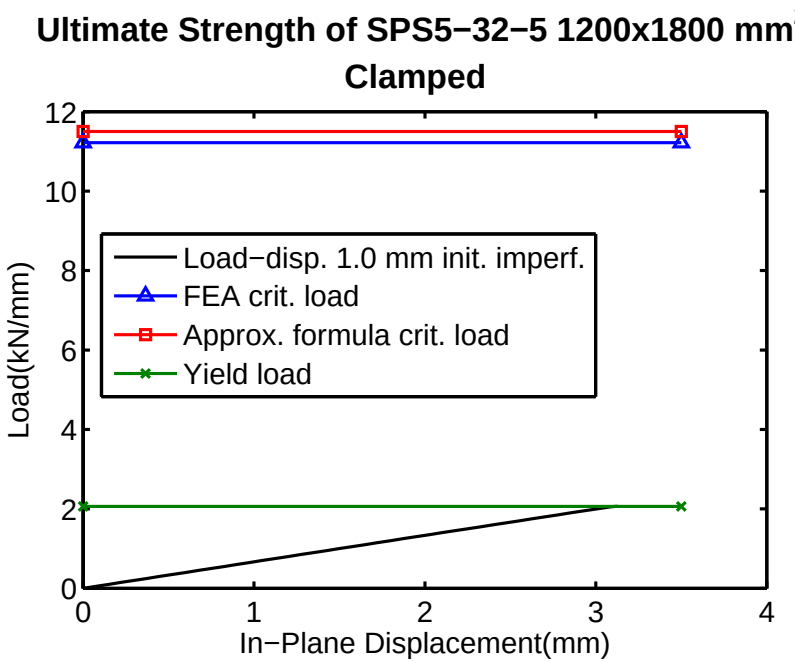

Figure 5.13: SPS5-32-5 1200x1800 mm^2 panel with simply supported boundaries subjected to in-plane shear load

Again yield is the limiting factor for the panels.

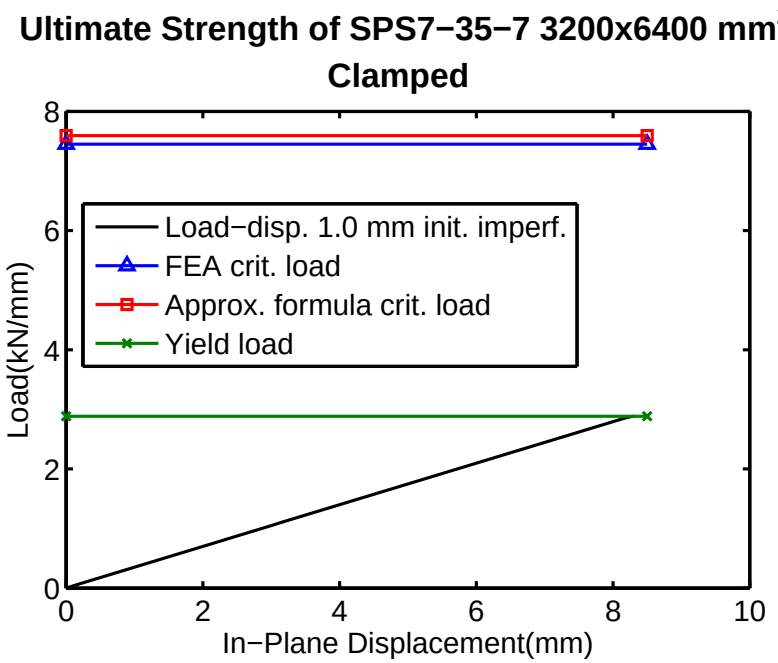

Figure 5.14: SPS7-35-7 3200x6400 mm^2 panel with clamped boundaries subjected to in-plane shear load

5.7 Summary

In most of the analyses of the extreme geometries performed in this work, the limitation of the ultimate in-plane shear load is due to yielding of the entire cross section. The exceptions are panels with thin core compared to the panel dimensions, especially with the less stiff, simply supported, boundary.

The thin panels are also the panels that are most sensitive to initial imperfections, especially when the two critical values are close to each other.

It can also be concluded that the two theories derived in Section 2.2 describes the ultimate capacity, and they agree well with finite element analyses.

Chapter 6

Interaction

6.1 In-Plane Shear Load and Lateral Pressure Load Interaction

6.1.1 Conventional Steel-Plated Structures

Interaction curves have been made for conventional steel-plated structures [4]. A conservative interaction curve based on curve fitting of square plates is given as

$$\left(\frac{\tau}{\tau_{u0}}\right)^{1.5} + \left(\frac{p}{p_{u0}}\right)^{1.2} = 1 \tag{6.1}$$

τ_{u0} is then the ultimate strength under pure edge shear and p_{u0} is the ultimate strength under pure lateral pressure. The lateral pressure p_{u0} is bounded between the upper and lower bound, and for a simply supported square panel, this is the same value for both bounds. For a clamped square panel the difference is significantly larger between upper and lower bound. Paik and Thayamballi [4] refer to a study by Fox in 1974, where he shows that for clamped square panels, the collapse load equals $42.85M_p/b^2$. This is slightly closer to the upper bound than the lower bound. According to the study performed in the current work, this value corresponds to the upper part of the "knee" for the clamped SPS panel which can indeed be a good reference value.

For the rectangular panels, $a/b > 1$, the upper bound solution seems to be used for both clamped and simply supported panels according to Paik and Thayamballi [4]. Upper bound and lower bound is almost identical for all panel aspect ratios when the boundaries are simply supported. For the clamped panel, the upper bound and lower bound reach the same value when the aspect ratio goes towards infinity. Using the upper bound sounds therefore reasonable.

There are several approaches to decide the ultimate strength under edge shear. Paik and Thayamballi [4] uses an empirical formula based on curve fitting from computed results.

Their results are compared to ENV 1993-1-1 of Eurocode 3: "Design of steel structures. General rules and rules for buildings." The formula of ENV 1993-1-1 is given as

$$\tau_u = \begin{cases} \tau_Y & \text{for } \lambda \leq 0.8 \\ [1 - 0.625(\lambda - 0.8)]\,\tau_Y & \text{for } 0.8 < \lambda < 1.2 \\ 0.9/\lambda\tau_Y & \text{for } \lambda \geq 1.2 \end{cases} \tag{6.2}$$

where

$$\lambda = \sqrt{\frac{\tau_Y}{\tau_E}} \tag{6.3}$$

τ_Y is the yield stress and τ_E is the elastic web shear buckling stress. There are also some more requirements for the stiffeners. For the SPS panels, more specifically the geometries studied in this work, almost all panels fall under the first category in Equation 6.2. The elastic buckling load is far higher than the critical yield load which means that the ultimate load is equal to the critical yield load. There are a few panels that fall under the two other categories too, but just using the elastic critical load seems to give a good estimate for the ultimate load.

6.1.2 Stiffened Plate in DNV Classification Rules for Ships

The DNV Classification Rules for newbuilding of ships [3] has another approach than the interaction curve for this load combination. For instance for a bulkhead plating, the following procedure is used. Firstly the thickness requirement for lateral pressure given in Equation 2.39 apply with the proper parameters. Then there is a criterion for minimum thickness of the panel depending on the area where the bulkhead is located. Buckling control is the next step. Depending on what area the bulkhead is located, different stability (usage) factors $\eta = \tau_a/\tau_c$, are used. τ_a is here the calculated actual shear stress in the bulkhead. τ_c is the critical shear stress in the bulkhead given from the Johnson-Ostenfeldt correction of the elastic Euler buckling in the elasto-plastic range.

$$\begin{aligned} \tau_c &= \tau_{el} \text{ when } \tau_{el} < \frac{\tau_f}{2} \\ &= \tau_f \left(1 - \frac{\tau_f}{4\tau_{el}}\right) \text{ when } \tau_{el} > \frac{\tau_f}{2} \\ \tau_f &= \text{ von Mises yield stress of the material in shear} \\ &= \frac{\sigma_f}{\sqrt{3}} \end{aligned}$$

The ideal elastic buckling shear stress, τ_{el}, is given by Allen and Bulson [17] to be

$$\tau_c = \frac{K\pi^2 E}{12\,(1-\nu^2)} \left(\frac{t'}{b}\right)^2 \tag{6.4}$$

where $K = 5.34 + 4\left(\frac{b}{a}\right)^2$ is the buckling coefficient for simply supported panels, E is the modulus of elasticity and $t' = t - t_k$ is the thickness of the plate without the extra added thickness to account for corrosion.

6.1.3 Interaction for SPS Panels

The theoretical interaction curve used in this work is based on curve fitting from the results obtained by finite element analyses on the range of different geometries. The interaction curve in Equation 6.1 was used as a basis and the power terms were adjusted. The interaction curve suggested in this study is given as

$$\left(\frac{Q}{Q_{ult}}\right)^{2} + \left(\frac{p}{p_{ult}}\right)^{1.2} = 1 \tag{6.5}$$

where Q_{ult} is the lowest of the two shear force criteria described in Section 2.2 and p_{ult} is for most cases the upper bound limit, but details on this will be presented later in this section.

SPS3-15-3 3200x6400 mm^2

SPS3-15-3 with dimensions 3200x6400 mm^2 is the panel with the thinnest cross section over the largest panel. The interaction curve for this panel is given in Figures 6.1 and 6.2 for clamped and simply supported boundaries respectively.

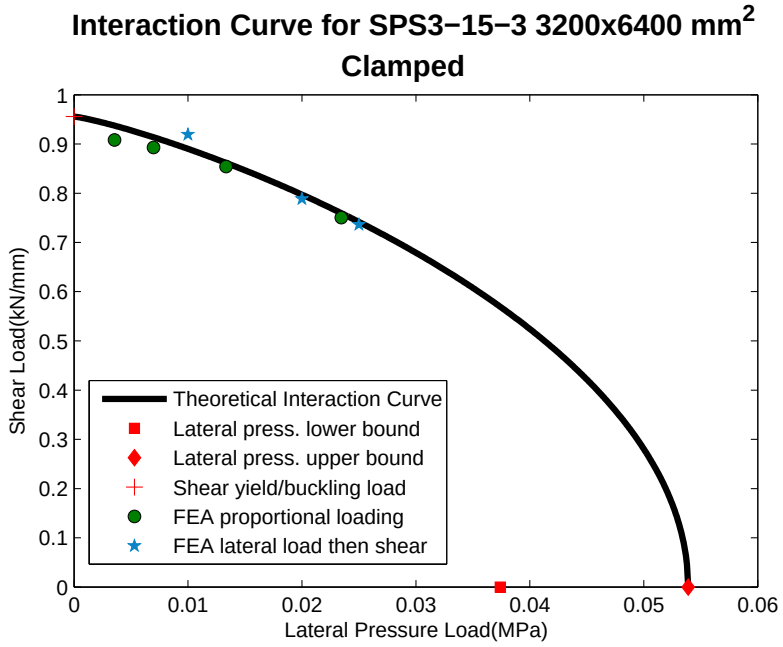

Figure 6.1: Interaction curve with the combination of in-plane shear loading and lateral pressure load on a SPS3-15-3 3200x6400 mm^2 clamped panel

As can be seen in Figure 6.1, only a few finite element points are included, and all of the points are in the left part of the curve where the shear load is dominant and lateral

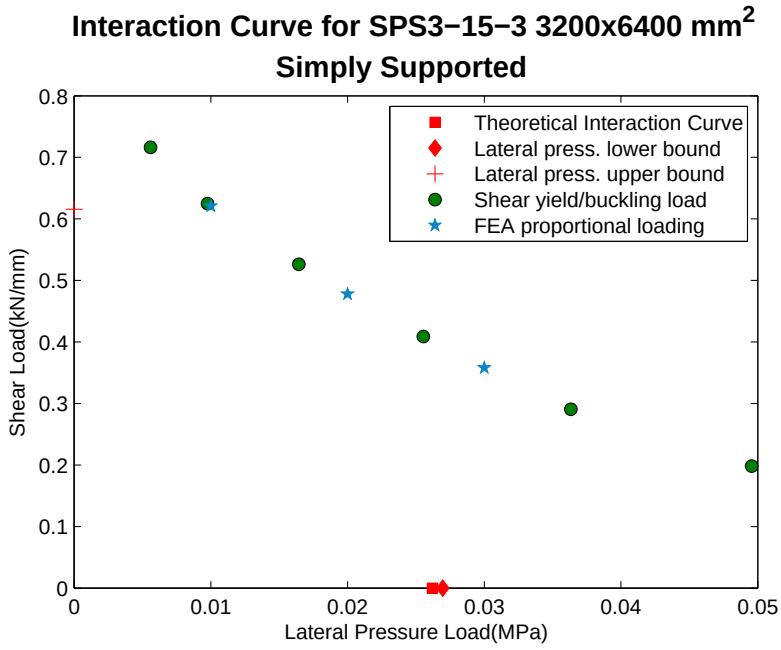

Figure 6.2: Interaction curve with the combination of in-plane shear loading and lateral pressure load on a SPS3-15-3 3200x6400 mm^2 simply supported panel

load is small. A lot more analyses are performed, but since the panel take up lateral pressure in the membranes when the deflection is large enough, no clear limit line can be found in the analyses. However when the lateral load is small and the shear load is high, the response curve flattens out or sometimes even starts decreasing, and an ultimate load value can be obtained. There is good correspondence between the two different loading sequences except for the leftmost part. The proportional loading is lower than both the theoretical interaction curve and the loading where lateral load is applied first. This is a result of the initial imperfection of 5.0 mm on the proportionally loaded panel. As can be seen in Figure 5.2 the panel with 5.0 mm initial imperfection has an ultimate strength slightly lower than the elastic critical load. Since the panel where lateral load is applied first has no initial imperfection before the lateral load is applied, the two loading sequences give different results where imperfections influence the results. It can also be noted that after the lateral load is increased, the two results agree very well. This means that the initial imperfection is most critical when the panel is mostly or only subjected to in-plane shear force.

The simply supported panel in Figure 6.2 has completely different interaction behaviour. As can be seen in Figure 5.1 the peak value for the curve with imperfection of 5.0 mm is 0.67 kN/mm, which is about 8% higher than the estimated elastic critical value used as reference value in the interaction curve. The leftmost point found by finite element analysis is showing a shear load of 0.71 kN/mm which is higher than the finite element

analysis of pure shear load with initial imperfection of 5.0 mm. As soon as lateral load is applied, the out-of-plane deflection from this load dominates the imperfection. When the panel is forced into a mode that is not the critical buckling mode, the panel can be loaded higher than the elastic critical load, but the panel will be unstable. If the panel snaps into the critical mode, the panel will collapse if the shear load is higher than the elastic critical load. The next point from the finite element analysis is within the expectations for an interaction curve and would fit the theoretical curve if the reference value for shear was taken as the value found by element analysis with 5.0 mm imperfection. Figure 4.2 shows that the membrane effects become significant when the lateral load is between 10 kPa and 20 kPa. This is also the case in the interaction curve, thus the rest of the curve become less interesting since the deflections now are the crucial topic.

SPS3-35-3 2000x2000 mm^2

In Figures 6.3 and 6.4 is the square SPS3-35-3 panel with dimensions 2000x2000 mm^2.

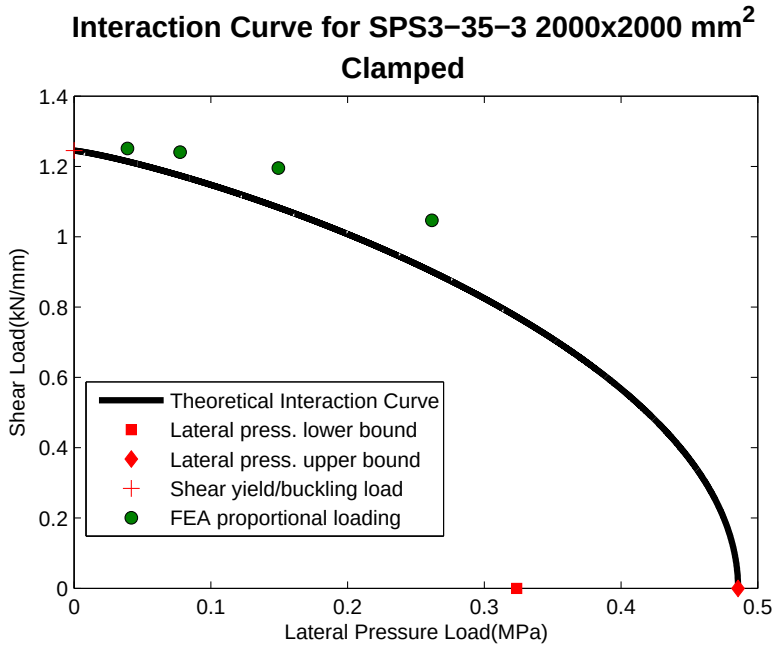

Figure 6.3: Interaction curve with the combination of in-plane shear loading and lateral pressure load on a SPS3-35-3 2000x2000 mm^2 clamped panel

For both panels in Figure 6.3 and 6.4 shear yield is the failure mode. The elastic critical load is around 8 times higher than the critical yield load for the clamped panel. Since the steel faces are the same thickness as for the previous panel the shear yield load is almost the same for these cases. Yield load for the panel in Figure 6.3 is slightly higher since the core is thicker and can carry a little more load, but this difference is really small and can

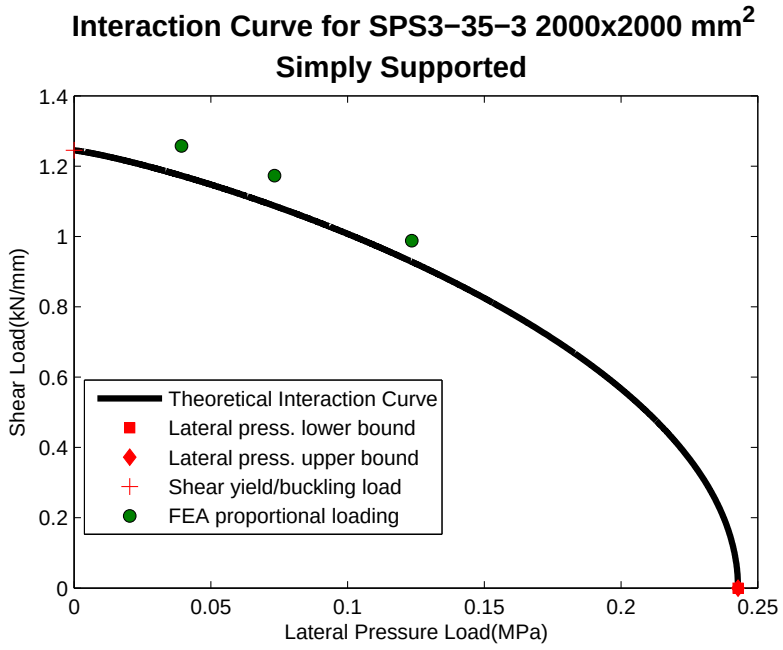

Figure 6.4: Interaction curve with the combination of in-plane shear loading and lateral pressure load on a SPS3-35-3 2000x2000 mm^2 simply supported panel

be neglected. Since the dimensions of the panel are smaller, and the distance between the two face sheets are larger, the elastic critical load is much higher for this panel. The same conclusion can be made for the simply supported panel.

Point number three from the left in Figure 6.3 is the finite element result that has the largest error to the theoretical interaction curve with 9% on the conservative side. The finite element results indicate that the shear capacity is not reduced as quickly as the theoretical interaction curve says when the lateral load increases. For instance if the power used on the p/p_{ult}-term is increased from 1.2 to 1.5, the results become better. The power 1.2 is however used to be conservative for all panels. To achieve a more correct interaction curve for the SPS panels under the load combination described in this report, a larger range of panels must be studied.

Upper bound theory seems to give the best reference value for both types of boundary conditions. Lower bound is far too conservative for the clamped panel. For the simply supported panel, upper and lower bound gives the same value.

SPS3-35-3 3200x6400 mm^2

The next panel is almost identical to the first panel in this section. Only difference is the core thickness which is the same as in the second panel studied. The interaction curves can be found in Figures 6.5 and 6.6.

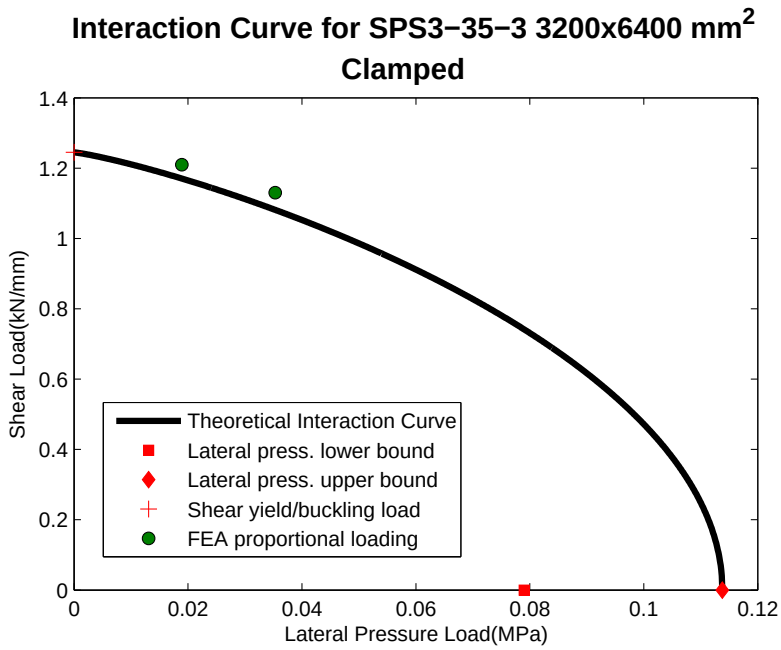

Figure 6.5: Interaction curve with the combination of in-plane shear loading and lateral pressure load on a SPS3-35-3 3200x6400 mm^2 clamped panel

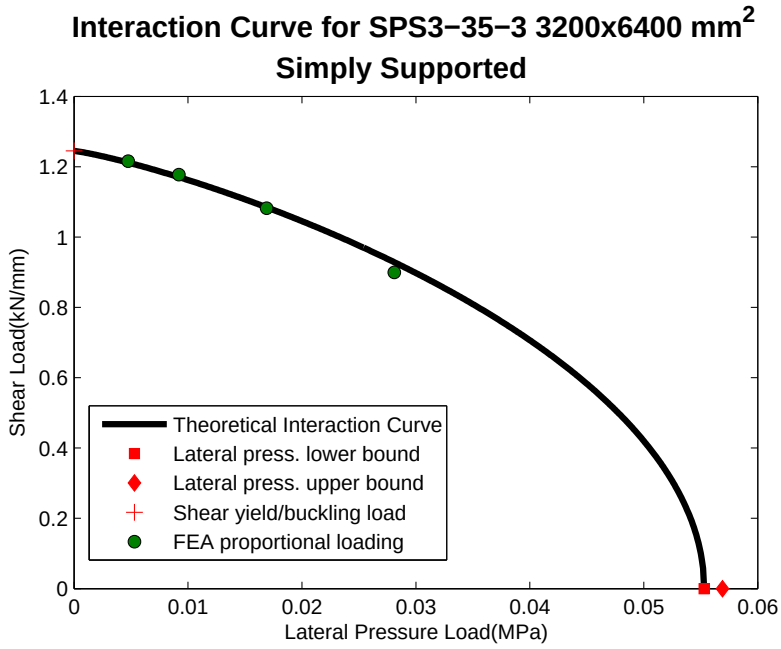

Figure 6.6: Interaction curve with the combination of in-plane shear loading and lateral pressure load on a SPS3-35-3 3200x6400 mm^2 simply supported panel

Both panels in Figures 6.5 and 6.6 fails in shear due to yielding over the cross section. The dimensions are equal to the first panel described in this chapter except the core thickness. This difference increases the elastic critical load without making the critical yield load any higher. The result is a different failure mechanism from that for the first panel.

When it comes to the pure lateral case, this panel has the same properties as the first panel. The length and width are large compared to the height of the cross section which leads to flexible panels with large deformations. This panel is however slightly stiffer than the first panel due to the thicker core, so this panel shows the same interaction curve as the second panel described. Whether the deformations are acceptable when the panel is subjected to mostly lateral pressure need to be decided from application to application, but some form of displacement limit should be considered.

Finite element results seem to agree well with the interaction curve suggested in this study. In the simply supported panel in Figure 6.6 the lower bound solution is chosen as the reference value since it seems to give a better fit, but the lower bound and upper bound are so close in this case that using the upper bound would work as a reference value as well.

SPS5-32-5 1200x1800 mm^2

Next panel studied, a SPS5-32-5 1200x1800 mm^2 panel, is in the middle range. The faces are slightly thicker than the previous panels and the core is around the same thickness as the previous panel. This is also the panel in the range of study with the smallest width and length

In these two interaction cases both load sequences has been tested. In Figures 6.7 and 6.8 the two different load sequences seem to agree well with each other and also with the suggested interaction curve. There is one point that stands out on the simply supported panel in Figure 6.8. That is the rightmost point and the reason is that membrane effects has started to become significant and the load-displacement curve no longer show a clear ultimate load.

When subjected to pure in-plane shear, yield will be the determining failure mode since the elastic critical load is five times higher than the yield load. On the lateral pressure side, the upper bound limit is the reference value that gives the best interaction curve. The upper bound solution gives however a large deflection for pure lateral pressure loads. As can be seen in Figure 4.19 the curve flattens out after the "knee" before it increases at a far higher deflection where the upper bound value can be found. This means that the load does not need to be reduced much before the deformation is acceptable for most applications. So when the safety factor is applied to the lateral loading, the deformation will most likely be of no concern.

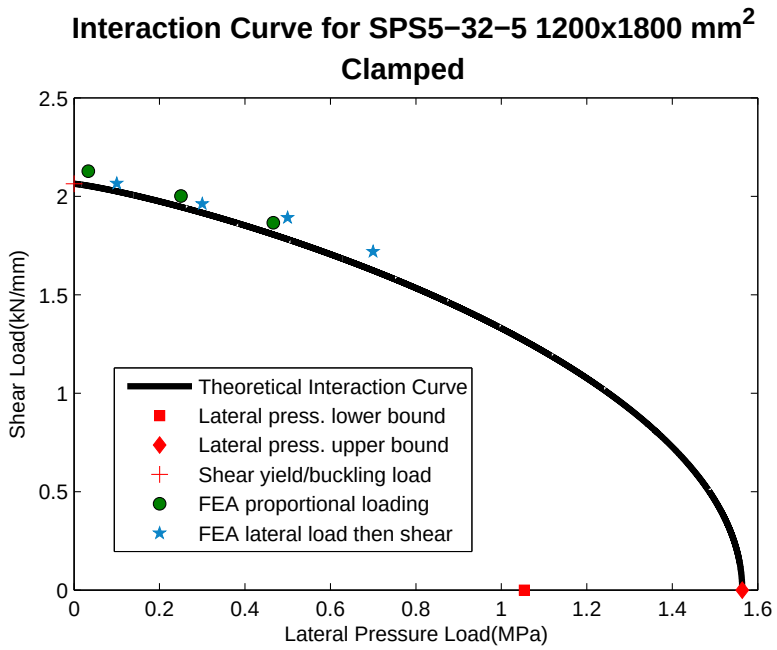

Figure 6.7: Interaction curve with the combination of in-plane shear loading and lateral pressure load on a SPS5-32-5 1200x1800 mm^2 clamped panel

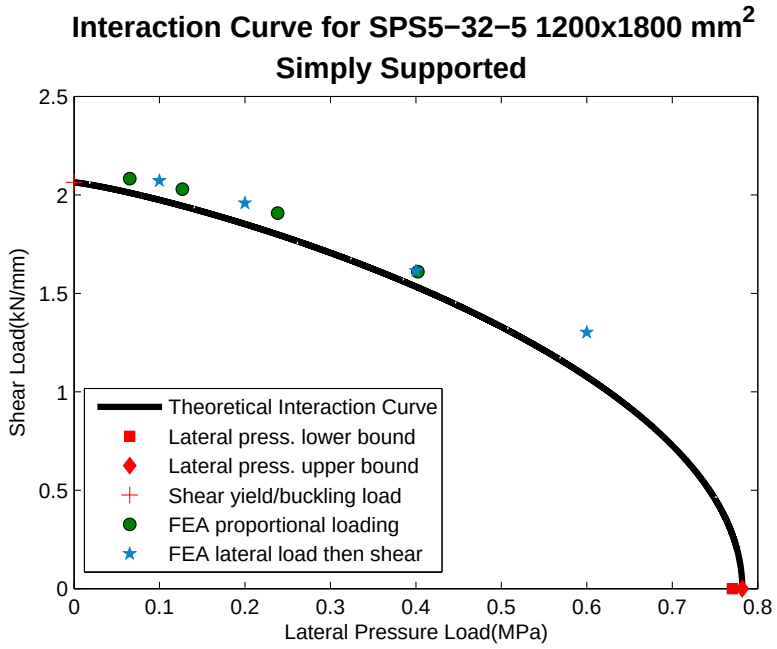

Figure 6.8: Interaction curve with the combination of in-plane shear loading and lateral pressure load on a SPS5-32-5 1200x1800 mm^2 simply supported panel

SPS7-35-7 3200x6400 mm^2

Another panel in the mid-range is the SPS7-35-7 with dimensions 3200x6400 mm^2. The interaction curves are shown in Figures 6.9 and 6.10.

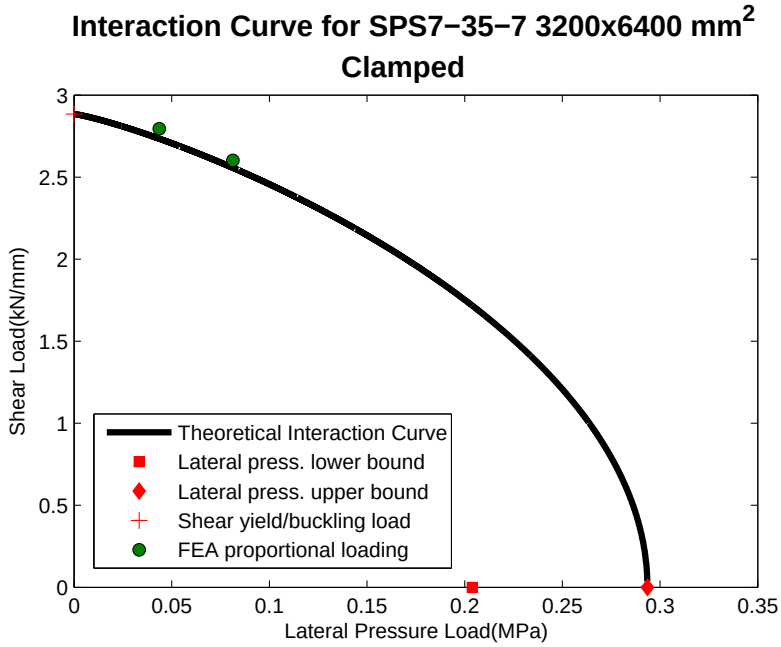

Figure 6.9: Interaction curve with the combination of in-plane shear loading and lateral pressure load on a SPS7-35-7 3200x6400 mm^2 clamped panel

Shear yield is the failure mode also for this panel when subjected to pure in-plane shear load. Due to the thicker steel faces, this panel can carry higher in-plane shear load than the previous panel. For the clamped panel in Figure 6.9, the two finite element results that were possible to obtain, correspond well with the interaction curve when the upper bound solution is used as the reference value.

The simply supported panel in Figure 6.10 also gives good finite element results compared to the suggested interaction curve. It is also possible here to obtain several more results that give a clear ultimate capacity. The rightmost point is however an exception. Here the membrane effect becomes significant before the ultimate capacity is reached. Also the second rightmost point reaches far too high deflections before ultimate capacity is reached. For this panel a lower bound reference value seems to give the best interaction curve. The difference between upper bound and lower bound is on the other hand so low, so it would not be a large error if the upper bound was used either.

If the three rightmost points are studied alone, they tend to show a similar behaviour to the panel in Figure 6.2. It can quickly be noted that the ratio between the thickness of

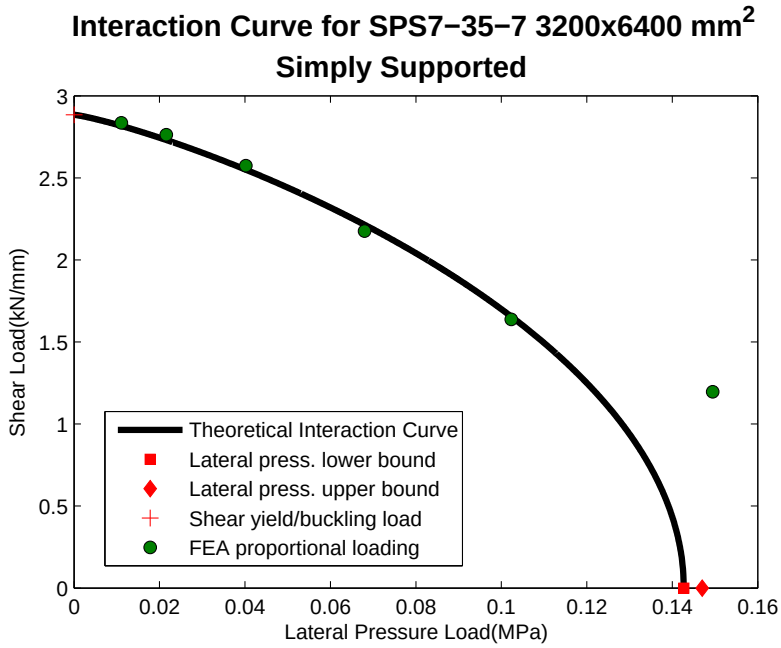

Figure 6.10: Interaction curve with the combination of in-plane shear loading and lateral pressure load on a SPS7-35-7 3200x6400 mm^2 simply supported panel

the face sheets and the core are equal for these two panels. Of course the SPS7-35-7 can be loaded higher since the panel is thicker, but it responds the same way as the SPS3-15-3 when subjected to mostly lateral pressure.

When the panels are subjected to mostly shear, they respond differently. Due to the difference in the steel face thickness, the SPS7-35-7 panel yields, and the SPS3-15-3 buckles. Yielding is much less sensitive to initial imperfections than buckling is and will therefore behave more stable close to the pure shear case.

SPS10-15-10 2000x2000 mm^2

Figures 6.11 and 6.12 shows the next panels in this study, square panels with thick faces and a thin core.

The reference values for in-plane shear and lateral pressure are for these panels the same as in most of the earlier cases. Yield limit and upper bound are used for the two loadings respectively. In Figure 6.11 it seems that some of the finite element results are not corresponding that well to the interaction curve. This is because no clear ultimate limit could be found on the load-displacement curve. The curves almost flatten out, but still have a small slope. Values used in the interaction curve are just the last points taken from the analyses. This is not entirely accurate and results in the differences described above. The simply supported panel in Figure 6.12 shows a similar mismatch for some of the points,

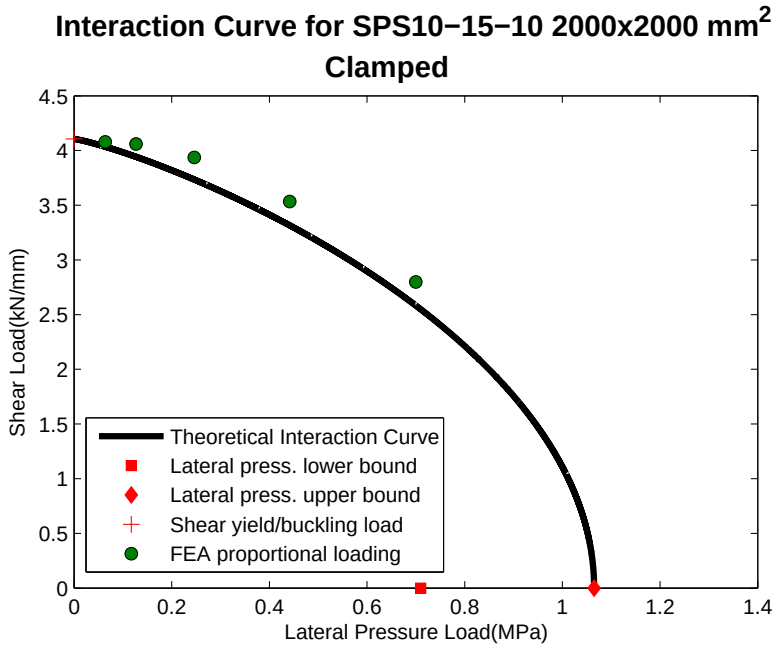

Figure 6.11: Interaction curve with the combination of in-plane shear loading and lateral pressure load on a SPS10-15-10 2000x2000 mm^2 clamped panel

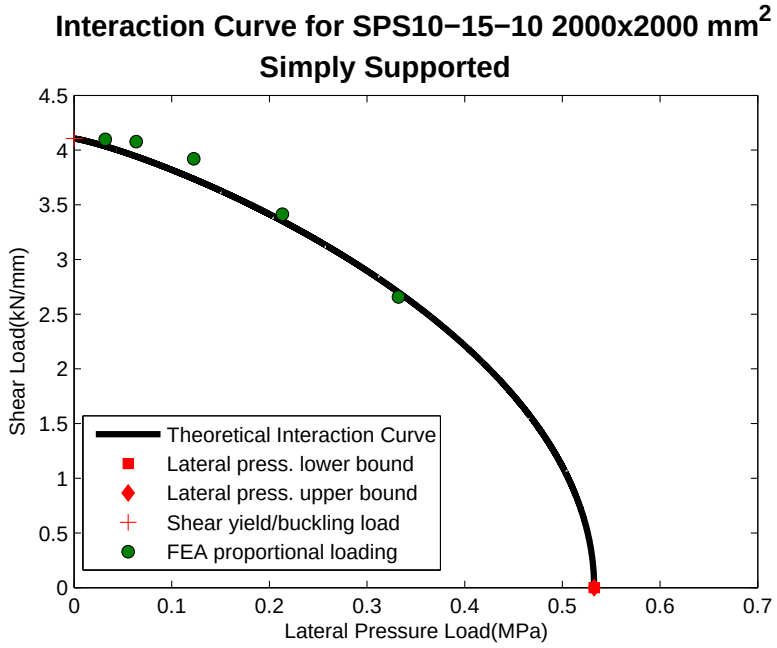

Figure 6.12: Interaction curve with the combination of in-plane shear loading and lateral pressure load on a SPS10-15-10 2000x2000 mm^2 simply supported panel

but overall there is a good correspondence between the interaction curve and the finite element results.

SPS10-15-10 3200x6400 mm^2

The last but one geometry studied in this report for two-way interaction is the SPS10-15-10 with dimensions 3200x6400 mm^2.

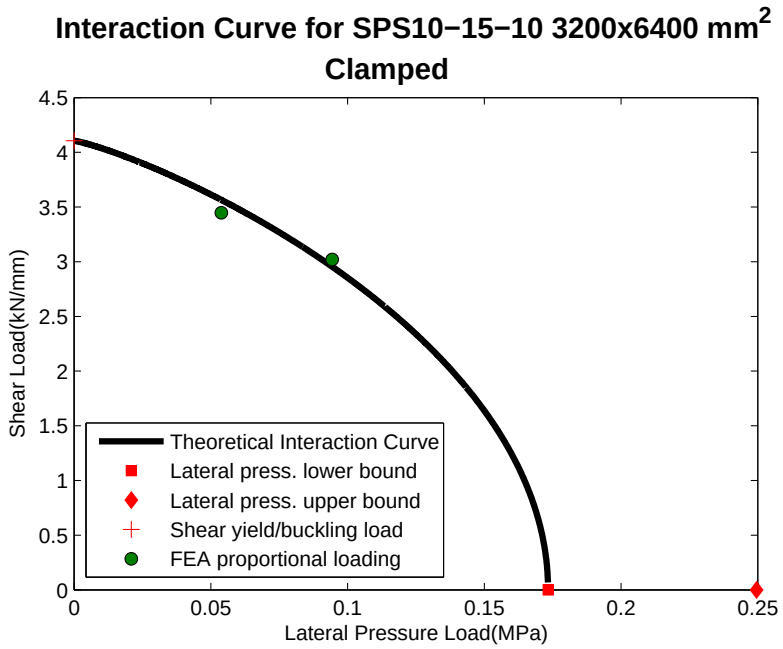

Figure 6.13: Interaction curve with the combination of in-plane shear loading and lateral pressure load on a SPS10-15-10 3200x6400 mm^2 clamped panel

The difference in boundary condition for this geometry gives a large difference in the panel behaviour. Figure 6.13 shows the clamped panel with around the same behaviour as most of the other panels in this study. Only two results from finite element analyses were showing a clear ultimate load but the deviation from the curve seems to be quite good for both of them. In this case the in-plane ultimate shear load is given as the yield load, and the lower bound solution is used for pure lateral load. For all the cases above, the upper bound solution can be used as a reference value for pure lateral pressure, so this panel is standing out.

The reason for this difference lies in the choice of reference value for in-plane shear. Another element analysis was performed with 5.0 mm initial imperfection for the pure shear load case. The result from this analysis was an ultimate load of around 3.64 kN/mm, which is 11.4% less than the theoretically predicted ultimate load. Considering that 5.0

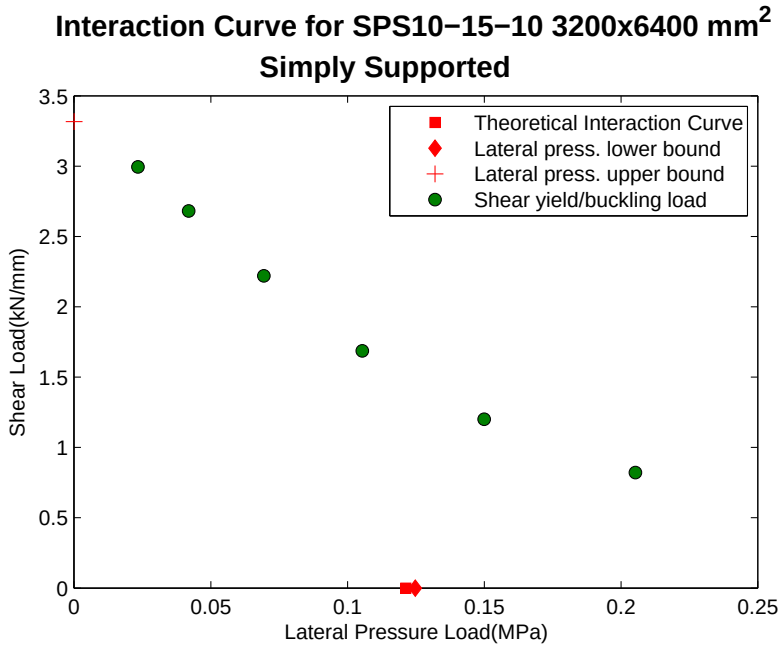

Figure 6.14: Interaction curve with the combination of in-plane shear loading and lateral pressure load on a SPS10-15-10 3200x6400 mm^2 simply supported panel

mm imperfection on a 3200x6400 mm^2 panel is little, it can be concluded that this panel is very sensitive to initial imperfections. As can be seen in Figure 5.10 the difference between the critical yield load and the elastic critical load is small. In a stress versus slenderness plot, this panel would lie just to the left of the transition point between yield and buckling. This is the point where the load is most dependent of initial imperfection, so the deviation between the theoretical yield load and the actual load obtained in this study can be explained from this phenomenon. In a dimensioning context, this is vital to bear in mind. When the new reference value obtained from the element analysis is used together with the upper bound theory for lateral pressure, the interaction curve corresponds well with the two other finite element analyses and is slightly conservative.

The simply supported panel in Figure 6.14 is more similar to the SPS3-15-3 3200x6400 mm^2 panel with simply supported boundaries. Critical load in shear is the elastic critical load. The same aspects as was described for the SPS3-15-3 panel apply for this panel too. Main difference is that this panel is closer to the transition point described in the previous paragraph and the sensitivity to initial imperfection applies.

SPS10-35-10 2000x2000 mm^2

Last two-way interaction analyses are on the thickest panel in the range of panels studied in this work, a square SPS10-35-10 panel with length and width 2000 mm. Interaction curves can be found in Figures 6.15 and 6.16.

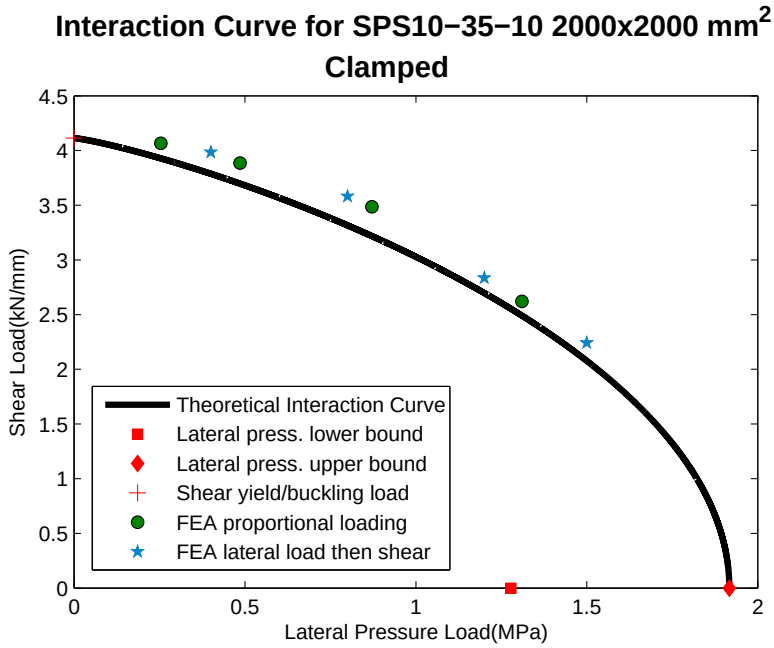

Figure 6.15: Interaction curve with the combination of in-plane shear loading and lateral pressure load on a SPS10-35-10 2000x2000 mm^2 clamped panel

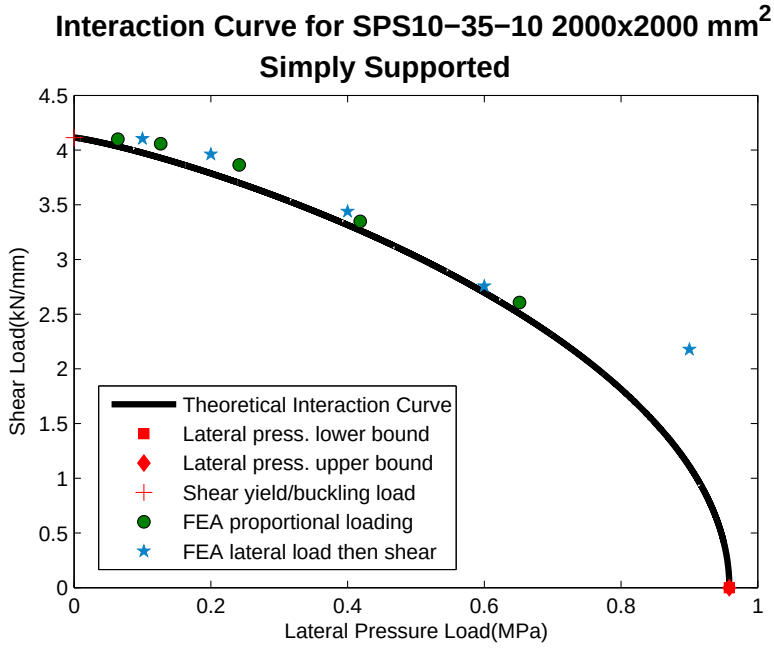

Figure 6.16: Interaction curve with the combination of in-plane shear loading and lateral pressure load on a SPS10-35-10 2000x2000 mm^2 simply supported panel

Both interaction curves in Figures 6.15 and 6.16 corresponds well to the finite element results. There is also a good correspondence between the two different types of load sequences. The rightmost finite element result on the simply supported panel does not agree well with the suggested curve, but this can be expected based on the discussions made earlier.

Conclusions from the analyses

For most of the panels in this study, the suggested interaction curve seems to give a relatively good estimate of the ultimate capacity of panels subjected to in-plane shear and lateral pressure, being slightly conservative. The reference value for in-plane shear load are mostly taken as the yield load, but there are a few exceptions where buckling occurs. When the two different shear criteria estimate quite different values, the lower of the two gives the best estimate of the ultimate capacity. In this case, initial imperfections do not influence the results greatly. However, when the two shear criteria are close in value, attention to the initial imperfections is important, since these may reduce the ultimate capacity considerably.

The upper bound solution seems to give the best estimate of ultimate capacity under lateral pressure load. For almost all panels, using upper bound as reference value gives the most optimum interaction curves. The exceptions are on two simply supported panels with the aspect ratio of 2 and one clamped panel. All of these panels can use the upper bound solution as well, as was discussed earlier in this section under the respective panels. Upper bound theory and lower bound theory are almost identical for simply supported panel under lateral pressure loading. For square panels they actually are identical, so for simply supported panels there is no need to investigate which one will be the best reference value. Figure 2.5 shows a larger span between upper and lower bound for clamped panels. The two values embrace the "knee" in all curves where such a "knee" exists. The lower bound solution is mostly indicating where the "knee" starts to form, while the upper bound solution shows a point little above the place where the curve has flattened, the mechanism is formed and the membrane effect starts to become significant. If this curve characteristic is compared to any of the load-displacement curves where the ultimate capacity was possible to obtain, the lower bound solution is far too conservative, and the upper bound is much closer.

In Section 2.1.1 where the upper bound yield line theory is described, it is mentioned the disadvantage of the theory; that there is no control of deflections. For some of the panels this is a problem and needs to be addressed. Design rules for standard ship applications do not normally specify any displacement limit explicitly, but for high speed light craft applications limits of 1-3% of the panel width are often used. This means that the upper bound generally can be used to represent the ultimate capacity reference for pure lateral pressure, but a separate deflection criterion should be applied during the process of

dimensioning the panels.

As mentioned earlier in this thesis, it is assumed that debonding does not occur.

6.2 In-Plane Shear Load, Lateral Pressure Load and Uni-Axial Compression Load Interaction

Possible reference values for uni-axial compression load was studied in a preliminary work [6] and was found to be quite similar as for the shear case. Either the panel collapse due to full yielding over the entire cross section or the panel buckles and collapse due to excessive yielding. The latter was not spotted for any of the panels tested in this work, but the range of panels was limited for axial compression load cases, so further studies should be performed on this load case.

In this study it is for simplicity assumed that only the steel faces carry axial load, but this should give a good estimate. To establish a three-way interaction surface, it is performed many finite element analyses to get a wide range of comparison data. Firstly the boundaries of the surface were studied. That is, lateral load and shear load, lateral load and axial load, and axial load and shear load. Based on these analyses, interaction curves have been made on the three separate load combinations. In the end, these three interaction curves have been combined to establish a formula for the interaction surface. The suggested interaction surface formula found in this work is given as

$$\left(\frac{N}{N_{ult}}\right)^2 + \left(\frac{Q}{Q_{ult}}\right)^2 \left[1 - \left(\frac{p}{p_{ult}}\right)^{1.2}\right]^{1/3} = \left[1 - \left(\frac{p}{p_{ult}}\right)^{1.2}\right]^{4/3} \tag{6.6}$$

where N_{ult} is the reference value for axial load, Q_{ult} is the reference value for shear load, and p_{ult} is the reference value for lateral pressure load.

Figure 6.17 shows an interaction surface for the SPS5-32-5 panel with dimensions 1200x1800 mm^2 and clamped boundaries. Reference values for lateral pressure load and in-plane shear load are equal to the ones used earlier. Full yield over the entire cross section is by far the most critical reference value for uni-axial compression load. This value can be found to be 4.26 MN when the steel with 355 MPa yield stress is used. The elastic critical load is around 3 times higher.

Figure 6.17 show that the suggested interaction surface gives a good estimate of the ultimate capacity when compared to the finite element analyses performed. Same problem occurs for three-way interaction as for the two-way interaction. When the lateral pressure becomes dominant, it is difficult to obtain a clear ultimate value that corresponds to allowable deformations and the given surface.

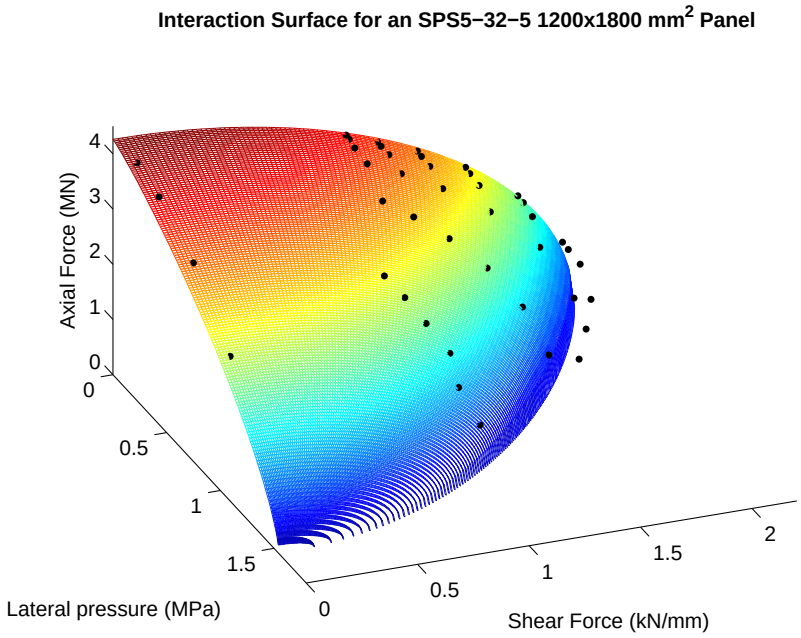

Figure 6.17: Three-way interaction between uni-axial compression load, in-plane shear load and lateral pressure load on a SPS5-32-5 1200x1800 mm^2 clamped panel

To check the suggested surface interaction formula, also a completely different panel than studied before is used. This panel is a SPS6-25-6 with dimensions 2800x4200 mm^2 and clamped boundaries. For this panel the upper bound theory is used for lateral pressure and the yield load is used for in-plane shear. Both these reference values give a good correspondence with the panel behaviour. Uni-axial compression load leads however to more difficulties. The elastic critical load and yield load is relatively close, the yield load being the lower of the two. As was described earlier in this chapter for one of the two-way interaction curves, this closeness in critical values results in a panel which is sensitive to imperfections. For three-way interactions, this leads to problems. If the load combination is in-plane shear and axial load, one reference value for axial load is optimal, and for the load combination lateral load and axial load, another reference value should be used. This means that when the surface approaches the case with pure axial load, the value obtained is not unique, it is path-dependent. One possible approach to this problem is of course to use the smaller of the values but uncertainties are connected to this. How does the panel respond to initial imperfections combined with these loadings for instance? This question of imperfections and reference values need to be studied closer in future work.

6.3 High Strength Structural Steel versus Normal Strength Structural Steel

In Section 3.2 it is shown the properties of the materials used in this work. For all cases the high strength structural steel is used. For shipping applications however, the normal strength structural steel is more often used. A few analyses are performed to see how the change in steel strength influences the panel behaviour.

From the in-plane shear theory section two different theories were presented. Only one of these formulations will change depending on the yield stress of the panel, that is, the full yield criterion. As shown in Section 5.7 most of the panels already fails due to yielding, but for the two cases where the two criteria were almost identical, yield will now clearly be the lowest value. This will make initial imperfections less governing and the three-way interaction curve discussed in the previous section can now be made.

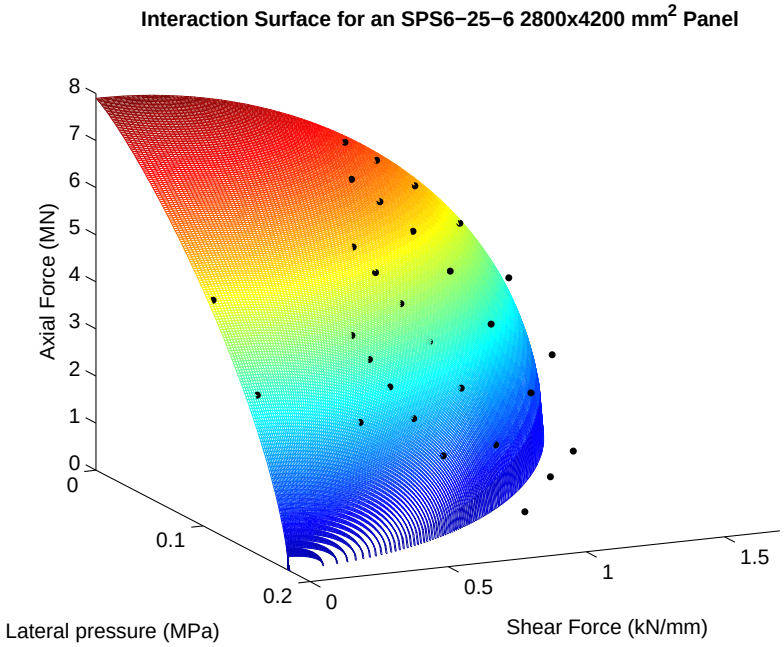

Figure 6.18: Three-way interaction between uni-axial compression load, in-plane shear load and lateral pressure load on a SPS6-25-6 2800x4200 mm^2 clamped panel with normal strength structural steel

A clear reference value can be defined for all the three types of loading, and the interaction curve can be seen in Figure 6.18. Also for this panel the finite element results corresponds well to the suggested surface. Some panels that earlier experienced pure buckling will now maybe get the same problem as the panels mentioned here, but those panels will be of less interest, since they are too flexible for the other sets of loading types.

For many of the panels studied in Chapter 4 a characteristic "knee" was difficult or impossible to find since the panels were too flexible. If the steel used in the faces are of the normal strength type, this "knee" will emerge as can be seen in Figures 6.19.

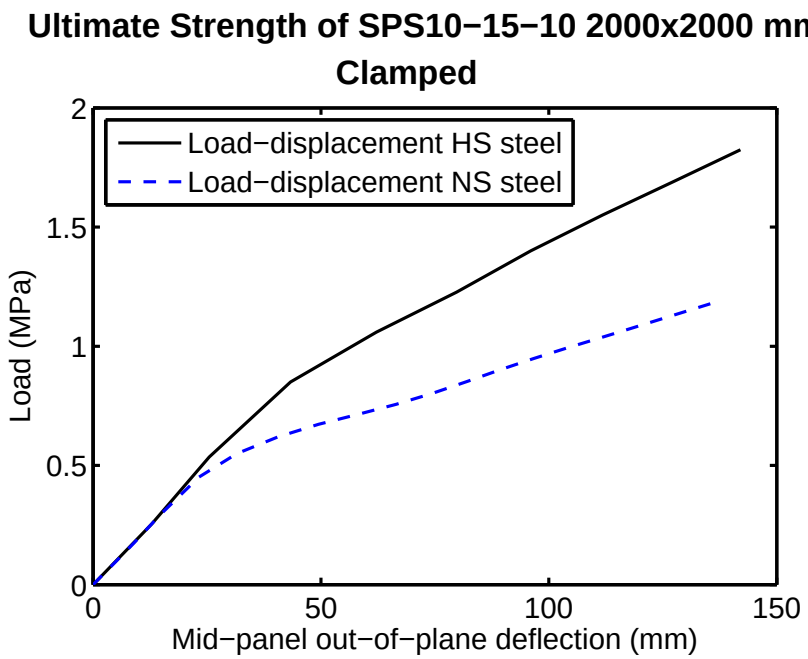

Figure 6.19: Load-displacement curve for the SPS10-15-10 2000x2000 mm^2 clamped panel with normal strength steel and high strength steel

Since the yield stress and modulus of elasticity is not connected, the two materials follows the same path up to a certain level, where the stiffness is greatly reduced on the normal strength steel and not so much reduced for the high strength steel. This gives a more well-defined "knee", and this "knee" also occurs at an earlier stage with respect to deformation. Both these factors are of interest for further studies on the panels.

The thick panels, such as the SPS10-35-10 panel, can carry a large lateral pressure load. In Chapter 4 where this is presented, transverse shear stress over the cross section is also discussed. For the thickest panels, this shear stress is really high and debonding might be the limiting factor. If a face with a lower yield stress is used, ultimate capacity becomes more critical again and dimensioning can be based on this instead of bond strength. Since the bond strength is independent of the yield stress in the steel, the normal strength steel can perform as good as the high strength steel.

Last factor that will be discussed in this context is fatigue. For some panels fatigue issues are more critical than the loading itself, and the resistance against fatigue is almost

identical for the two steel types. The yield stress needs to be far higher before it influences fatigue strength. This means that in situations where fatigue is the critical factor, the two types of steel perform about identical. The extra strength in the HS steel cannot be used.

Chapter 7

Summary and Conclusions

Finite element analyses have been performed on 9 different SPS panels to determine their ultimate strength under lateral pressure, in-plane shear load and for some cases also in-plane uni-axial compression load. Both separate loading and different load combinations are considered. The panel behaviour under the separate loading cases is studied more closely and theoretical approaches are compared to find design criteria that can be used at a later stage. The theories considered in this report are the yield line theory (upper bound) [1], a lower bound theory by Jones [2] and the DNV Class Rules [3] for lateral pressure, and von Mises yield criterion and elastic critical load for in-plane shear load. For in-plane uni-axial compression load, yielding and buckling are used as reference values.

The geometries of the sandwich panels in this report are mostly of the extreme sort with regard to the three ratios, face to core thickness, panel aspect ratio and panel thickness to width. This will help categorising the panels and show what factors that influences the ultimate capacity. Some panels with intermediate dimensions are also studied.

Most of this study is performed with thick shell elements from ABAQUS. The elements are compared to solid elements and give satisfactory results for ultimate strength, and since they require less computational time than the solid elements, they are a good candidate. There are however situations where the solid elements must be used, and that is situations where local strains in the faces can be important. This is for instance when fatigue is studied on a welded edge. The thick shell elements do not spot these local increases in strain. For both types of elements, mesh refinement analyses are performed to verify convergence. Since the finite element method is a form of Rayleigh-Ritz, the solution converges from the non-conservative side.

Two different load sequences are studied in this thesis for two-way combinations between in-plane shear load and lateral pressure load. This is to check whether the loading is path-dependent or not and if it is path-depended, the most critical path must be found. It seems from this study that for the given load combinations, the ultimate strength is not path-dependent, but when the analysis were expanded to three-way interaction, problems

occurred for a panel where yield load and buckling load were almost identical under in-plane uni-axial compression load.

The thin panels subjected to pure lateral pressure show an almost linear behaviour on the load-displacement curve and the region between the upper and lower bound does not indicate any change in the panel behaviour. This indicates that the deformations are so large, that the small deformation assumption in the upper and lower bound theory is violated. The theory still makes a good reference point for the lateral pressure in an interaction curve. These thin panels should not however be located on places where large lateral pressure loads occur.

Thick panels show a well-defined "knee" which is between the upper and lower bound for the clamped panel. Upper and lower bound for simply supported panels are almost identical and always above the "knee". Upper bound is used as reference value for lateral pressure in the interaction curves.

Many of the panels experience large out-of-plane deflections when subjected to lateral pressure. This needs to be accounted for, either by making criteria on allowed displacement, or making the panels stiffer. For instance using the normal strength steel instead of the high strength steel makes the ultimate limit state occur at smaller deflections. Further studies are required to derive a criterion for allowed displacement.

As was mentioned earlier in this report, lateral load is not making the panel rupture before the load is very large, but transverse shear stresses can increase and give problem with both failure in the core and also debonding. Bonding strength is already studied a lot, but further ongoing studies are crucial to get a good understanding of the strength for dimensioning purposes. For some of the thick panels, the transverse shear stress is high.

Using the normal strength structural steel instead of the high strength steel will reduce the ultimate capacity such that the bond strength and ultimate capacity are closer in value. Since the modulus of elasticity is the same for both types of steel, the normal strength steel will also show a more defined "knee" and the material behaviour is easier to study. For the two different steel types mentioned in this report, the difference in fatigue resistance is very small, so in cases where the panel is limited by fatigue, stronger steel than the normal steel will be a waste, since the high strength steel will not reach its full potential. This is an interesting topic with respect to the price of the materials as well.

There are two modes of failure when the SPS panels are subjected to in-plane shear load. Either the panel yields over the entire cross section or the panel buckles and collapses shortly after due to yielding. Most of the panels fail due to yielding over the entire cross section, but there are some exceptions for the thin panels in the study. For dimensioning purposes the smaller of the two should be used, but if the two values are close, special attention need to be taken on imperfections since the panels are sensitive to even small

variations in the imperfection.

For the load combination with in-plane shear load and lateral pressure load, it is difficult to define an ultimate load when the lateral pressure is dominant. This may be expected since the panel has much more capacity than the upper bound theory prescribes when subjected to pure lateral pressure. As the in-plane shear load become more dominant, peak values can be obtained on the load-displacement curves. This can be seen in the interaction curves where all finite element results are on the leftmost part of the curve. Some of the finite element results also show different behaviour when the lateral pressure load is very small on the thin panels. This is due to sensitivity to imperfections as was mentioned in the previous paragraph.

For some of the panels there may be better estimates for the theoretical interaction curve suggested, but the formula given in this thesis is made to give conservative results for all the panels studied. Further studies on a larger range of panels are however needed to check the performance of the formula suggested, or maybe different formulae need to be used for the different "types" of panels.

A formula for the interaction surface for the three load types in this study is suggested to be

$$\left(\frac{N}{N_{ult}}\right)^2 + \left(\frac{Q}{Q_{ult}}\right)^2 \left[1 - \left(\frac{p}{p_{ult}}\right)^{1.2}\right]^{1/3} = \left[1 - \left(\frac{p}{p_{ult}}\right)^{1.2}\right]^{4/3}$$

This formula described the two panels with three-way interaction in this study well, but extensive studies need to be performed on a wide range of geometries to ensure the performance of the formula. It can also be noted that if the in-plane uni-axial load is set equal to zero in the expression, the two-way interaction formula used in this report emerges.

REFERENCES

[1] F. Zhou. *Ultimate Strength of Clamped Steel-Elastomer Sandwich Panels under Combined In-Plane Compression and Lateral Pressure*. PhD thesis, Virginia Polytechnic Institute and State University, Blacksburg, Virginia, 2008.

[2] N. Jones. *Structural Impact*. Cambridge University Press, 1989.

[3] Det Norske Veritas. Hull structural design, ships with length 100 metres and above. *Rules For Classification of SHIPS, Newbuildings*, July 2009.

[4] J. K. Paik and A. K. Thayamballi. *Ultimate Limit State Design of Steel-Plated Structures*. John Wiley & Sons Ltd, England, 2003.

[5] J. Little. *Sandwich Plate System Panels under In-plane Load and Uniform Lateral Pressure*. Master thesis. University of Alberta, Department of Civil and Environmental Engineering, Edmonton, Alberta, 2007.

[6] J. Fladby. *Ultimate strength of SPS panels under combined loadings: Preliminary studies*. Report no/DNV Reg No.: / 12A63TY-2 Det Norske Veritas, Høvik, Norway, 2009.

[7] O. Buyukozturk. *Mechanics and Design of Concrete Structures, Outline 11, Yield Line Theory for Slabs*. Massachusetts Institute of Technology, 2004.

[8] Z. Sobotka. *Theory of Plasticity and Limit Design of Plates*. Elsevier, Amsterdam, 1989.

[9] N. Jones. *A Lower Bound to the Static Collapse Pressure of a Fully Clamped Rectangular Plate*. Report No. 71-20 MASSACHUSETTS INSTITUTE OF TECHNOLOGY, Department of Ocean Engineering, Cambridge, Massachusetts, 1971.

[10] C. Mürer. *Background and Motives of DNVs Hull Structural Rules*. Det Norske Veritas, 1995.

[11] M.A. Brooking Y. Heo M.S. Kim A.E. Martino S.J. Kennedy and H. Ocakli. *Development of Design Equations for Steel Sandwich Panel Construction*. Marine and Offshore Composites, RINA HQ, London, UK, 3-4 Februrary 2010.

[12] W.S. Ericksen E.W. Kuenzi and J.J. Zahn. Shear stability of flat panels of sandwich constructions. *U.S. Forest Products Laboratory Report 1560*, Revised 1962.

[13] M. Stein and J. Neff. *Buckling Stresses of Simply Supported Rectangular Flat Plates in Shear*. Technical Note No. 1222, Langley Memorial Aeronautical Laboratory, Langley Field, Va, 1947.

[14] D. Zenkert. *An Introduction to Sandwich Structures, Student Edition*. Stockholm, 2005.

[15] M.E. Plesha R.D. Cook D.S. Malkus and R.J. Witt. *Concepts And Applications of Finite Element Analysis*. John Wiley & Sons Inc, USA, 2002.

[16] Dassault Systèmes Simulia Corp. *ABAQUS Documentation Manual 6.9-1*, 2009.

[17] H.G. Allen and P.S. Bulson. *Background to Buckling*. McGraw-Hill, Berkshire, 1980.

Appendices

Appendix A

MATLAB Code

```
function koeffShearBuckling

Ef = 206000;%MPa
nuf = 0.3;
Ec = 750;   %MPa
nuc = 0.36;

a = 6400;   %mm
b = 3200;   %mm
t = 3;      %mm
tc = 15;    %mm

d = t + tc;
Gc = Ec/(2*(1+nuc));

D = Ef*t*d^2/(2*(1-nuf^2));
S = Gc*d^2/tc;

mMax = 6;
deltaK = 0.01;

%symmetric

phi = [1:0.02:5];
M = zeros(1,size(phi',1));
for k=1:size(phi',1)
clear DETER;
stop = true;
K = 0;
f = 0;
```

```
g = 0;
    while stop
        i=1;
        j=1;
        g = f;
        for m = 1:mMax
            for n = 1:mMax
                if mod((m+n),2)==0
                    for p = 1:mMax
                        for q = 1:mMax
                            if mod((p+q),2)==0
                                if mod((n+q),2) && mod((m+p),2)
                                    DETER(i,j) = m*n*p*q/((m^2-p^2)*(n^2-q^2));
                                    j=j+1;
                                elseif n==q && m==p
                                    DETER(i,j)=(m^2+n^2*phi(k)^2)^2*...
                                        (t^3*Ef/(D*6*(1-nuf^2))+1/(1+pi^2*D/...
                                        (S*b^2)*(m^2/phi(k)^2+n^2)))/...
                                        (32*phi(k)^3*K)*pi^2;
                                    j=j+1;
                                else
                                    DETER(i,j) = 0;
                                    j=j+1;
                                end
                            end
                        end
                        j=1;
                        i=i+1;
                    end
                end
            end
        f = det(DETER);
        if f > 0 && g < 0
            stop = false;
            M(k) = K;
        elseif f < 0 && g > 0
            stop = false;
            M(k) = K;
        end
        K = K + deltaK;
    end
end
```

```
%plot(phi,M);

%antisymmetric

T = zeros(1,size(phi',1));
for k=1:size(phi',1)
clear DETER;
stop = true;
K = 0;
f = 0;
g = 0;
    while stop
        i=1;
        j=1;
        g = f;
        for m = 1:mMax
            for n = 1:mMax
                if mod((m+n),2)
                    for p = 1:mMax
                        for q = 1:mMax
                            if mod((p+q),2)
                                if mod((n+q),2) && mod((m+p),2)
                                    DETER(i,j) = m*n*p*q/((m^2-p^2)*(n^2-q^2));
                                    j=j+1;
                                elseif n==q && m==p
                                    DETER(i,j)=(m^2+n^2*phi(k)^2)^2*...
                                        (t^3*Ef/(D*6*(1-nuf^2))+1/(1+pi^2*D/...
                                        (S*b^2)*(m^2/phi(k)^2+n^2)))/...
                                        (32*phi(k)^3*K)*pi^2;
                                    j=j+1;
                                else
                                    DETER(i,j) = 0;
                                    j=j+1;
                                end
                            end
                        end
                    end
                    j=1;
                    i=i+1;
                end
            end
        end
        f = det(DETER);
```

```
        if f > 0 && g < 0
            stop = false;
            T(k) = K;
        elseif f < 0 && g > 0
            stop = false;
            T(k) = K;
        end
        K = K + deltaK;
    end
end

R = zeros(1,size(phi',1));
for i=1:size(T',1)
    if T(i) < M(i)
        R(i) = T(i);
    else
        R(i) = M(i);
    end
end
figure(1);
axes('LineWidth',1.5,'FontSize',14);
hold on;
box on;
axis([0.2 1 5 8.5]);
plot(1./phi,R,'-k','LineWidth',1.5);
K0 = 16/3+4./phi.^2;
K0Cl = 9+17/3*b^2/a^2; %Clamped panel
K = K0./(1+pi^2*D/(S*b^2).*(K0-1-1./phi.^2));
KCl = K0Cl/(1+pi^2*D/(S*b^2).*(K0Cl-4/3*(1+b^2/a^2)));
T = Ef*t*d^2*pi^2/(2*(1-nuf^2)*b^2)*KCl/1000

plot(1./phi,K,'-b','LineWidth',1.5);
plot(0.5,634/D*b^2/pi^2,'rx','LineWidth',1.5);
hold off;
title('Buckling Coefficient vs Panel Aspect Ratio','FontSize',14);
legend('Numerical solution of determinant','Approximate design formulae',...
    'Finite element analysis','Location','NorthWest');
set(legend,'LineWidth',1.5);
xlabel('1/\phi','FontSize',14);
ylabel('K','FontSize',14);
N = Ef*t*d^2*pi^2/(2*(1-nuf^2)*b^2)*R/1000;
```

```
figure(2);
plot(1./phi,N,'-k')
hold on;
P = Ef*t*d^2*pi^2/(2*(1-nuf^2)*b^2)*K/1000;
plot(1./phi,P,'-b');
plot(0.5,634/1000,'rx');
hold off;
title('Buckling Load vs Panel Ratio');
legend('Numerical solution of determinant','Approximate design formulae',...
    'Finite element analysis','Location','NorthWest');
xlabel('1/\phi');
ylabel('N_{xy}(kN/mm)');
```